STRUCTURE ANALYSIS AND LESION DETECTION FROM RETINAL FUNDUS IMAGES

A thesis submitted for the degree of Doctor of Computer Science

by

ANA GUADALUPE SALAZAR GONZALEZ

Department of Information Systems and Computing

Brunel University December 2011

Abstract

Ocular pathology is one of the main health problems worldwide. The number of people with retinopathy symptoms has increased considerably in recent years. Early adequate treatment has demonstrated to be effective to avoid the loss of the vision. The analysis of fundus images is a non intrusive option for periodical retinal screening.

Different models designed for the analysis of retinal images are based on supervised methods, which require of hand labelled images and processing time as part of the training stage. On the other hand most of the methods have been designed under the basis of specific characteristics of the retinal images (e.g. field of view, resolution). This compromises its performance to a reduce group of retinal image with similar features.

For these reasons an unsupervised model for the analysis of retinal image is required, a model that can work without human supervision or interaction. And that is able to perform on retinal images with different characteristics. In this research, we have worked on the development of this type of model. The system locates the eye structures (e.g. optic disc and blood vessels) as first step. Later, these structures are masked out from the retinal image in order to create a clear field to perform the lesion detection.

We have selected the Graph Cut technique as a base to design the retinal structures segmentation methods. This selection allows incorporating prior knowledge to constraint the searching for the optimal segmentation. Different link weight assignments were formulated in order to attend the specific needs of the retinal structures (e.g. shape).

This research project has put to work together the fields of image processing and ophthalmology to create a novel system that contribute significantly to the state of the art in medical image analysis. This new knowledge provides a new alternative to address the analysis of medical images and opens a new panorama for researchers exploring this research area.

Contents

List of Figures

List of Tables

Acronyms

DIARETDB1 Diabetic Retinopathy Database 1

DRIVE Digital Retinal Images for Vessel Extraction

STARE STructured Analysis of the Retina

AHE Adaptive Histogram Equalization

MRF Markov Random Field

TPR True Positive Rate

FPR False Positive Rate

ROI Region of Interest

GT Ground Truth

Oratio Overlapping ratio

MAD Mean Absolute Distance

He Hard Exudates

Se Soft Exudates

Acknowledgments

For my family; with special thanks to my mother for her support and faith in me, to my father for my early education that made the solid base for this achievement.

I am grateful to my supervisors Professor Xiaohui Liu and Dr. Yongming Li for their enthusiastic guidance and advice throughout my research.

To all the people that contributed to the development of the research, to Tomi Kauppi, J. J. Staal and A. Hoover for making their retinal images datasets publicly available.

Thanks also to all the members of CIDA research group, for their friendship, interesting discussions and valuable comments that contributed to my research work.

Finally, I would like to express my gratitude to the Mexican National Council of science and technology for the funding of my research project.

Thank you.

To my loved little Cliff, thank you for your support, patient, encouragement and for the mornings of breakfast in the bed.

List of publications

A. Salazar-Gonzalez and Y. Li and X. Liu. Retinal Blood Vessel Segmentation via Graph Cut. *In Proceedings of the 11th International Conference on Control, Automation, Robotics and Vision, ICARCV.* 1:225-230, 2010.

A. Salazar-Gonzalez and Y. Li and X. Liu. Optic Disc Segmentation by Incorporating Blood Vessel Compensation. *In Proceedings of IEEE SSCI, International Workshop on Computational Intelligence In Medical Imaging.* 1:1-8, 2011.

A. Salazar-Gonzalez and Y. Li and D. Kaba. MRF Reconstruction of Retinal Images for The Optic Disc Segmentation. *Health Information Science. Lecture Notes in Computer Science.* Springer Berlin / Heidelberg 7231:88-99, 2012. (Best paper award)

A. Salazar-Gonzalez and Y. Li and X. Liu. Retinal optic disc and blood vessels: the segmentation of overlapping tissues. *Journal of Health Information Science and Systems.* 2012.

A. Salazar-Gonzalez and Y. Li and X. Liu. Automatic graph cut based segmentation of retinal optic disc by incorporating blood vessel compensation. *Journal of Artificial Intelligence and Soft Computing Research.* 2012.

Chapter 1

Introduction

1.1 Overview

The research on medical science field has been and will always be of the common interest for the humankind. Since ancestral time the study of the human body has been concentrate to understand how it works in order to prevent diseases and heal the sickness.

With the invention of new systems and the developing of new technologies the research in the medicine field have had a great impulse. In particular, the development of the medical imaging field has been revolutionary with the availability of new techniques to acquire and process digital images. This revolution have required of significant innovation in computational techniques for the different aspects of image processing. In addition medical images analysis represents an excellent option as non invasive process for the diagnostic and control of diseases.

Medical imaging research involves the analysis of different type of im-

ages such as bones, brain, heart, kidneys, retina, etcetera, that require of different processing techniques. On the other hand tomography, ultrasound and magnetic resonances images cannot be process with a unique methodology; in this direction the type of acquisition process of these images is by itself an independent area of research. The research in the medical imaging has contributed to control and prevent diseases such as arthritis, cerebral tumours, kidney dysfunctions, glaucoma, retinopathy, etcetera.

One of the main health problems that has increased worldwide recently is the retinopathy. Retinopathy is an asymptomatic disease of the retina with the major consequence of the loss of the vision. Periodical eye screening is recommended specially for people under high risk.

Different efforts have worked for the prevention of the blind condition due to a retinopathy. The analysis of retinal images represents a non invasive process to perform the diagnosis and control of patients. Interactive and automatic systems for the analysis of retinal images have been designed. Early models are based on supervised systems. These systems have probed their eficiently in different methods. Unfortunately supervised systems require of high processing time and hand labeled image as part of the training process. Due to the systems have been training using images with specific characteristics the system comprises its performance to image with similar features.

The state of the art on retinal image analysis has the need of an unsupervised systems that perform the analysis of retinal images without human supervision or interaction. In this research we have worked for this kind of

system. A system that take advantage of high image processing techniques, a flexible system that incorporate prior knowledge and that can perform without parameters adjustments for different datasets images.

The purpose of this chapter is to provide and introduction to this research, the retinal image analysis. First we present briefly some of the medical terms in the opthalmologic area. The retinal structures are described, and glaucoma and retinopathy conditions are defined.

Later, we place our research into the current state of the art and the key issues of our research are discussed. The contribution to knowledge of our research is presented next, by highlighting the innovative part of our research. Finally the structure of the thesis is described in order to create a row map for the reader.

1.2 Glaucoma

The term of glaucoma refers to a group of diseases characterized by optic neuropathy. These are characterized by structural changes (optic disc appearance) and functional deficit (measured by visual field change) [Johnson et al., 2003]. Intraocular pressure is used to diagnose glaucoma patients when is not possible visualize the optic nerve and the visual fields cannot be measured. However, even when intraocular pressure is an important risk factor for glaucoma, it is not part of the definition.

In general there are three cases of glaucoma. In the majority of the cases the cause of the glaucoma is primary, it means the disease appears

without known cause. In second instance the glaucoma occurs as a consequence of another form of ocular pathology (e.g. diabetic retinopathy) that increase the intraocular pressure, leading to optic nerve damage. The last case is the congenital glaucoma and is rare.

The second cause of glaucoma represents the 20% of all the cases in a population and is the one on which is more factible to have an early detection. If a patient has the precedent of ocular retinopathy or any other condition that can result on retinal damage (e.g. diabetes) periodical eye screening is strongly recommendable. Receive adequate treatment on the early stages of the disease is crucial in order to avoid the loss of vision.

1.3 Diabetic Retinopathy

Diabetes has turned in a great health threat worldwide in a brief period. According to the World Health Organization (WHO) [Wild et al., 2004], the prevalence of diabetes was estimated in 2.8% of worldwide population, about 171 million people in 2000. This number is projected to increase to 366 million in 2030; it will represent the 4.4% worldwide population. The study indicates that the diabetes epidemic will continue if obesity levels remain constant.

[Fong et al., 2004] defines the diabetes as a condition mainly defined by the high hyperglycaemia level enough to risk of microvascular damage: retinopathy, nephropathy and neuropathy. The type 1 diabetes is a form of diabetes mellitus that results form the autoimmune destruction of the pan-

creas cells that produce insulin. As a consequence the insulin production in the pancreas is permanently damaged. Due to the insulin administration dependency of to the patient, this conditions is commonly refer as "insulin dependent diabetes". On the other hand type 2 diabetes is a metabolic disorder that is characterized by high blood glucose due to the increased resistance to insulin. Most diabetic people have type 2.

The diabetes may cause abnormalities in the retina (diabetic retinopathy), kidneys (diabetic nefropathy), and nervous system (diabetic neuropathy) [Johnson et al., 2003]. The diabetes is also a major risk factor in cardiovascular diseases. The diabetic retinopathy is a microvascular complication of diabetes, causing abnormalities in the retina, and in the worst case, blindness. About 10,000 diabetic people worldwide lose the vision each year. There is evidence that retinopathy begins its development at least 7 years before the clinical diagnosis of type 2 diabetes. If the diabetic retinopathy is not detected and the patient does not receive appropriated treatment it is very likely that glaucoma will be followed.

Retinal treatment is more effective at reducing visual loss when it is applied in the first stages of the disease. But unfortunately patients with retinopathy are often asymptomatic. In this way the early detection of any sign of retinopathy is complex and very important. Regular eye examinations represent an effective approach to detecting and treating diabetic retinopathy. They can avoid the blindness and are cost effective. Systematic evaluations have been developed with effective results, when the treatment is applied in the first stages.

However, despite the recommendations many diabetic patients at risk of blindness due to severe retinopathy stage are not receiving eye examinations and the corresponding treatment [Fong et al., 2004]. The evaluation systems required capacitate physicians, and an adequate evaluation protocol. However, there are concerns about the cost of the development, implementation and maintenance of the appropriated screening scheme. As a means to reduce this cost, the potential ability of an automated detection system to reduce this workload by the use of computerised algorithms on digital retinal images has been investigated exhaustively.

1.4 Retinal eye screening

As mention in the previous section periodical eye screening is highly recommended for patients under certain risk (e.g. diabetic patients). Retinal image analysis is a non invasive option to perform this procedure. Also it permits the analysis of a massive number of images in a relatively short time. The process to acquire a retinal image is quite especialised. One of the techniques to acquire retinal images is the use of a fundus camera. This type of camera operates as a conventional camera, but instead of having a film, they use an image sensor [Patton et al., 2006]. Details about the image acquisition procedure are presented in Chapter 2.

Figure 1.1 shows an example of digital fundus image and the retinal elements. The main distinguished structures are the blood vessel network, the optic disc and the macula.

Blood vessel network is the set of thin elongated structures of dark red

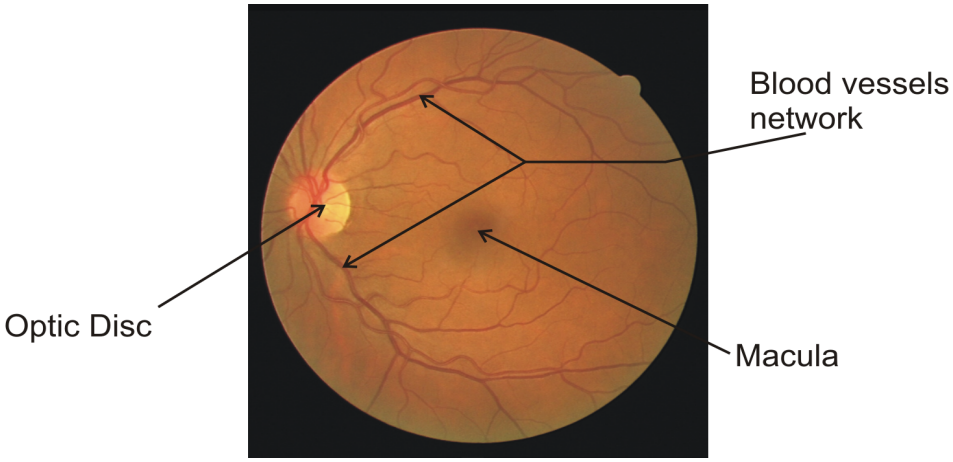

Figure 1.1: Retina structures: blood vessels, optic disc and macula.

colour. Blood vessels converge into the largest bright round area knows as optic disc. Retinal structures, such as optic disc and blood vessel, can provide valuable information about the health condition of the retina. For this reason is important to keep control and detect any change on their morphology. Nevertheless the main indicator of the presence of a disease is the appearance of lesions.

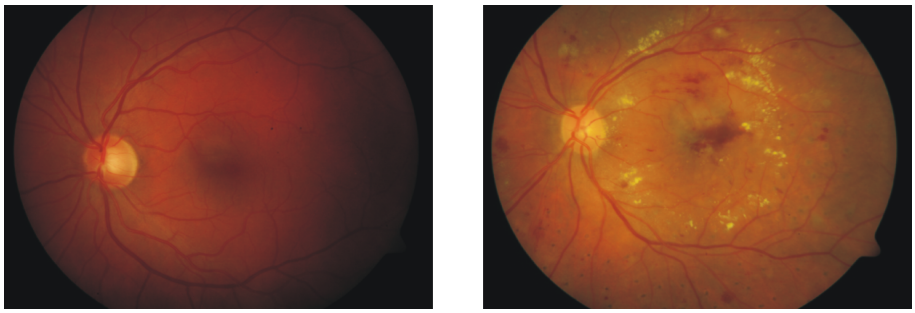

Figure 1.2: Retinal images. Left: healthy retina. Right: retina with clear sign of lesions.

Figure 1.2 shows a clear example of a healthy retina and a retina with

lesions. In general we can classify the retinal lesions as bright and dark lesions. Bright lesions are characterized by yellowish bright colour and depending of their shape, texture and location these can be hard exudates, soft exudates or cotton spots. Haemorrhages and red spots are the type of dark lesions and are characterized by their dark red colour.

The detection of retinal lesions can be complex, especially for dark lesions that are characterised by their poor contrast with the background. On the other hand lesions have similar features of colour and texture with retinal structures. Bright retinal lesions (e.g. exudates) share properties of colour with the optic disc, and dark lesions with blood vessels.

1.5 Current State of the Art

The retinal analysis models can be classified in two groups. The first group includes the systems that address the analysis directly on the lesions. These type of models are concentrated on the enhancement and detection of the lesions [Osareh et al., 2009], [Niemeijer et al., 2007b], [Garcia et al., 2009], [Sanchez et al., 2009], [Fleming et al., 2007], [Welfer et al., 2010b], [Li Yun et al., 2008]. The second group adopts as methodology the segmentation the retinal structures as a first step. These structures are then used to extract valuable information about the retinal morphologic. Once that retinal structure have been segmented, they are used to facilitate the detection of lesions [Walter et al., 2002], [Sanchez et al., 2004], [Sopharak et al., 2008], [Fang et al., 2010].

Early methods for the analysis of retinal images are based on supervised systems. The system is trained by using a set of retinal images labeled by hand. These marks are used to extract information about the region of interest. Later, by using this information the system creates a model of the object to segment and uses this model to segment the region of interest in other retinal images.

Supervised systems demand, as part of the training process, a set of hand labeled retinal images. Also the training stage requires of computing processing time. Both conditions increase the amount of necessary resources in order to implement the system. Furthermore, if the system has been trained in a collection of retinal image with particular features (e.g. illumination, resolution, field of view), the system will compromise its performance to images with similar characteristics.

Often the systems designed for the segmentation of the retinal structures (e.g. blood vessels and optic disc) consider that the image has been captured in a particular position and the analysis is based under this template [Sanchez et al., 2009], [Niemeijer et al., 2007a]. This kind of assumption limited the performance of the method to the type of retinal images that have been captured in this way.

The state of the art has the need of an automatic and unsupervised system to analyse retinal images. The system should not be limited to perform on retinal images with specific characteristics of resolution or field of view. The system should be able to perform on retinal images from different datasets without need of adjustment of parameters or recalibration.

Blood vessels and optic disc should be segmented by using high level image processing techniques that consider not only their colour or intensity, but also their shape. Traditional techniques for the analysis of images need to be adapted to cover the specific needs of medical images.

Another important issue to address is the experimental work. Until recently years the experimental work has been carried out independently. The amount of data set images goes from ten to hundreds of them; and the images features are not that clear to create a conclusion about the performance of the evaluated method. This makes complicated the comparison of results with other methods.

The evaluation of the methods needs take place by using a controlled methodology where the conditions do not work in favour of some techniques. In this direction public datasets that provided hand labelling of the region of interest are very useful to carry out experimental work. Some of the available public datasets provide hand labelled of the retinal structures that can be used as ground truth to evaluate the segmentation results.

For the specific case of retinal lesions the DIARETDB1 dataset provides a new hand labelling system. In this dataset the retinal images where marked independently by some experts in the area. The experts not only marked the lesions, also they graded the confidence of their markings. As a result the ground truth is a collection of lesion markings with different levels of confidence that reflect the knowledge of the experts. DIARETDB1 dataset has opened a new gate for the evaluation of retinal lesion detection,

where the methods can be evaluated by using more than one expert opinion.

1.6 Key Issues

Medical image analysis is a fascinating research field. The development of new technologies to capture medical images has revolutionized the medicine area. New techniques to process and analyse medical images have opened a new panorama for the computer assisted diagnosis.

The challenge of medical image analysis implies deal with poor contrast images. In general medical images are characterized for their fuzzy boundary between elements and high noise due to the capture process. In particular retinal images present very low contrast between blood vessels and their background. The colour distribution of vessels and their background are very similar which difficult the vessel network segmentation. The optic disc is the brightest round area, it presets good contrast with its background. Nevertheless there special issues to address for its segmentation, such as vessel crossing.

We can divide our retinal method analysis in three major procedures: blood vessel segmentation, optic disc segmentation and retinal lesions detection. As a first steps the retinal structures are segmented. The segmentation of the structures allows extracting features that can provide information about the health condition of the eye. Later, the structures are masked out in order to create an adequate area to detect the lesions. Figure 1.3 presents the general methodology scheme of our system. The

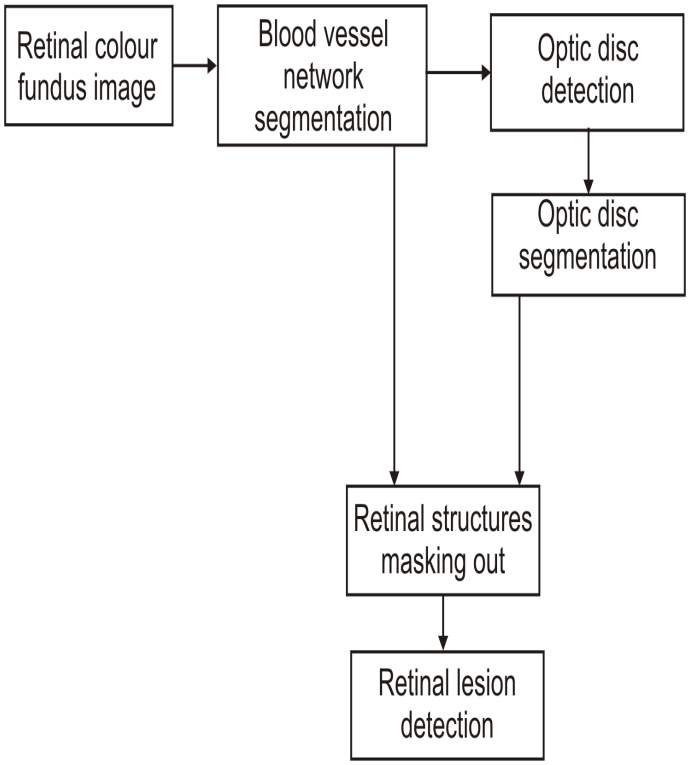

Figure 1.3: Retinal analysis methodology squeme.

three main process of our method are summarized next.

1.6.1 Blood vessel segmentation

Retinal blood vessels are thin elongated structures that converge into the optic disc. Their morphology is taking in consideration for the diagnosis of patients.

The contrast between vessels and their background is very low especially in the poor illuminated areas. A simple threshold cannot deal with the vessel segmentation. The vessels pixels intensity has a wide range of values due to the non illumination homogeneity. This distribution overlaps the background distribution.

As many other researches we identify the green channel as the best one to perform the vessels segmentation. The best contrast between vessels and their background appears in the green channel. We have preprocessed the green channel in order to enhance this contrast. As a result of applying a modified version of adaptive histogram equalisation on the green channel of retinal images vessels are enhanced from their background. From the enhanced images a prior rough segmentation is obtained and graph cut theory is used to obtain the final segmentation of vessels.

The segmented vessels are a good start to proceed with the rest of the analysis. Vessels can be used to localize other retinal structures such as the optic disc. Also because vessels location is known they can be considered to perform the optic disc segmentation by discriminate them or incorporate

them to the process. Frequently some vessels structures are detected as part of the retinal lesions, if vessels are discriminated from the searching field for the lesions detection, false positives can be reduced.

Chapter 4 provides details of our vessel segmentation method where experimental results are presented and discussed.

1.6.2 Retinal optic disc segmentation

Even when optic disc has colour similitude with bright lesions, the optic disc is a much bigger collection of pixels. Also vessels converge into the optic disc, making it unique with this characteristic. These conditions can be used to detect and segment the retinal optic disc.

The main issue to address is the overlapping of vessels with the optic disc. The optic disc appears as a round object which boundary is interrupted by vessels crossing, this make its segmentation difficult. On the other hand vessels inside of the optic disc are part of the object to segment (foreground), while vessels outside of it are part of the background, this complicates the separation of structures.

The overlapping of tissues is a common case in medical image analysis. Most of the methods designed to deal with this issues address the problem by segmenting the overlapping structures as a first step in order to discriminate them later. We have addressed this problem by using prior blood vessel segmentation. Two methodologies were designed and implemented. The first one considers blood vessels pixels as unknown and reconstruction process is used to fill the gaps. As a result the optic disc appears as a well

defined object, and then it is segmented. The second methods incorporates blood vessel network into the optic disc segmentation formulation.

The implementation of these methods, based in the graph cut theory, let us explore two opposite research lines and compare results. Chapter 5 presents the implementation details for both methods and the results of experimental work. The methods were tested using the same experimental conditions. Results are compared with other methods in the literature, and the advantage and drawbacks of each method are discussed.

1.6.3 Retinal lesions detection

As mention before the presence of lesions in the retina is the main indicator of a case of disease. Different methods have been designed in order to detect and segment retinal lesions. Some methods have chosen concentrated the analysis to specific type of lesions, such as hard exudates.

In general bright lesions (e.g. exudates) are easier to detect than dark lesions (e.g. haemorrhages). This due to their high contrast with the background. Frequently candidate lesions pixels are selected as first step, and later the selection is pruned to produce the final segmentation. Some of the methods perform first the segmentation of retinal structures in order to discriminate this areas and reduce the searching field for lesions. This procedure reduce the number of false positives.

Many researchers have focused their work in the detection and segmentation of retinal lesions. Nerveless is questionable in which grade a perfect

segmentation of lesions will support the diagnosis process. If the purpose of the diagnosis is determine the presence or absence of lesions, then the exact definition of lesions boundaries is not that relevant. On the other hand if the objective of the detection of lesions is to apply a corrective treatment a high definition of lesions boundaries results important.

1.7 Contribution to Knowledge

During the developmento of our research several methods were designed and implemented for the segmentation of retinal structures and the detection of lesions. These innovative methods are contributing in the creation of new knowledge in the area of medial imaging analysis. We have summarized the contribution of our research project next.

- The design of an automatic and unsupervised system for the analysis of retinal images. Much of the work on retinal images segmentation has been based on supervised systems. These type of systems requiere of a training process, which demands of high processing time. Also the creation of training images requires of time and work to label them. Futhermore, due to the need of a training set of hand labeled images, supervised methods are limited to perform on retinal images with similar characteristics than the ones used for training. Our methods are initialized automatically, and they perform the segmentation of retinal structures in an unsupervised manner. These particular features provided flexibily to our methods to perform on image with different characteristics, such as illumination, resolution, field of view, etcetera.

- Incorporation of prior knowledge. The segmentation is considered an ill-posed problem, where more than one solution can be accepted as correct. In order to find the optimal segmentation prior knowledge can be used to reduce the searching field. For first time graph cut technique has been considered to segment retinal images. Graph cut is an energy based segmentation method. The selection of this technique has permited to incorporate prior knowledge to guide the search for the optimal solution.

- Segmentation of overlapping tissues (blood vessels and optic disc). Blood vessels are the main interference for the segmentation of the optic disc. Vessels inside the optic disc are part to the object to segment, but vessels outside of the optic disc correspond to the background. Until now vessels have been discriminated (eliminated) for the segmentation of the optic disc. We have explored to complementary research metodologies, discimination and incorporation of vessels. Experimental results provide new knowledge to be taken as a base to address the segmentation of overlapping tissues in the medical imaging field.

- Dark and bright retinal lesions detection. In general bright lesions are easier to detect than dark lesions. This due to the high level contrast with their background. Current methods designed for the detection of retinal lesions are concentrated in the detection of brigth lesions, leaving to a side dark lesions. Our method detects any suspicious area that do not match with the general background template, this

includes dark and bright lesions.

- Confidence based evaluation for the retinal lesion detection. Until now the evaluation of the methods for the detection of lesions has been performed based on a unique ground truth. By means of the DIARETDB1 dataset use we perform the evaluation of detected lesions based on the confidence marks made by more than one expert.

- Creation of ground truth for the optic disc in public datasets. A common interest within the research comunnity in retinal imaging is the availability of ground truth images to perform experimental work. Different public retinal datasets are available, but unfortunately they do not included a ground truth of the optic disc. We have created hand labelling of the optic disc on two public dataset, DRIVE and DIARETDB1. These ground truth sets are available and have been shared within the research comunity.

1.8 Structure of Thesis

The analysis of the current background literature is presented in Chapter two. The most relevant methods for the analysis of retinal images have been selected. They have been classified by the eye structure analysis, blood vessels and optic disc. Different methods for the blood vessel and optic disc segmentation are presented and compared.

Chapter three is dedicated to present the research design and methodology. The process to capture a retinal image is explained, we have included

the definition of the related terms. The public datasets used for our experimental work are described along with their particular characteristics. The graph cut technique and its traditional formulation are detailed, and medical images analysis methods based on this technique are reviewed. Finally topology cut technique and its participation in our experimental work are described.

In our research the analysis of retinal images can be divided in three stages; the segmentation of blood vessels, the optic disc segmentation and the retinal lesions detection. The segmentation of the blood vessels is detailed in Chapter four. We describe the main issue for the blood vessel segmentation using the graph cut technique, and the proposed solution is detailed. Experimental results are used to evaluated and compare our method using public datasets.

The segmentation of the optic disc is presented in Chapter five. The main obstacle for the optic disc segmentation are the blood vessels. We use prior blood vessel segmentation to perform the segmentation of the optic disc. Two different methods were developed. As most of the proposed methods in the literature, one of our methods eliminate the blood vessels prior to the optic disc segmentation by using image reconstruction. As a result the optic disc appears as a well defined object ready to be segmented. The second method incorporates the blood vessel information into the graph formulation.

Chapter six presents the detection of retinal lesions procedure. The segmented structures (blood vessels and optic disc) are masked out of the

retinal image. Using the masked image a background template is created and used to detect the objects that do not match the general background. The evaluation of the method for the detection of retinal lesions is based on terms of confidence using the ground truth created by opticians.

Finally Chapter seven discusses the contributions of the research and describes the overall benefits of the proposed system in the medical images analysis domain. Future considerations of new research and related ideas are also discussed.

Chapter 2

Background

Recently medical image processing has gained a notable interest within the research community. Due to the non invasive characteristic the analysis of medical image represents an excellent option to carry on the diagnosis and control of diseases. With the availability of new methods to acquire medical images and the creation of new techniques to process them the analysis of medical images has revolutionised the medicine field.

The analysis of retinal images has been used as an instrument to detect signs of retinopathy. The morphology of retinal structures, such as blood vessels and optic disc, is an important indicator for diseases like diabetes, hypertension and retinopathy. A regular inspection of the retinal represents an effective action to detect the symptoms of these diseases.

To address the analysis of retinal images different approaches have been considered. These include the use of active contours, machine learning systems, neural networks, mathematic morphologic and wavelets. In this chapter we make a review of the relevant literature in the area of retinal

image analysis. We have considered the retinal image analysis systems, particularly the ones dedicated to the retinal structure segmentation(e.g. optic disc, blood vessels).

This chapter has been divided into three major sections. Firstly we are dedicated to review the methods designed for the segmentation of retinal blood vessel. Secondly retinal optic disc segmentation techniques are presented. Finally the methods dedicated to the analysis of retinal lesions are summarized and discussed.

2.1 Retinal blood vessels segmentation

Blood vessels can be seen as thin elongated structures in the retina, with variation in width and length, that converge into the optic disc. An accurate segmentation of the blood vessels is the first step to extract features and fundamental information to create a diagnosis, evaluate treatments progress and keep control of diseases.

An adaptive local thresholding based in a verification multithreshold probing scheme is proposed in [Jiang and Mojon, 2003] to detect the vessel network on retinal images. Considering an image resulted from a thresholding process on the retinal image, the method claims to be able to decide if any region on the binary image can be accepted as an object by using a classification procedure. The method is performed on a series of different thresholds and the final segmentation is obtained by combining the results from the individual thresholds.

An automatic method to localize and segment the retinal blood vessels is presented in [Hoover et al., 2000]. The method uses local and global vessel features cooperatively to segment the vessel network. It utilizes a matched filter response, followed by a threshold probing process. A relevant contribution of the work of Hoover and his collaborators is the creation of the STARE dataset. STARE dataset is a collection of retinal fundus images. Part of these images were selected by Hoover's research team to perform blood vessel hand labeling and create a ground truth to evaluate segmentation results. Their work has been referred by different authors, and is used in this research to perform evaluation of blood vessel segmentation.

Wu [Wu et al., 2006] proposed an adaptive detection method which consists of three stages. The methods starts by enhancing the blood vessels using an extended adaptive histogram equalization. Later a Gabor filter response with different orientations is used to extract features. And finally a tracing process of the vascular networks is applied as postprocessing.

Mendonca [Mendonca and Campilho, 2006] addressed the vessel segmentation problem by detecting the vessel centerline as the first step, followed by a vessel filling using global intensity characteristics and local vessel width information. Four directional difference of offset gaussian filters are used to select vessel centerline pixels candidates. They are validated based on the characteristics of the line segments. The final segmentation is obtained by using an iterative region growing method that integrates the contents of several binary images resulting from vessel width dependent morphological filters. Usman [Usman Akram et al., 2009] proposed as the

first step the use of a 2-D Gabor wavelet to enhance the vascular network. After enhancement process blood vessel are detected by using an adaptive thresholding.

Supervised methods have been proposed to perform the retinal blood vessel segmentation. In [Staal et al., 2004] the system is based on extraction of image ridges, which coincide approximately with vessel centerlines. The ridge is used to compose primitives in the form of line elements. This line elements are used to divide the image into patches by assigning each pixel in image to the closest line element. For each pixel feature vectors are computed by using the properties of the patches and line elements. Then the feature vectors are classified using a kNN classifier and sequential forward feature selection. A notable contribution of this work is the creation of DRIVE dataset. DRIVE is a collection of 40 retinal images, with two sets of blood vessels hand labeling. In this research, as many other works, one of the hand labeling sets is used as ground truth to evaluate blood vessel segmentation results, while the other set is taken as second observer.

An automatic system for the segmentation of retinal blood vessel is presented in [Soares et al., 2006]. The method is based on feature vector classification. The feature vectors are composed of pixel intensity, and two dimensional Gabor wavelet transform responses taken at multiple scales. The Gabor wavelet is used as noise filtering and vessel enhancement in a single step. Finally Bayessian classifier with class conditional probability density function is used to classify pixels as vessels or non vessels. Based on a training set of labeled pixels obtained from manual segmentation the probability distributions are estimated.

In [Martinez-Perez et al., 2007] an automatic system for the segmentation of retinal blood vessels is proposed. The method is based on multiscale feature extraction. Using gradient magnitude and maximum principal curvature of the Hessian tensor features as vessel width, size and orientation are extracted. Later, a multiple pass region growing procedure progressively segments the blood vessels by using the feature information together with spatial information about the pixel neighborhood.

An automatic and unsupervised multiresolution vessel segmentation method using normalized cuts is presented in [Cai and Chung, 2006]. Making use of the gradient matrix of the Lucas-Kanade equation the method detects a candidate window where a vessel possibly exists. The normalized cut criterion is used to search a local intensity threshold to segment the vessels in a candidate window. If a vessel is detected, this is tracked to select the next candidate window. The final segmentation is completed by combining all the results obtained from different resolutions levels.

Recently a method based on the divergence of vector fields was presented in [Lam and Yan, 2008]. By using the Laplacian operator the method detects vessel candidates. Later the centerlines are detected using the normalized gradient vector field. Finally the segmentation is refined by pruning the spurious candidate vessels according to the detected centerlines. The idea is to remove a pixel from the candidate vessel list if this pixel is far away from the detected centerline.

Frequently vascular retinal segmentation methods are designed for a

specific dataset. In order to perform on retinal images with different characteristics parameters are adjusted to adapt them for different imaging conditions. It is important to have a segmentation algorithm that does not depend on parameter configuration, so the analysis can be unified for images of different datasets.

2.2 Retinal optic disc

The optic disc appears as the brightest round object in the retinal images. The segmentation of the optic disc is not an easy problem to resolve, and it requires a specialized procedure. Apart from the variation in shape, colour and size there are other complications to address. The proportional area occupied by the optic disc inside of a fundus image depends on the field of view FOV taken by the camera. Methods based on the standard size and shape of the optic disc limit their performance to images with specific characteristics.

One of the main obstructions for the optic disc segmentation is the outgoing blood vessels breaking the optic disc boundary. This added to the non uniform illumination make the segmentation of the optic disc complicated even for the human eye. In general the best conditions to perform the segmentation of retinal structures are found in healthy images. Images with some sings of retinopathy are turbid and as a consequence more complicated of analyze.

The research proposals dedicated to the optic disc analysis can be re-

viewed in two groups. The first group is dedicated to the methods whose only purpose is the location of the optic disc without perform its segmentation. Some of these methods have demonstrated an achievement of 100% in the location of the optic disc. The second group includes the methods which locate and perform the segmentation of the optic disc. In the next sections we make a review of the current techniques of both groups.

2.2.1 Optic disc location

The optic disc location based on prior vessel segmentation has demonstrated to be the most reliable method. A confident blood vessel segmentation is required in order to perform a successful optic disc localization.

Hoover et al [Hoover and Goldbaum, 2003] proposed a method for optic disc location based on the fuzzy convergence of the blood vessels. In the absence of a confident convergence result the algorithm will identify the optic disc location as the brightest region in the image. The evaluation of the method is performed separately for healthy retinas (31 images) and diseased retinas (50 images). These work presents a good argumentative support to explain the implicated difficulties for the analysis of retina images with a disease.

In [Tobin et al., 2007] the optic disc location relies on prior vascular system segmentation. Next, spatial features are determined; these features describe the density, thickness, and orientation of the vessels in relation to the position of the optic disc. The optic disc position is used to localize the macula by determining the horizontal line of the retina using a vascular

geometric model.

In [Youssif et al., 2008] the retinal vessels are segmented by using a 2-D Gaussian matched filter and a vessel direction map is created. The vessels are then thinned, and filtered using local intensity, to finally represent the optic disc centre candidates. The minimum difference between the matched filter result and the vessel direction around each candidate provides an estimation of the optic disc location.

A supervised location method for the optic disc position was presented in [Niemeijer et al., 2008]. Prior vessel segmentation and a kNN regression are used to approximate the optic disc location. The model is trained by using a set of 200 images. Another supervised method for the optic disc location is presented by Kauppi et al in [Kauppi and Kalviainen, 2008]. The proposed method performs a training stage, where PCA is adopted to determine an eigenspace that characterizes the optic disc in retinal colour images. Templates extracted from the training images are used to localize the optic disc.

Table 2.1 shows the compilation of methods designed for the location of the optic disc. During the experimental work one of the issues to attend is the lack of a common data set to test the algorithms. The methods have been evaluated using different collection of retinal images. This complicates the comparison of methods performance.

Method	Num. images	Optic disc location
Fuzzy convergence [Hoover and Goldbaum, 2003]	81	89%
Vessel features [Tobin et al., 2007]	345	90.4%
Vessel direction matched filter [Youssif et al., 2008]	81 (STARE)	98.77%
	40 (DRIVE)	100%
kNN regresor [Niemeijer et al., 2008]	250	99.2%
Decorrelated templates [Kauppi and Kalviainen, 2008]	61 DIARETDB1	100%
PCA [Li and Chutatape, 2004]	89	99%
Point distribution model [Niemeijer et al., 2007a]	500 (healthy)	98.4%
	100 (pathological)	94%
Multi-scale hybrid Snake [Welfer et al., 2010a]	89 DIARETDB1	97.75%
	40 DRIVE	100%

Table 2.1: Methods for the location of the optic disc.

2.2.2 Optic disc segmentation

Different methods for the segmentation of the optic disc have been designed. The convergence of vessels is a recursive method to localize the optic disc in order to perform its segmentation later. The current methods have made used of morphological operations, active contour models, Hough transform and PCA to perform the definition of the retinal optic disc boundary.

Morphological operations have been used to perform the segmentation of the optic disc. An algorithm for the segmentation of the optic nerve is presented in [Chrastek et al., 2005]. The method was designed to perform in scanned laser tomography images. Morphological operations is used for the localization of the optic disc as first step. Later, the search space is constrained using the Hough transform, and finally the optic disc contour is defined using an active contour model.

[Welfer et al., 2010a] presents an adaptive method using mathematical morphology for the optic disc segmentation on fundus images. The convergence of the blood vessels is used to detect the optic disc centre. Later, watershed transforms from markers are used to find the optic disc boundary. The main vessels arcade is used to initialize internal and external markers, and estimate a first boundary shape. Using the estimated boundary shape, new internal and external markers are obtained. Morphological erosion is applied to the selected boundary and then is used as new internal marker.

One of the first works to use active contour models to identify the optic disc boundary is presented in [Mendels et al., 1999]. Morphological filtering technique and active contour model are used to find the boundary of the optic disc. Preprocessing technique based on local minimal detection and morphological filtering is used to minimise incorrect boundary detection due to blood vessel interference. Later, the optic disc boundary is determined by an active contour driven by a gradient vector flow.

The method proposed in [Aquino et al., 2010] performs the segmentation of the optic disc by the use of morphological and edge detection techniques, followed by the circular Hough transform. Prior to the segmentation of the optic disc blood vessels are eliminated. The method assumes that a linear shape can be detected by using a rotating linear structuring element to calculate the statistical variance of gray level values of pixels along the shape.

An unsupervised segmentation method is proposed in [Yang et al., 2006], a multi-scale hybrid Snake is used to segment the optic disc. The

method places the initial curve considering the dark area around the central bright region in Heidelberg retinal tomographs. In [Lowell et al., 2004] the optic disc location is achieved using a specialized correlation filter, which matches key elements of the structure of the optic disc. The correlation peak gives the approximate center of the optic disc. The model is a circle defined by the center, and evenly spaced radial spokes. The method performs the segmentation of the optic disc using a deformable Contour Model.

In [Li and Chutatape, 2004] principal component analysis (PCA) is proposed to localize the optic disc. Making use of the top-down strategy the system extracts the common characteristics among the training images dataset. These common characteristics are used to detect the similar object (optic disc) in a retinal image. For the optic disc boundary detection a modified active shape model is used. The system constructs a point distribution model from a training set, and then the model is used to search for an object with similar shape in the rest of the retinal images.

Niemeijer et al [Niemeijer et al., 2007a] addresses the problem by fitting a single Point Distribution Model to the retinal images. The model contains points in the center and four extremes of the optic disc; the distances from the extremes to the center point are interpolated to find a radius **r**. A rough segmentation is marked by drawing a circle around the center point with radius **r**. The disadvantages of supervised systems are the requirement of a training process and hand labeled images, which is resources consuming.

Table 2.2 shows a compilation of the different methods for the optic

disc segmentation. We have divided them into supervised and unsupervised methods. It is possible to appreciate that supervised methods have reached slightly better performance than unsupervised methods. The use of public datasets, susch as DIARETDB1 and DRIVE, to evaluated the performance of the methods is very important in order to make fair the comparison of results with other methods. The characteristics of the datasets used in our experimental work are described in Chapter three.

Supervised Methods		
Method	Num. images	Overlapping ratio
Active shape model [Li and Chutatape, 2004]	35	94%
Point distribution model [Niemeijer et al., 2007a]	500 (healthy)	94%
	100 (pathological)	85%
Unsupervised Methods		
Multi-scale hybrid Snake [Yang et al., 2006]	10	85.01%
Adaptive morphologic [Welfer et al., 2010a]	89 DIARETDB1	43.65%
	40 DRIVE	41.47%
Circular Hough transform [Aquino et al., 2010]	1200 MESSIDOR	86%

Table 2.2: Methods for the segmentation of the optic disc.

2.3 Retinal Lesions

As mention before, retinal lesions are the main indicator of the presence of a disease. We can classify the retinal lesions as bright and dark. Figure shows some samples of retinal lesions. Exudates are example of bright lesions these can be classified as hard exudates and soft exudates. Hard exudates are characterized by their sharp edges, while fuzzy edges are characteristics of soft exudates. Both of them are bright yellowish objects clearly

distinguished from the background.

Dark lesions are characterised by their deep red colour. These can be divided into heamorrhages and red spots. Dark lesions are difficult to localize due to the similar colour distribution with the background. The sample of retinal images presented on the Figure and the marking of the lesions were taken from the DIARETDB1 dataset.

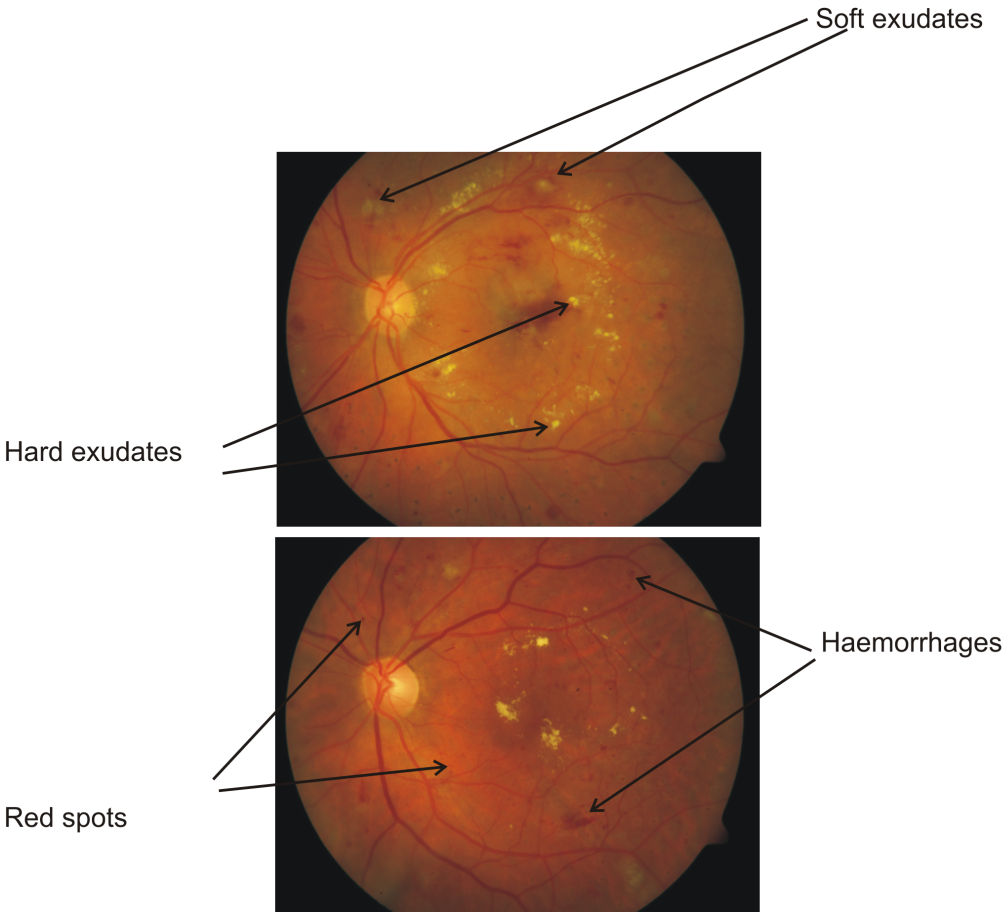

Figure 2.1: Retinal lesions. Bright lesions: hard and soft exudates. Dark lesions: red spots and haemorrhages.

In general bright retinal lesions are easier to detect and segment; this due to their high contras with the background. For this reason, methods designed for the detection of retinal lesions are frequently focused on the detection of bright lesions, such as exudates.

Due to the colour characteristics shared by the optic disc and bright lesions, very frequently the optic disc is detected and segmented prior to the retinal lesion analysis. In [Walter et al., 2002] an unsupervised system for the detection of hard exudates based on morphological operations is presented. As a first step the optic disc is segmented using morphological operations and the watershed transform. Later, exudates candidates are selected and their boundaries defined. Morphological operations are used to minimize the obstruction of vessels in the optic disc in order to facilitate its segmentation. Prior to select exudates candidates vessels are eliminated by using morphological closing. Because the morphological operations are applied to the whole image the shape of other structures is altered and a reconstruction process is needed. By following this methodology the risk of losing crucial information, including lesions, is high.

Boosted soft algorithm is used to obtain a coarse segmentation of hard exudates and optic disc in [Fang et al., 2010]. Later, vessels are detected by using Gabor wavelet filters and SVM classifier with multi channel features and contour cue. The convergence of vessels is detected and assumed as the optic disc centre. In order to segment the optic disc the size of this is estimated by using double ring filter. Finally by using a SVM classifier the hard exudates candidates are pruned and the final detection is achieved. The method assumes the optic disc as a perfect circle shape in order to

facilitate its segmentation. This assumption block the vessels interference but it is not always the case to find a perfect circle as optic disc, especially in retinas with some kind of disease. The size of the optic disc is estimated by using proportions with the matched filter used to determine the optic disc centre. This methodology restricts the method performances to retinal images with a certain field of view where the proportion of the optic disc in the image is within the requirements of the method.

Morphological operators are used for exudate detection in [Sopharak et al., 2008]. The retinal images are preprocessed by a median filter to reduce the noise and by a contrast limited adaptive histogram equalization (CLAHE). Later, by using morphological operators the optic disc is detected and masked out. A complex process of morphological closing, thresholding, fill holes and morphological reconstruction is then applyed to finally detect the exudates.

In [Sanchez et al., 2004] the method addresses the hard exudate detection by considering two of their features: "yellowish" color and sharp edges. As a first step the optic disc and blood vessels are detected and removed from the retinal images. Later, colour segmentation based on the statistical classification is used to detect the "yellowish" objects and the ones with sharp edges are selected and assumed as hard exudates. A exudate detection is considered as successful when the detected region overlaps at least 50% of its area.

An unsupervised method for the detection of hard exudates is presented in [Sanchez et al., 2009]. The histogram of the enhanced retinal image is

modelled using a mixture model. From the histogram shape, two heavy tails are distinguished and assumed as foreground area (vessels, optic disc and lesions). The low intensity tail is assumed as representation of dark lesions and haemorrhages, while the high intensity tail includes optic disc and bright lesions. From the high intensity tail optic disc is segmented. The segmentation is performed by using mathematical morphology to select candidate pixels; this selection is then prune by restricting the selection to the pixels in the neighborhood of the main vessels. The main vessels are detected by using a two dimensional vertical oriented filter. The method assumes that the primary four vessels normally emanate near vertically from the optic disc. This assumption limited the performance of this method to the type of retinal images where the optic disc has been captured under the exact conditions to clearly display the four main vessels crossing vertically the optic disc.

Frequently the retinal lesion detection methods begin with a coarse segmentation of exudates candidates reducing the searching area. Later the process is completed by a refine process to define the lesion edges. In [Welfer et al., 2010b] an automatic method designed for the detection of exudates is presented. The method is based in mathematical morphologic and performes in two stages: coarse exudate detection and fine exudate detection. An automatic detection of retinal exudates is proposed in [Fleming et al., 2007]. Exudate candidates are selected by using a multi-scale morphological process. These candidates are then classified based on locally evaluated features to generate a likelihood that each candidate is exudate, drunsen or background.

Supervised methods based on a training process using a set of hand label images are used to perform the retinal lesion analysis. A machine learning based system designed for the detection and differentiation of retinal lesions is presented in [Niemeijer et al., 2007b]. The method starts with a coarse classification considering the probability of a pixel to be part of a lesion. Later this selection is reduced by selecting the pixels with high probability to be a bright lesion, finally they are classified into the different types of bright lesions. An automatic system for the detection of retinal hard exudates is presented in [Garcia et al., 2009]. As a first step luminosity and constrast are normalized in the retinal images and exudate region candidates are segmented. In order to classify the candidate regions a set of features are extracted from them and used as inputs to the neural networks classifer. The algorithm proposes the use of three different NN to compare the performance: multilayer perceptron (MLP), radial basis function (RBF) and support vector machine (SVM).

An automatic identification of exudates besed on computational intelligence is presented in [Osareh et al., 2009]. The retinal images are preprocessed using techniques of colour normalization and contrast enhancement. Later the retinal images are segmented using fuzzy c-means clustering. To separate the segmented regions into exudates and non exudates, a set of features (e.g. colour, size, edge strength, and texture) are extracted. The features are ranked by a genetic algorithm, and the best are selected. Finally the selected feature vectors are classified by a multilayer neural network system.

In [Li Yun et al., 2008] after a contrast enhancement preprocessing a

set of features are extracted from the retinal images. These features are used to classify the image in one of the four different stages of the diabetic retinopathy declared by the method. Classification was achieved using a three layer feedforward neural network. The method classified correctly 8 out of 11 images in the case of moderate retinopathy, 4 of 5 in the case of severe retinopathy and 10 of 12 for proliferative retinopathy.

Figure summarizes the current methods for the analysis of retinal lesions. It can be appreciated that all of these methods are concentrated on the detection of retinal bright lesions, particularly exudates. The work presented in [Niemeijer et al., 2007b] classify the retinal lesions into exudates, wool cotton spots and drunsen, all types of bright lesions.

Due to the high number of pixels in a retinal image that are not part of a lesion, the specificity value is very near to 100% and is not very meaningful. Chapter six analyses in deep this issue in the evaluation of results and proposes the evaluation in term of sensitivity and predictive value. These parameters are meaningful and are frequently used to measure the performance of the retinal detection methods.

2.4 Summary

In this chapter we have reviewed the relevant literature related to the analysis of retinal images. This has included the methods designed for the segmentation of blood vessels and optic disc. Also we reviewed the current methods for the detection of retinal lesions. The contributions and limita-

Retinal lesion methods			
Method	lesion	Num. images	Sensitivity
Boosted soft segmentation [Fang et al., 2010]	He	83(DIARETDB1)	88.54
Mixture model [Sanchez et al., 2009]	He	40	90.2
Fuzzy C-means [Osareh et al., 2009]	Ex	80	90.2
Morphologic reconstruction [Walter et al., 2002]	Ex	15	92.8
Machine learning [Niemeijer et al., 2007b]	Bl	300	95
	Ex		95
	CW		70
	Dr		77
Neural Network classifier [Garcia et al., 2009]			
(MLP)	He	67	88.14
(RBF)	He	67	88.49
(SVM)	He	67	87.61
Morphological operators [Sopharak et al., 2008]	Ex	40	80
Color and sharp edges [Sanchez et al., 2004]	He	20	79.62
Coarse-to-fine strategy [Welfer et al., 2010b]	Ex	47(DIARETDB1)	70.48

Table 2.3: Methods for the analysis of retinal lesions, lesion based criterion. Ex=exudates, He=hard exudates, Bl=bright lesions, CW=cotton wool spots, Dr=drunsen.

tions of the methods in the literature and the needs of the current state of the art have been highlighted.

In the next chapter we present the approach of our research. An overview of the research design is presented. Also the process of capture a retinal image and the features to be considered are explained. Details of the experimental set up and the characteristics of the retinal datasets used in the development of our research are explained.

Chapter 3

The approach

The aim of this research is to create a system to assist the periodical retinal screening process which is highly recommended for patients in risk of conceiving a retinopathy. We have worked for the development of an automatic and unsupervised system capable to perform the analysis on retinal images with different characteristics (e.g. resolution, field of view, etcetera).

In this chapter we present the approach of our research. Firstly an overview of the research design is presented and the Graph cut technique introduced; we include the background theory, the energy function cost formulation and the traditional edge weights assignation. Relevant methods for the analysis of medical images based on the graph cut technique are reviewed.

Next, the process to capture a retinal image is detailed and the retinal datasets used for the development of our research are presented. The particular characteristics of the datasets are highlighted.

Finally, we explain some of the prior work made to carry out experimental work. The work includes hand labelling of retinal images in order to create a ground truth to evaluate the results and quantification of data.

3.1 Graph Cut technique

The design of our research can be divided into three major parts. The first two include the segmentation of retinal structures, such as optic disc and blood vessels. The third part is concern to the detection of retinal lesions.

By detecting the convergence of prior segmented vessels the optic disc centre is localized to proceed with its segmentation. The optic disc is segmented by using to complementary methods. One of them eliminates the vessels prior to the segmentation of the optic disc, while the second incorporates the vessels into the formulation of the method. Finally, the structures are masked out from the retinal image and a background template is created. The template is used to detect the regions that do not match with the general background, and these regions are taken as suspicious lesions places.

The segmentation of retinal structures is based in the minimization of a energy function. This energy function represents the relationship of the elements in the image (pixels) with their neighbourhood, and with prior knowledge of the foreground and background. The use of this technique, known as Graph Cut, permits the incorporation of prior knowledge into the formulation in order to guide the model and find the optimal segmentation. This feature is particularly useful in medical image analysis, where prior

information (e.g. shape) about the object to segment is available.

Graph cut is a widely used technique for interactive image segmentation in computer vision and medical image analysis [Boykov and Jolly, 2000, Chittajallu et al., 2009, Zhu-Jacquot and Zabih, 2008, Boykov and Funka-Lea, 2006, Boykov and Jolly, 2001, Kolmogorov and Boykov, 2005]. Graph cut is a energy based object segmentation technique. Energy based segmentation methods are characterized by the optimization technique designed to minimize the energy function generated from the image data.

Graph cut technique is characterized by the optimization of a cost function defined on a discrete set of variables. The general idea is to map the image onto a graph with weighted connections. The graph is then cut (separating foreground and background), minimizing the energy function and producing the optimal segmentation for the image. The energy function consists of regional (computing likelihoods of foreground and background) and boundary terms (calculated by pixel intensity, texture, color, etc). Discrete graph cut is easy to implement, and is flexible to include various forms of regional, boundary, or geometric constraints.

A graph $G(\nu, \epsilon)$ is defined as a set of nodes ν and edges ϵ connecting neighboring nodes. An example of graph is shown in Figure 3.1. There are two special nodes called terminals, S source (foreground) and T sink (background). Edges between pixels are called n-links, while t-links are referred to the edges connecting pixels to terminals. All graph edges $e \in \epsilon$ including n-links and t-links are assigned some non negative weight (cost). The edge weight assignment depends on different applications scenarios,

but it should ensure that the energy function minimization will produce the optimal segmentation.

In our research we have used different approximations to assign weights to the edges: flux incorporation for blood vessel segmentation [Salazar-Gonzalez et al., 2010] and the traditional boundary and regional terms for the optic disc segmentation [Boykov and Jolly, 2001]. Also, in the course of our experiments we developed an special foreground t-link weight for the specific application of the optic disc segmentation [Salazar-Gonzalez et al., 2011].

A cut is a subset of edges $C \in \epsilon$, that separate the graph into two regions: foreground and background. $G(c) = \langle \nu, \epsilon \backslash C \rangle$. Each cut has a cost which is defined as the sum of the costs of the edges that it severs. A globally minimum cut on a graph with two terminals can be computed efficiently in low order polynomial time via standard maxflow.

In general the process to solve a problem using the energy minimization theory consists of two stages. The first one is to formulate the energy function, which is usually the combination of terms that correspond to different constrains of the problem. In the second stage the energy function is minimized and the graph is separated in two parts, background and foreground.

The constraints imposed by the regional and boundary terms in the set of labels $A = (A_1, ...A_p, ...A_P)$ assigned to each pixel p in the image P are described by the cost function $E(A)$. The energy function consisting of regional (computing likelihoods of foreground and background) and

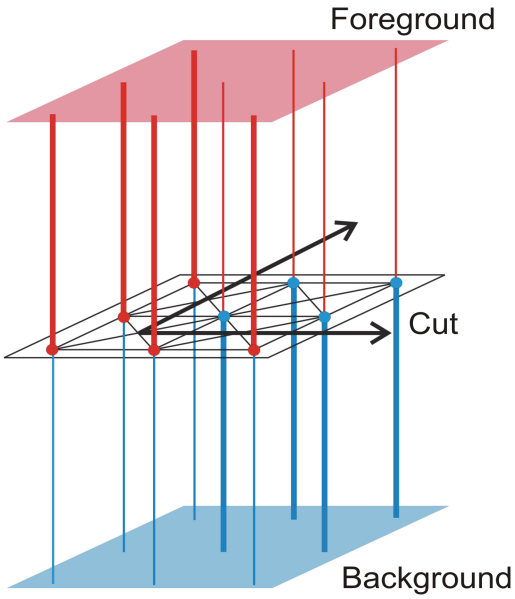

Figure 3.1: Example of a graph, terminals S (foreground) and T (background)

boundary terms (calculated by pixel intensity, texture, color, etc).

$$E(A) = \lambda \cdot R(A) + B(A) \tag{3.1}$$

where

$$R(A) = \sum_{p \in P} R_p(A_p) \tag{3.2}$$

$$B(A) = \sum_{p,q \in N} B_{p,q} \cdot \delta(A_p, Aq) \tag{3.3}$$

and

$$\delta(A_p, Aq) = \begin{cases} 1 & \text{if } A_p \neq Aq \\ 0 & \text{otherwise} \end{cases}$$

$B(A)$ and $R(A)$ represent the boundary and regional constraints. $B_{p,q}$ shows the discontinuity between pixel p and its neighborhood, and generally has a large value when the pixels p and q are similar and close to zero when they are very different. At the same time the value of $B_{p,q}$ will depend on the distance between pixels p and q. Pixels in the immediate neighborhood are considered with more relevance than the ones in the distant neighborhood.

Traditional formulation of the graph cut technique [Boykov and Jolly, 2001] is based in the intensity of the pixels to the describe the discontinuity between p and its neighborhood and calculate $B_{p,q}$. It also sets up the t-links weight by using initialized seeds to calculate the likelihood of the pixel p to belong to the foreground and background models. The graph link weights are traditionally assigned using the Table 3.1.

This function assigns a strong link between pixels with similar intensities, and a weak link if pixels are not very similar between them. Also, this assignment of edge weights considers the distance between pixels $dist(p, q)$. So, in the case of similar intensity discontinuities the distance will be the discriminant factor.

3.1.1 Medical image analysis models based on Graph Cut technique

Graph cut segmentation is based on the minimization of an energy function. This energy function represents the relationship between pixels within an image and is subject to regional and boundary constraints. Graph Cut algorithms use a global cost function to find the optimal segmentation, but

edge	**weight (cost)**	**for**
p, q	$B_{p,q}$	$p, q \in N$
p,S	$\lambda \cdot R_p(\text{“bkg”})$	$p \in P, p \notin (O \cup B)$
	K	$p \in O$
	0	$p \in B$
p,T	$\lambda \cdot R_p(\text{“obj”})$	$p \in P, p \notin (O \cup B)$
	0	$p \in O$
	K	$p \in B$

$$K = 1 + \max_{p \in P} \sum_{q:p,q \in N} B_{p,q}$$

$$B_{p,q} \propto exp(-\frac{(I_p - I_q)^2}{2\sigma^2}) \cdot \frac{1}{dist(p,q)} \tag{3.4}$$

Table 3.1: Traditional edges weight declaration [Boykov and Jolly, 2001].

it is possible to constrain the solution space of the segmentation problem. In the field of medical image segmentation a significant amount of prior knowledge is available and can be used for this purpose.

The segmentation of medical images represents a challenge within the image processing field. The poor contrast between different tissues, the overlapping of structures and the non well defined boundaries are some of the problems to deal with. In general the traditional formulation of the graph cuts technique based only on pixel intensity results in poor segmentation when applied to medical images. So, why is graph cut technique a recurring algorithm used for in the medical images analysis? We can highlights three major reasons:

- Additional constraints. Image segmentation is an ill-posed problem, therefore it is possible there exists more than one acceptable solution. Additional constrains need to be imposed in order to achieve the desired segmentation [Chittajallu et al., 2009]. Graph cut formulation is an excellent option due to its facility to add prior knowledge into the energy function as regional and boundary constraints. Prior shape templates have been successfully added into the graph formulation constraining the solution space of the segmentation problem and generating good segmentation results.

- Interaction or automatic segmentation. Because of the nature of graph cuts formulation it is possible create an interactive system where the user can initialize foreground or background seeds, as well as control parameters in the energy function(e.g. λ). On the other hand if those parameters have been set up and the initialization of seeds is automatic, the technique will result in an automatic segmentation system. The opportunity of being able to select between interactive or automatic system gives the graph cut the flexibility needed in the case of medical images analysis.

- N-D segmentation. Graph cut segmentation is easy to extend to a N dimension images [Boykov and Funka-Lea, 2006].

After the publication of the first work for the interactive segmentation of medical images using graph cuts [Boykov and Jolly, 2000], a great number of proposals using this technique on specific medical structures segmenta-

tion have been published.

Frequently prior shape models are incorporated into the graph cuts formulation as an additional energy term. The first proposal to incorporate prior shape into the graph cuts algorithm is presented in [Freedman and Zhang]. The work proposes a graph cut algorithm for interactive segmentation that incorporates shape priors. In addition to regional and boundary terms, the algorithm uses information about a level set function of a template to define the graph weight links. The method uses a fixed shape template aligned with the image by the user input. The success of this method is limited to when the fixed template and the desired segmentation match under an uncertain threshold.

In [Slabaugh and Unal] the graph cut segmentation is performed using an elliptical shape prior. The method provides a fast solution but it can only be applied when the object to be segmented is similar to an ellipse shape. The method is applied to segment human faces and structures from pelvic magnetic resonance images (e.g. vessels and lymph nodes). The method computes the graph over a set of pixels in a narrow band around the ellipse. When the cut is complete the model is actualized by finding the best ellipse that fit the points of the segmentation. Then, a new graph is constructed within the new narrow band. The method iterates until the solution converges. Later on in [Zhang et al., 2009] a modification of this model is used to perform the segmentation of cervical lymph nodes on sonograms. The ellipse shape constraint is adaptively estimated from previous segmented contours.

The work presented in [Zhu-Jacquot and Zabih, 2008] proposes a graph cut segmentation method for medical images that incorporates statistical shape priors to increase robustness. The method is applied on kidney images that does not present well defined boundaries. Statistical shape information of the region of interest is represented using the mean shape and eigenshapes obtained through PCA analysis of a set of aligned training shapes. EM approach is used to minimize the energy function and alternately update the GMM and shape parameters while fixing the segmentation (M step) and use the GMM and shape prior to facilitate the image segmentation (E step).

Cerebral white matter is segmented from MRI using probabilistic Graph Cuts and geometric shape priors in [Chowdhury et al.]. The edges capacities are calculated according to the probability of pixels to belong to different segmentation classes. Prior shape template is used to generate a subgraph (a graph using just a section of the image). The probabilistic graph cut is first run on the entire graph (e.g. whole image) and then on the constraints based subgraph.

A framework for the automatic segmentation of brain MRI tissues is presented in [Song et al.]. The method uses a graph cut atlas based registration methodology optimized within an iterative model. By registering pre-segmented brain MRI to a canonical atlas space probabilistic prior atlas are generated. The prior shape information is included in the t-link weights.

In [Ababneh and Gurcan, 2010] graph cut technique is used to segment knee bone osteoarthritis images. The method proposes the use of content

based features to achieve segmentation without the need for any user interaction. The method performs a block wise scanning of the image to locate the images blocks with features similar to typical bones features obtained from a training data set. This first detection is used to initialize the seeds and later construct the graph.

An automatic segmentation of the left and right cerebral hemispheres from MRI is described in [Liang et al., 2007]. Prior to the segmentation the image is preprocessed, normalized and the ventricular are filled with high intensity. Using a registered template an approximate segmentation of the three major regions is obtained. Later, the prior segmentation forms are shrinking by using morphological processing and these are used to initialize the seeds for the graph cut algorithm.

Texture features have been added to the traditional graph cut formulation resulting in an improved segmentation. An interactive semi-automatic framework for the segmentation of the ductal network in x-ray breast images is presented in [Nuzhnaya et al.]. The modified graph cut algorithm uses texture analysis to incorporate features of skewness, coarseness, contrast, energy and fractal dimensions.

Graph cut segmentation can easily be extended to a N-D segmentation. In [Boykov and Funka-Lea, 2006] a generalization for the N-D segmentation problem using the graph cuts technique is presented. A 3D semi-automatic graph cut liver segmentation method is presented in [Esneault et al.]. The method is characterized by a graph descriptor of contrast medium injected CT volume. The graph weights are described after a first interactive train-

ing phase.

A graph cut method for the segmentation of the left ventricle is presented in [Lin et al., 2005]. A 4D prior model of the left ventricle is determined using a historically analysis cases. The model is scaled and rotated and a 2D spatial prior is calculated for each image. The spatial prior is then incorporated in the energy function as well as regional and boundary constraints.

The method presented in [Chen and Shapiro, 2008] encodes size constraints as sides constrains into the graph cut for the 3-D segmentation. Global upper and lower bounds on the contour of the object to be segmented are determined by using a training data set.

[Chen and Ruan, 2010] makes use of the graph cut technique to perform the segmentation of MRI brain tumor. The method uses eigenvector characteristics and the dependence between objects to be segmented for the image descriptor. The segmentation is performed in 3-D images using a 2-D geometrical contour model.

A Forearm 3-D graph cut segmentation method is presented in [Furnstahl et al.]. The method incorporates knowledge about intensity, bone shape and local structures into the energy function.

Some methods have adapted the graph cuts formulation to incorporate new constraints. In [Chittajallu et al., 2009] topology priors are incorporated as global constraints. Also, a new way to cut the graph was designed

in order to consider the topology constraints during the process. This model is used in our experiments to compare the segmentation performance in the retinal image.

Fuzzy cut is an innovative adaptation of graph cuts technique designed for the segmentation of medical images. A fuzzy teoretic model is used to incorporate knowledge driven constraints into the MAP-MRF formulation. The segmentation problem is addressed as the maximum a posteriori (MAP) estimation of markov random fields (MRF), which in essence is equivalent to the minimization of the Gibbs energy function. Fuzzy connectivity and fuzzy location priors are used in combination to define the first and second order clique potential of the Gibbs energy function.

3.2 Retinal image capture

Fundus photography is a highly specialized form of medical imaging technique dedicated to capture the retinal for the study and treatment of disorders of the eye. A fundus camera is a low power microscope with an attached camera designed to photograph the interior surface of the eye, including the retina, optic disc, macula, and posterior pole (i.e. the fundus).

The optical design of fundus cameras is based on the principle of monocular indirect ophthalmoscopy [Saine and Tyler, 2002]. A fundus camera provides an upright, magnified view of the fundus of the retina. The observation light is focused via a series of lenses through a doughnut shaped aperture (see Figure 3.2), which then passes through a central aperture,

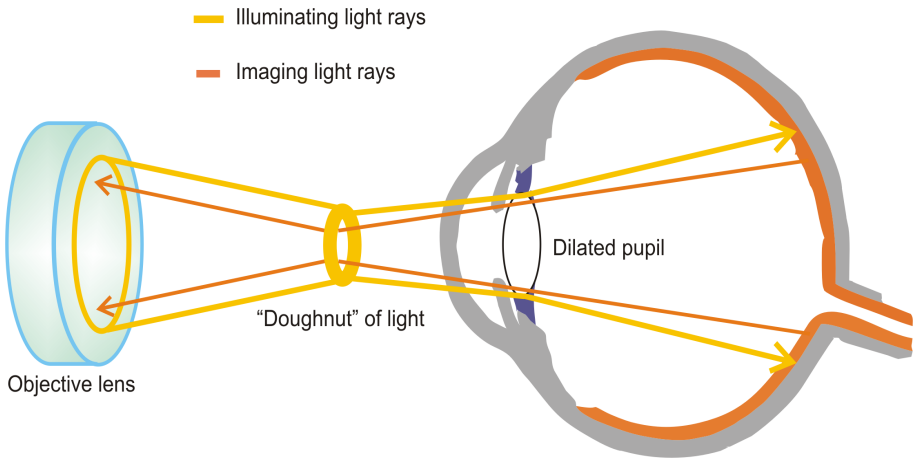

Figure 3.2: Retinal image capture. The "doughnut" light (yellow) pass through the cornea and the image forming rays (orange) passes through the non-illuminated hole in the "doughnut" and is reflected by the mirror to the capturing medium (e.g. film or digital CCD).

before passing through the camera objective lens and through the cornea onto the retina.

The light reflected from the retina passes through the un-illuminated hole in the doughnut formed by the illumination system. As the light paths of the two systems are independent, there are minimal reflections of the light source captured in the formed image. The image forming rays continue towards the low powered telescopic eyepiece. When the button is pressed to take a picture, a mirror interrupts the path of the illumination system allow the light from the flash bulb to pass into the eye. Simultaneously, a mirror falls in front of the observation telescope, which redirects the light onto the capturing medium, whether it is film or a digital CCD (charge-coupled device). Because of the eyes tendency to accommodate while looking though a telescope, it is imperative that the exiting vergence is parallel in order for an in focus image to be formed on the capturing

medium.

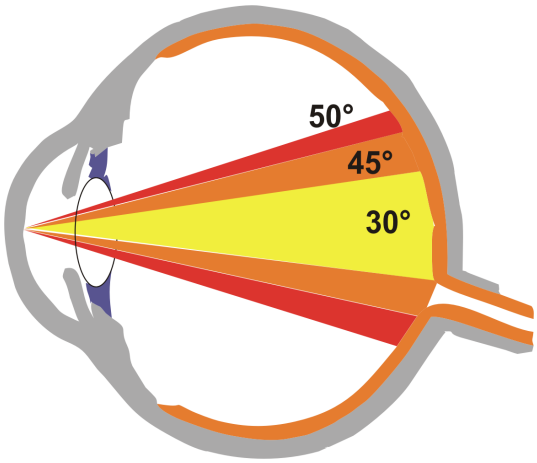

Figure 3.3: Different angles of view for the retinal image capture process (e.g. An angle of 30 creates a film image 2.5 times larger than life.

Fundus cameras are described in terms of the angle of view FOV (field of view). FOV is the optical angle of acceptance of the lens (see Figure 3.3). A typical camera have a FOV between 30 to 50 degrees of retinal area. A retina captured with a 30 of FOV creates a film image 2.5x larger than life. If the image is captured with smaller FOV the magnification will be increased (e.g. FOV = 15, magnification= 5x). The magnification of the captured image can be controlled through zoom or auxiliary lenses. Figure 3.3 shows different angles of view for the retinal image capture process. Representative fundus images taken with different FOV are presented in figure 3.4, the optic disc size can be taken as a reference to compare the magnified view. For a FOV of 30 the optic disc appears bigger in the field of view than for a FOV of 50.

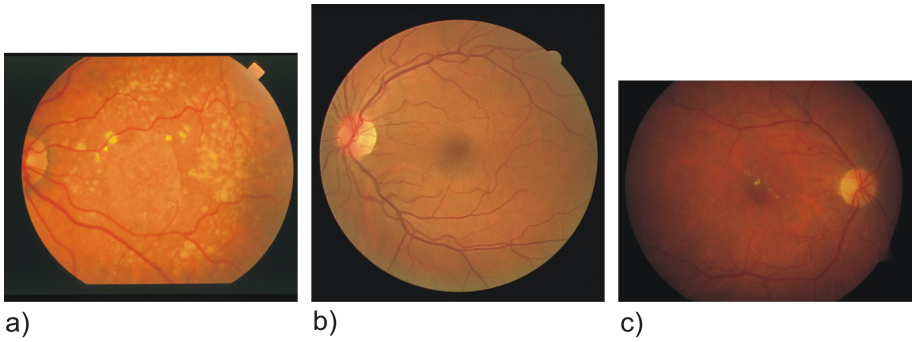

Figure 3.4: Fundus images taken with different angles of view FOV. a) FOV = 35 (STARE dataset), b) FOV = 45 (DRIVE dataset) and c) FOV = 50 (DIARETDB1 dataset)

3.3 Retinal image data sets

Retinal images datasets are important for the development of algorithms and techniques for the analysis of the retina. Retinal datasets are a collection of images that have been selected under a specific criterion. Using a common representative image dataset to evaluate algorithms permits to create a confident comparison between different techniques. In our research we have used three different datasets to evaluate the segmentation results.

3.3.1 DIARETDB1 dataset

DIARETDB1 [Kauppi et al., 2007] is a particular dataset of retinal images created by Tomi Kauppi and his research group. The dataset is compound of 89 colour images of which 84 contain at least one indication of diabetic retinopathy. Images were captured to 50 degree field of view using a digital fundus camera. They have a resolution of 1500×1152 pixels.

The uniqueness of this dataset is the ground truth marking for the

lesions. The images were marked independently by 4 medical experts considering the type of lesions separately. Four type of lesions were considered: hard exudate, soft exudate, red spots and hemorrhages. The experts were instructed to report the confidence of their markings as well. The marking confidence is defined in three levels: Confidence $< 50\%$, Confidence $> 50\%$ and Confidence 100%. These levels represent the certainty of the decision over the mark. The markings of the four experts were combined considering the level of confidence to create a unique ground truth for each image for each type of lesion. So, for each image in the dataset four ground truths are available, one for each type of lesiosn.

The fact that the ground truth was generated independently by each expert avoids the mutual influence on their marking decisions. DIARETDB1 dataset does not include ground truth for the retinal structures (e.g. blood vessels and optic disc). For this reason blood vessel segmentation on DIARETDB1 was unable to be evaluated. And in the case of optic disc segmentation we create the hand labeling on the DIARETDB1 and this was used as ground truth.

3.3.2 DRIVE dataset

DRIVE dataset [Staal et al., 2004] consists of 40 images which were captured from a Canon CR5 non-mydriatic 3CCD camera at 45° field of view (FOV). The images have a size of 768×584 pixels, eight bit per color channel. The dataset includes masks to separate the FOV from the rest of the image. The data set provides blood vessels ground truth. Hand labeled images are available in two sets (set A and set B). The set A offers the

manual labeling for all the images in the dataset, while the set B provides the manual labeling just for half of them.

For the DRIVE dataset, hand labeling set B is taken as a second observer and set A is used as ground truth to evaluate the segmentation results.

3.3.3 STARE dataset

The STARE dataset [Hoover et al., 2000] consists of 20 colour images captured by a TopCon TRV-50 fundus camera at 35° FOV. The size of the images is 700×605 pixeles. This dataset does not include FOV mask. The mask images were created by using a simple threshold for each channel of color, taking the matching results. The STARE dataset provides ground truth for blood vessels. The ground truth is divided in two sets of hand labeled images performed by two observers.

The second hand labeling set in STARE is taken as second observer, while the first set is used as ground truth.

Table 3.2 summarizes the characteristics of the retinal datasets used in the development of this research. It is possible to appreciate that the DIARETDB1 dataset is the only one that provide ground truth of lesions. Unfortunately it does not include hand labelling of retinal structures, such as blood vessels and optic disc. If is required to evaluated a method for the segmentation of the optic disc or blood vessels in this dataset, a hand label of retinal structured must be created.

DATASET	No. Images	Resolution	FOV	Ground truth
DIARETDB1	89	colour 1550×1152	$50°$	Lesions labeled by 4 experts
DRIVE	40	colour 768×584	$45°$	Blood vessels in two different sets
STARE	20	colour 700×605	$35°$	Blood vessels in two different sets

Table 3.2: Characteristics of retinal images datasets.

3.4 Experimental set up

In order to evaluate the segmentation results we have made use of hand segmentation. The hand label of retinal structures is used as ground truth. Table 3.2 illustrates the available ground truths for each one of the public dataset.

Our retinal blood vessels segmentation method was used on the three datasets. The segmentation performance on DRIVE and STARE dataset was evaluated by using the provided ground truth. Unfortunately the evaluation was no possible in the case of DIARETDB1 dataset, because does not exist ground truth of retinal vessels for this dataset.

The experimental work for the optic disc segmentation was performed on DIARETDB1 and DRIVE datasets. These datasets does not provide a hand label of the optic disc that can be used as ground truth. As a consequence we have to create the hand segmentation of the optic disc on these two datasets in order to have a ground truth to evaluate the results.

The method designed for the detection of retinal lesions is evaluated on DIARETDB1. This datasets provides ground truth marks of the retinal lesions in four sets of images, one for each type of lesion. The marks intensity is within the gray level scale. The intensity level represents the confidence of the marking. The confidence level of the markings is very useful for the evaluation of results. The markings are taken as ground truth with different levels of confidence, and the results are evaluated by considering more than one experts opinion.
Unfortunately the confidence level is represented only by gray level intensity, and needs to be quantified in order to provide a meaningful numeric evaluation result. The process of the quantification of confidence is explained in Chapter six.

As part of the experimental work, we have used the topology graph cut technique to perform the segmentation of retinal structures. Because topology cut technique is a modified implementation of the graph cut technique, the comparison of results is meaningful.

Topology cut technique [Zeng et al., 2008] introduces a label attribute for each node to handle the topology constrains, and uses a distant map to keep track of the nodes that are closest to the boundary. The topology cut segmentation was performed on non preprocessed retinal image. Also the initialization of seeds was not automatic and should be marked by hand.

3.5 Summary

In this chapter we have reviewed the approach of the research work. The process of capture a retinal images has been detailed and the retinal datasets used in our research has been described. Also we have mentioned some of the preliminary work made to perform the experimental process. This work includes the hand label of the optic disc, quantification of confidence level for the lesions marks and the hand initialization of seed in retinal images to use the topology cut technique.

We have also introduce the basis technique for the segmentation of retinal structures. Graph cut is an energy function based technique successfully used for the segmentation of structures in medical images. Nevertheless special design of the graph is needed in order to attend the specific characteristics of the object to segment.

Chapter four explains one of the drawbacks of the graph cut technique to segment thin elongated structures, such as blood vessels. It also explains the formulation to overcome this issue.

In Chapter five the graph cut technique is used to segment the retinal optic disc. Two complementary methods were designed. And it will demonstrated the versatility of the graph cut technique to incorporate prior information.

Chapter 4

Blood Vessel Segmentation

4.1 Introduction

Blood vessels can be seen as thin elongated structures in the retina, with variation in width and length, that converge into the optic disc. An accurate segmentation of the blood vessels is the first step to extract features and fundamental information to create a diagnosis, evaluate treatments and keep control of the disease.

Frequently vascular retinal segmentation methods are designed for a specific dataset, or parameters are adjusted to adapt them for different imaging conditions. It is important to have a segmentation algorithm that does not depend on parameter configuration, so the analysis can be unified for images of different datasets.

The segmentation of blood vessels is a fundamental part in the analysis of retinal images. The morphology of blood vessels is an important indicator for diseases like diabetes, hypertension and retinopathy. Blood vessels

can be seen as thin elongated structures in the retina, with variation in width and length (see Figure 4.1). Frequently blood vessels are used to detect other structure in the retina such as optic disc.

Blood vessels and hemorrhage have similar colour features. For the analysis of retinal lesions we masked out the eye structures (blood vessels and optic disc) in order to minimize the false positives lesison detections.

Figure 4.1: left: retina colour images, right: blood vessel network

In this chapter we describe the automatic and unsupervised method designed for the retinal blood vessels segmentation. The method is based on the graph cut technique. The graph is constructed using a prior rough segmentation from a pre-processed image together with spatial pixel connection. In our research we use the segmented blood vessels to detect the center of the optic disc and later on the vessel network is masked out prior to the retinal lesion detection.

Frequently vascular retinal segmentation methods are designed for a specific dataset, or parameters are adjusted to adapt them for different imaging conditions. Some of the methods are based on vessels charac-

teristics such as width, which obviously will depend of the specific characteristics of the dataset (e.g. FOV). Our method performs the blood vessel segmentation without the need of parameters adjusments for differente datasets characteristics. The analysis is unified for images of different datasets.

Our approach takes as a first step the enhancement of blood vessels, followed by a rough segmentation, where prior information together with spatial pixel connection is used to construct the graph to obtain the final segmentation. Firstly we present some examples of the vessel segmentation using the traditional graph weight assignment and explain the need of a special graph formulation for the blood vessel segmentation. Later we explain our method, including prepocessing, prior rough segmentation and graph construction. Finally we present results of our method performing on two public datasets (DRIVE and STARE) and comparison with other methods. Also we applied our method to segment vessel in the DIARETDB1 dataset and we disscuss the results obtained.

4.2 Graph formulation for blood vessels segmentation

The segmentation of blood vessels using the graph cut technique requires special graph formulation. The minimization energy using the boundary term has a tendency to follow short edges, frequently referred to as "the shrinking bias" problem [Vicente et al., 2008]. This problem creates particular difficulties to segment thin elongated structures like the blood vessels.

Figure 4.2 shows the segmentation of blood vessels using the traditional graph formulation. Note that the segmentation follows short edges, and tends to "shrink" in the searching for the cheapest cost.

To improve the segmentation the image can be limited to a smaller area, this will reduce the searching field. Also from the energy function $E(A) = \lambda \cdot R(A) + B(A)$ it can be observed that λ controls the relation between boundary and regional terms. If λ is increased, the likelihood of the pixels belonging to foreground and background (t-links) gains strength over the regional term (n-links) and the segmentation will improve (Figure 4.2).

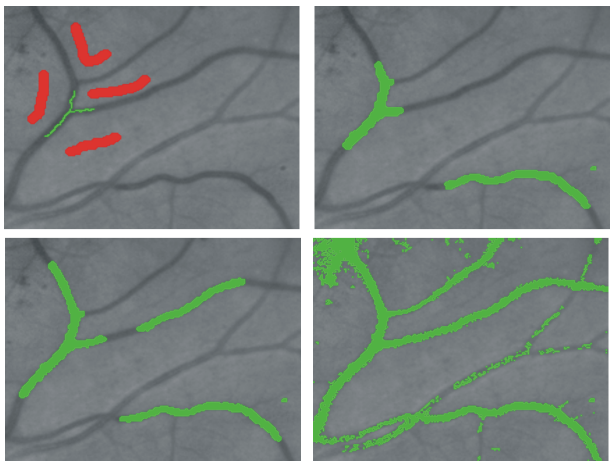

Figure 4.2: Blood vessel segmentation using the traditional graph formulation with different λ values. a) seeds initialization, b) $\lambda = 20$, c) $\lambda = 50$ and d) $\lambda = 100$

For the reason explained above, it is necessary to create an special graph formulation to perform the blood vessel segmentation. One of the proposals to overcome the shrinking bias problem is to impose an additional connectivity prior, where the user marks the constrain connectivities [Vicente et al., 2008]. We follow the approach presented in [Kolmogorov

and Boykov, 2005], which addresses the shrinking problem by adding the mechanism of flux into the construction of the graph. It has been demonstrated that the flux of any given field of vector **v** can be optimized in order to improve the segmentation of elongated narrowing structures, like vessels [Vasilevskiy and Siddiqi, 2002] and [Kolmogorov and Boykov, 2005]. The incorporation of flux can improve edge alignment and help to segment thin objects such as blood vessels by keeping a balance between shrinking (length) and stretching (flux) along the boundary.

In our implementation image gradients of rough blood vessels segmentation are taken as vectors $\boldsymbol{v}$, and the flux of these vectors is incorporated into the graph and optimized.

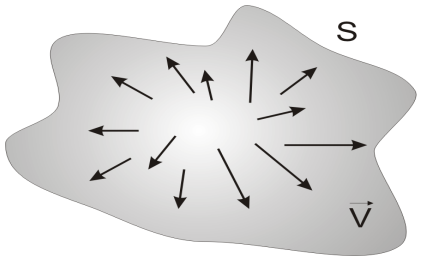

Figure 4.3: Flux of vectors $\vec{V}$ passing through surface S.

In our implementation the flow is described in terms of local image gradients. The spreading effect is equilibrated with the shrinking effect of the minimization energy using the boundary term. The main idea is to incorporate both parts of the vectors in the field, magnitude and direction.

Finsler metric, a class of continuous metric, can be approximated by discrete cut metric on regular grids. Finsler length can be represented by the

sum of two terms, which represent the symmetric and antisymmetric parts of the cut metric. The symmetric part of the cut provides the standard length of contour independently of its orientation, while the antisymmetric part of the cut metric is considered the flux of a given vector field through the contour [Kolmogorov and Boykov, 2005]. Both parts of the cut metric are calculated and used to construct the graph. Finally the graph is cut and the optimal segmentation is found.

4.3 Method

Our implementation can be divided into two main stages: preprocessing and graph construction. Figure 4.4 shows an overview of the method, which is described with detail next.

4.3.1 Preprocessing

The use of green channel for retinal image analysis has been considered in previous works [Staal et al., 2004, Hoover et al., 2000, Jiang and Mojon, 2003] due to its high contrast between blood vessel and retinal background. In the preprocessing stage the green channel is separated from the RGB retinal color image, this image is used to construct the symmetric part of the graph.

Similar to [Wu et al., 2006], we apply a contrast enhancement process to the green channel image. The intensity of the image is inverted, and the illumination is equalizated. The resulting image is enhanced using an

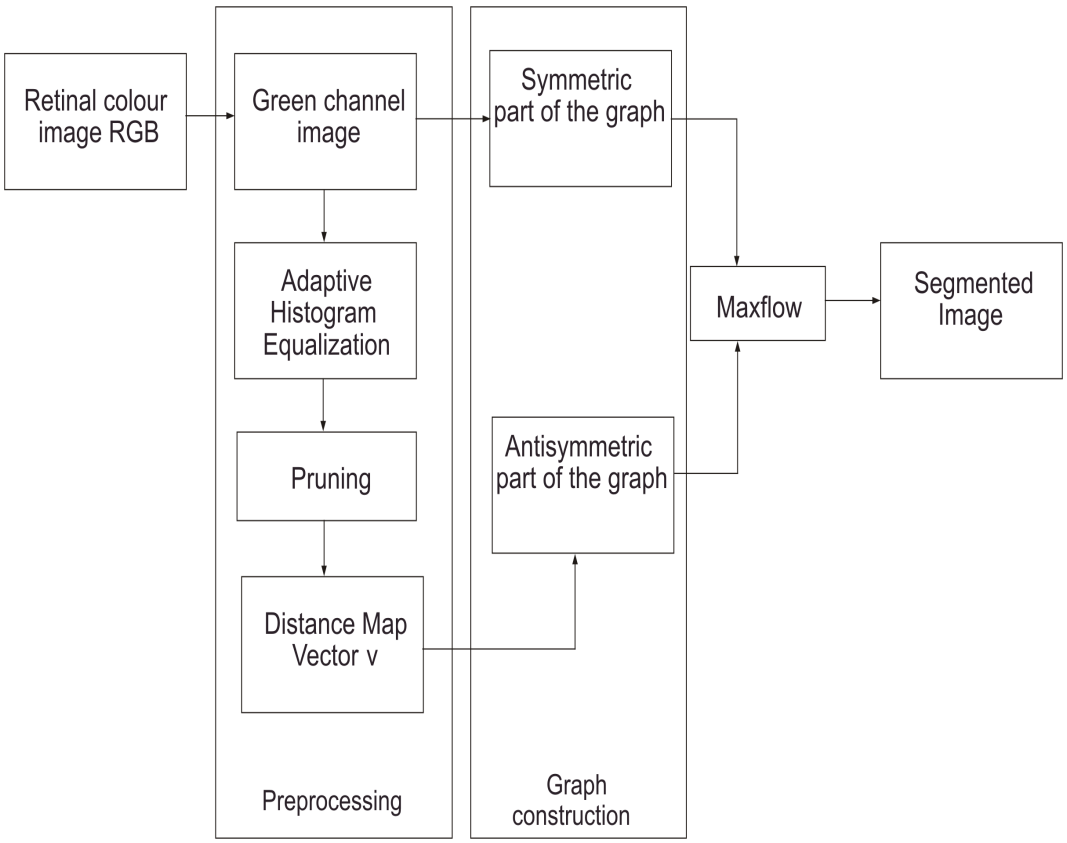

Figure 4.4: Blood vessel segmentation algorithm scheme

adaptive histogram equalization process:

$$I_{Enhanced} = \left(\sum_{p' \in R(p)} \frac{s\left(I_2\left(p\right) - I_2\left(p'\right)\right)}{h^2} \right)^r \cdot M \tag{4.1}$$

where I_2 is the green channel of the retinal colour image, $s(d) = 1\ if\ d > 0$ and $s(d) = 0$ otherwise, $M = 255$, p denotes the pixel and $p's$ is the pixel neighborhood specified by a square window with width h. Increasing r would also increase the contrast between vessel pixels and the background. Figure 4.5 shows some examples of the retinal images preprocessed using different values for h and r. It is possible to appreciate the blood vessels enhancement effect on the retinal images.

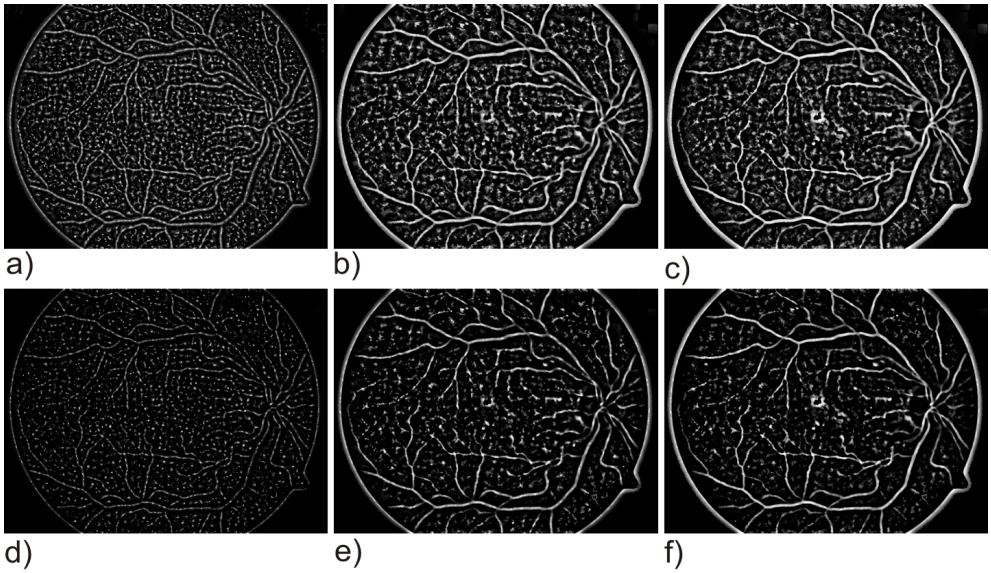

Figure 4.5: Pre-proceced retinal images using AHE. a) $h = 15$, $r = 3$, b) $h = 45$, $r = 3$, c) $h = 81$, $r = 3$, d) $h = 15$, $r = 6$, e) $h = 45$, $r = 6$, f) $h = 81$, $r = 6$

After experimental work the window was set up to $h = 81$ and $r = 6$. Figure 4.6 shows the resultant image after the enhancement process.

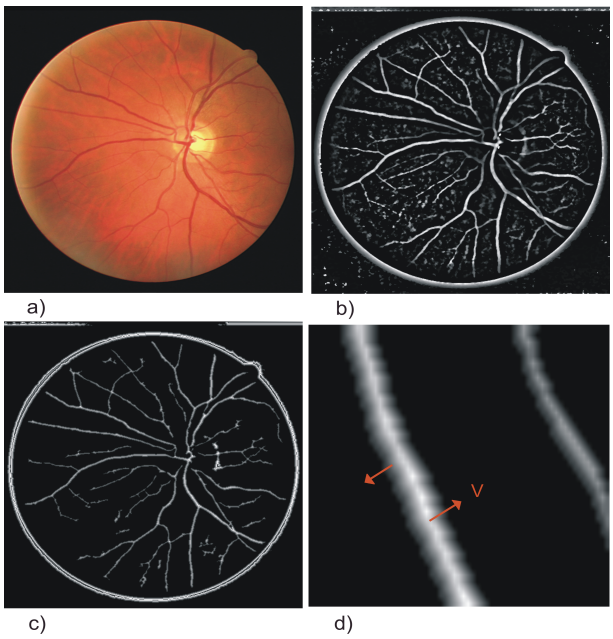

Figure 4.6: Retinal images preprocessing. (a) input image, (b) enhanced image, (c) distance map, (d) a sample of a vessel into the distance map

After the application of the AHE blood vessels are enhanced as well as other individual structures. These individual structures correspond to other retinal elements which morphology do not match with the background (e.g. retinal lesions). These blobs of pixels are not attached to the blood vessels because they are not part of them.

In experimental trial the independent blobs of pixels were classified in two groups. The first one included the blob with largest number of elements (blood vessel network). The second group included the rest of independent blobs (structures not attached to blood vessel network).

The pruning stage is designed to eliminate the blobs of pixels detached

from the vessel network. We apply a binary morphological open process, eliminating the groups of pixel with fewer than a certain number of elements E. Based on the analysis of the second groups (in the experimental trial) the maximum number of pixels for an independent blob that is not attached to the vessel network, was set to 200 ($E = 200$) pixels including a safety margin.

At this stage it is important to reduce the false positives to minimum, because this information will be used to construct the graph connections. Figure 4.6 shows the enhanced image after prunning. From the pruned image, we create a distance map by applying the distance transform. This image is used to calculate the direction and magnitude of the vector $\mathbf{v}$ for the blood vessel pixels. Figure 4.6 shows the distance map for the whole image and for a sample vessel, where we can see the center line as the brightest pixels and reduction in intensity to the direction of the edges (image gradients). This vector field is used to construct the antisymmetric part of the graph.

It is possible to appreciate the flux definition with more detail in the augmentated vessel showed in Figure 4.7. The vectors are defined from the vessel pixels to the nearest edge. Vectors in the center line have higher magnitude than the ones near to the vessel edges. Each vector have two components, one in each cartesian axe, X and Y. The flow of these vector will guide the segmentation and prevent "the shrinking bias" problem.

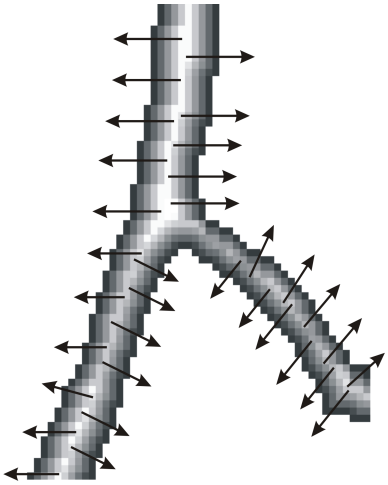

Figure 4.7: Distant map of vessel segment with the flux from the center line

4.3.2 Graph construction

Here we detail the construction of the graph based in [Kolmogorov and Boykov, 2005]. The graph construction can be divided in two parts: the symmetric and antisymmetric parts. The symmetric part g^+ corresponds to cut geometric length and is related directly with the n-link connections. The antisymmetric part g^- corresponds to a flux of vector field v over a cut and is used to define the t-links.

Symmetric part

The neighbor system can be described as a set of edges e_k, where $1 \leq k \leq N$, for N number of neighbors. e_k is the shortest vector connecting two pixels in the direction k. $W_k^+(p)$ is the weight of the edge e_k at pixel p. $\tilde{W}_k^+(p)$ is the set of the edge weights at pixel p for all directions. The corresponding edge weights are defined according to:

$$\omega^+ = \frac{1}{2} D g^+ \tag{4.2}$$

where D is a N x N matrix with entries

$$D_{ii} = -\frac{sin(\alpha_{i+1} - \alpha_{i-1})}{sin(\alpha_{i+1} - \alpha_i) sin(\alpha_i - \alpha_{i-1})} \tag{4.3}$$

$$\mathrm{D}_{ij} = \frac{1}{|sin(\alpha_j - \alpha_i)|} \quad if\ j - 1 = \pm 1\ mod\ N$$

$$\mathrm{D}_{ij} = 0\ for\ all\ others\ entries$$

where α_k is the angle of the edge e_k with respect to the positive axis X.

We consider a grid map of 16 neighbors with edges $e_k, k = 1, 2, ..., 16$ (see Figure 4.8). For each pixel p in the green channel image, the edge weight $\widetilde{W}_k^+(p)$ is computed according to formula (2). g^+ is calculated using the pixel intensity difference between the two nodes.

$$g^+ = K \cdot exp\left(\frac{-(I_p - I_q)^2}{\sigma^2}\right) \tag{4.4}$$

This function has a high value for pixels of similar intensities, when $I_p - I_q < \sigma$. But if the pixels are very different $I_p - I_q > \sigma$ the value is small, which represents a poor relation between the pixels, suggesting they belong to different terminals [Boykov and Funka-Lea, 2006].

$$\mathrm{D} = \begin{bmatrix}
4.828 & 2.613 & 0 & 0 & 0 & 0 & 0 & 0 & 0 & 0 & 0 & 0 & 0 & 0 & 0 & 0 \\
2.613 & 4.828 & 2.613 & 0 & 0 & 0 & 0 & 0 & 0 & 0 & 0 & 0 & 0 & 0 & 0 & 0 \\
0 & 2.613 & 4.828 & 2.613 & 0 & 0 & 0 & 0 & 0 & 0 & 0 & 0 & 0 & 0 & 0 & 0 \\
0 & 0 & 2.613 & 4.828 & 2.613 & 0 & 0 & 0 & 0 & 0 & 0 & 0 & 0 & 0 & 0 & 0 \\
0 & 0 & 0 & 2.613 & 4.828 & 2.613 & 0 & 0 & 0 & 0 & 0 & 0 & 0 & 0 & 0 & 0 \\
0 & 0 & 0 & 0 & 2.613 & 4.828 & 2.613 & 0 & 0 & 0 & 0 & 0 & 0 & 0 & 0 & 0 \\
0 & 0 & 0 & 0 & 0 & 2.613 & 4.828 & 2.613 & 0 & 0 & 0 & 0 & 0 & 0 & 0 & 0 \\
0 & 0 & 0 & 0 & 0 & 0 & 2.613 & 4.828 & 2.613 & 0 & 0 & 0 & 0 & 0 & 0 & 0 \\
0 & 0 & 0 & 0 & 0 & 0 & 0 & 2.613 & 4.828 & 2.613 & 0 & 0 & 0 & 0 & 0 & 0 \\
0 & 0 & 0 & 0 & 0 & 0 & 0 & 0 & 2.613 & 4.828 & 2.613 & 0 & 0 & 0 & 0 & 0 \\
0 & 0 & 0 & 0 & 0 & 0 & 0 & 0 & 0 & 2.613 & 4.828 & 2.613 & 0 & 0 & 0 & 0 \\
0 & 0 & 0 & 0 & 0 & 0 & 0 & 0 & 0 & 0 & 2.613 & 4.828 & 2.613 & 0 & 0 & 0 \\
0 & 0 & 0 & 0 & 0 & 0 & 0 & 0 & 0 & 0 & 0 & 2.613 & 4.828 & 2.613 & 0 & 0 \\
0 & 0 & 0 & 0 & 0 & 0 & 0 & 0 & 0 & 0 & 0 & 0 & 2.613 & 4.828 & 2.613 & 0 \\
0 & 0 & 0 & 0 & 0 & 0 & 0 & 0 & 0 & 0 & 0 & 0 & 0 & 2.613 & 4.828 & 2.613 \\
0 & 0 & 0 & 0 & 0 & 0 & 0 & 0 & 0 & 0 & 0 & 0 & 0 & 0 & 2.613 & 4.828
\end{bmatrix}$$

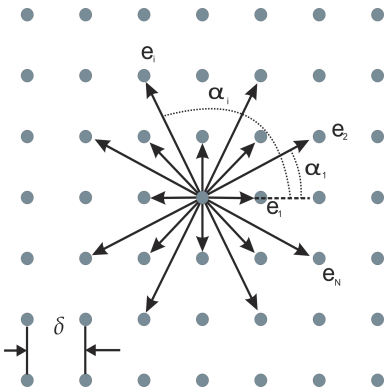

Figure 4.8: Neighborhood system for a grid in the graph for blood vessel segmentation.

Matrix D for a 16 neighborhood system.

Antisymmetric part

The antisymmetric part corresponds to a flux of vector field **v** over a cut. Specific weights for t-links are based on the decomposition of vector **v**. Different decompositions may result in different t-links whose weights can be interpreted as an estimation of divergence. We consider a decomposition along grid edges using a natural choice of n-links oriented along the main axes, X and Y. This decomposition leads to t-link weights as

$$t_p = \frac{\delta^2}{2} \cdot (Vx + Vy) \tag{4.5}$$

where Vx and Vy are the components of vector **v**, and δ is the size of the cell in the grid map. This is a particular scheme for computing divergence of vector **v**. We add edge $(s \rightarrow p)$ with weight $C * (-tp)$ if $tp < 0$, or edge $(p \rightarrow t)$ with weight $C * tp$ otherwise. The parameter C is related to the magnitude of the vector **v**, thus pixels in the center of the blood vessel have a higher connection to the source (foreground) than pixels in

the edge of the blood vessels. Because the distance map is calculated on the pruned image, vector **v** is defined just for the pixels detected as blood vessels in the rough segmentation. The initialization of t-link weights for the rest of the pixel is set as $(p \rightarrow s)$ with weight $t = 0$ and $(p \rightarrow t)$ with weight $t = K$, where K is the maximum weight sum for a pixel in the symmetric construction. Figure 4.9 shows the segmentation of blood vessels using different decompositions of the vector **v**, generating different t-link weights. The maxflow-v3.01 implemented by Komolgorov [1] is used in our implementation to compute the graph cut and find the final segmentation.

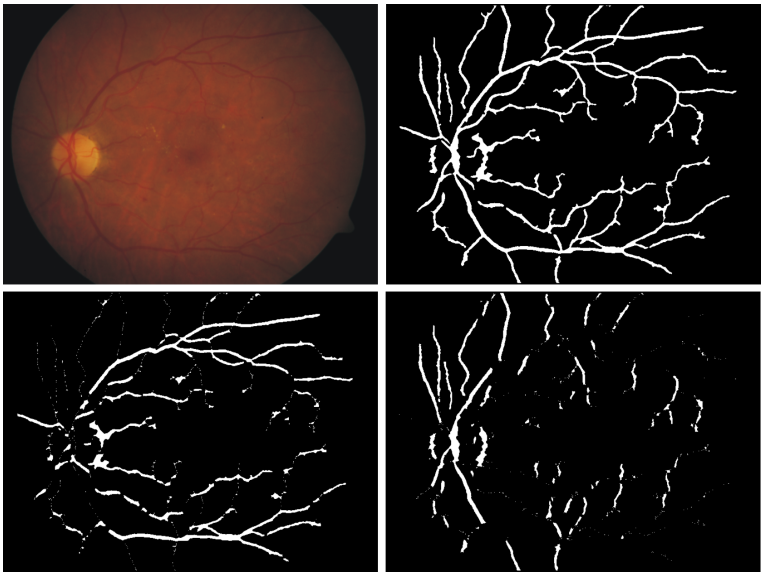

Figure 4.9: Top row: retinal image and blood vessel segmentation using decomposition of vector **v** along the main axes, X and Y. Bottom row: blood vessel segmentation using horizontal and vertical decomposition of the vector **v**.

[1] maxflow-v3.01 is available at
http://www.cs.ucl.ac.uk/staff/V.Kolmogorov/software.html.

4.4 Experiments and Results

Our method was tested on the three public datasets, the DRIVE [Staal et al., 2004], the STARE [Hoover et al., 2000] and the DIARETDB1 [Kauppi et al., 2007], with a total of 149 images. Unfortunately only DRIVE and STARE datasets include blood vessel ground truth to evaluate the segmentation quantitatively. Nevertheless, we have included some segmentation result images for the DIARETDB1 dataset.

The performance of segmentation is measured by true positive rate, false positive rate and accuracy rate. These meassurement parameters are defined as:

$$TPR = \frac{Tp}{GT_{vessel\,pixels}}$$

$$FPR = \frac{Fp}{GT_{Non\,vessel\,pixels}}$$

$$Accuracy = \frac{Tp\ +\ Tn}{Image_{pixels}}$$

where Tp, Fp and Tn are the number of true positives, false positives and true negatives respectively. $Image_{pixels}$ is the total number of pixel in the image. And GT is the ground truth image where the number of pixels marked as vessels $GT_{vessel\,pixels}$ and non vessels $GT_{Non\,vessel\,pixels}$ can be determined. Figures 4.10 and 4.11 show the segmented images and the manually labeled images for the DRIVE and the STARE datasets respectively. While Figure 4.12 shows some segmentated images on the

DIARETDB1 dataset.

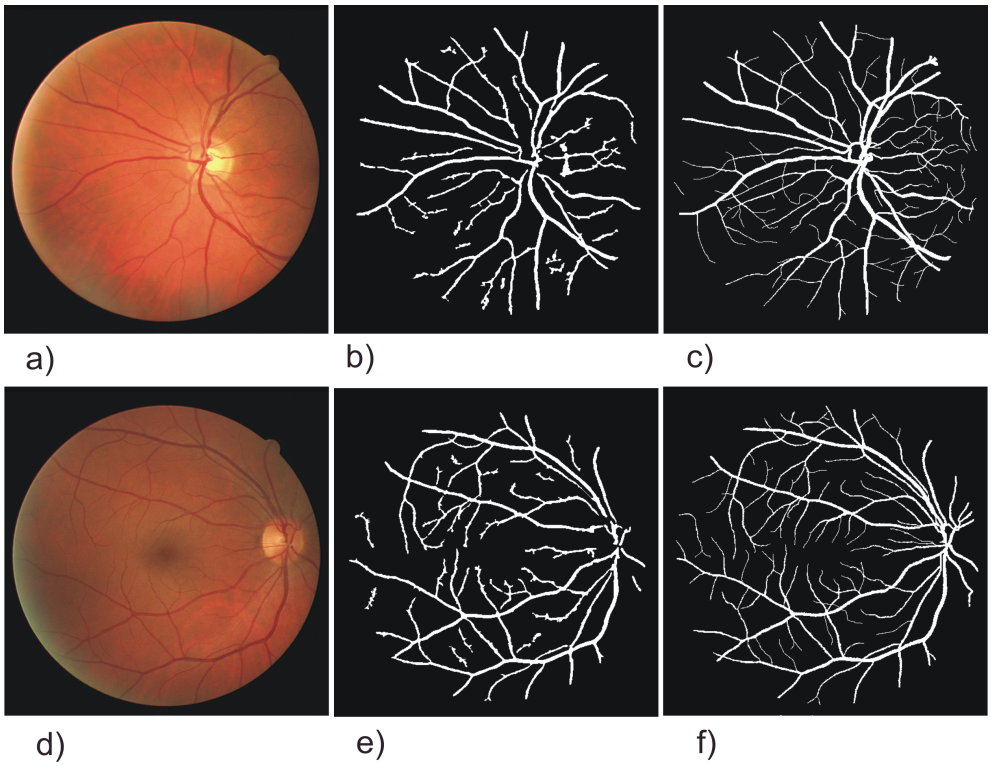

Figure 4.10: Blood vessel segmentation in the DRIVE dataset: a) and d) retinal images, b) and e) our segmentation results, and c) and f) manually labeled results.

For the two sample images presented in Figure 4.10 the segmentation evaluation reported $TPR = 0.6962$ and $TPR = 0.6716$ respectively; and $FPR = 0.0236$ and $FPR = 0.0208$. The accuracy reported was $Accuracy = 0.9518$ and $Accuracy = 0.9487$.

For the case of STARE sample images in Figure 4.11, the segmentation evaluation reported $TPR = 0.7315$ and $TPR = 0.7208$ respectively; and $FPR = 0.0434$ and $FPR = 0.0273$. The accuracy reported

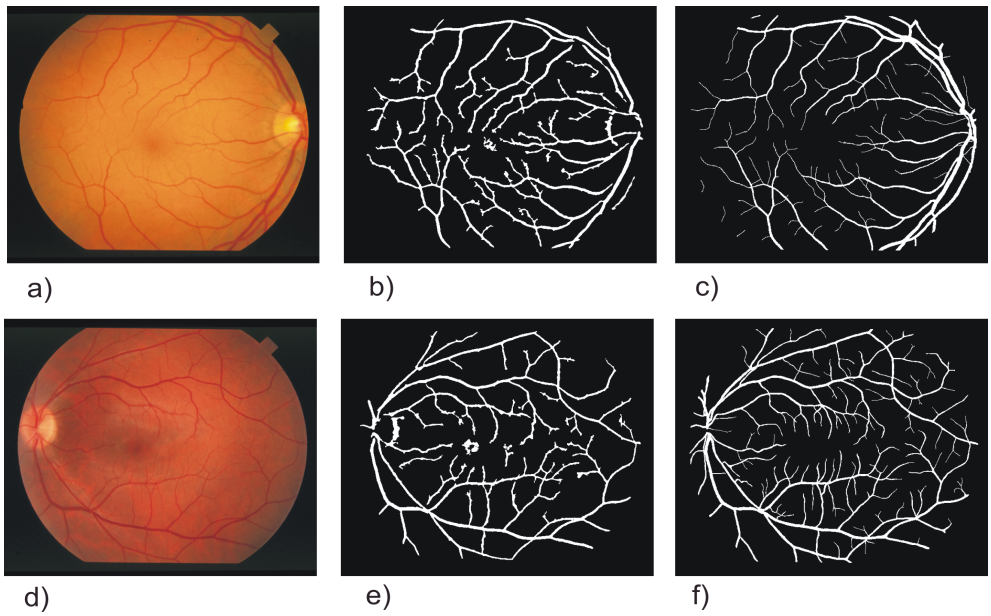

Figure 4.11: Blood vessel segmentation in the STARE dataset: a) and d) retinal images, b) and e) our segmentation results, and c) and f) manually labeled results.

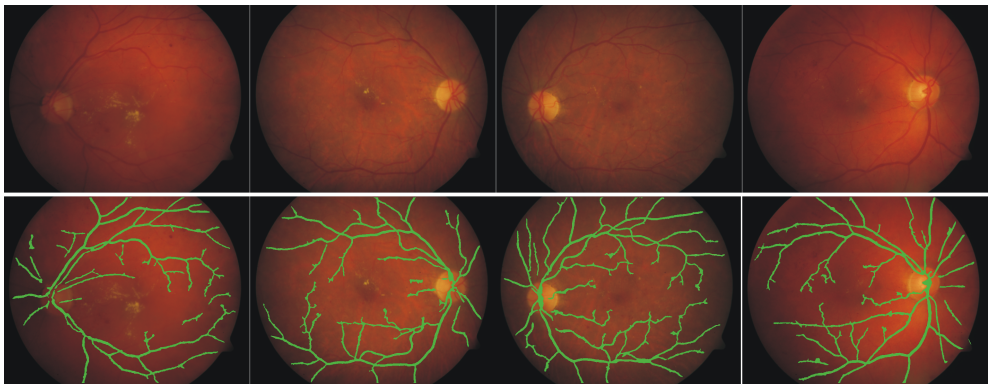

Figure 4.12: Blood vessel segmentation in the DIARETDB1 dataset. Top row: retinal colour images. Bottom row: Blood vessel segmentation on retinal images.

was $Accuracy = 0.9389$ and $Accuracy = 0.9502$.

The segmentation measure between two manual labellings for a same image establishes a reference to compare the average performance of other methods. For the DRIVE dataset set B is taken as a second observer. Segmentation in B is measured taking the manually labeled set A as a reference. At the same time the segmentation of the second observer in STARE is measured taking the first observer as a reference.

Tables 4.1 and 4.2 show the average performance of our method on the STARE and DRIVE datasets with a comparison to the results in Staal [Staal et al., 2004],Mendonca [Mendonca and Campilho, 2006], Martinez [Martinez-Perez et al., 2007] and Usman [Usman Akram et al., 2009]. We have also included the human observer rates. All the measured results used the same set as a reference, set A for DRIVE and first observer for STARE.

Method	TPR	FPR	Accuracy
Second human observer [Martinez-Perez et al., 2007]	0.8951	0.0438	0.9522
Hoover[Mendonca and Campilho, 2006]	0.6751	0.0433	0.9267
Staal[Staal et al., 2004]	0.6970	0.0190	0.9541
Mendonca[Mendonca and Campilho, 2006]	0.6996	0.0270	0.9440
Martinez[Martinez-Perez et al., 2007]	0.7506	0.0431	0.9410
Graph Cut	0.7197	0.0335	0.9479

Table 4.1: Performance comparison of the blood vessel segmentation on the STARE dataset.

The results show a TPR of 89.51% (STARE) and 77.6% (DRIVE) for the second observer segmentation. Most of the methods use the whole image to measure the performance. In [Staal et al., 2004] all the experiments are done on the FOV without considering the performance in the dark area

outside the FOV. The method in [Mendonca and Campilho, 2006] measures the performance on both the whole image and the FOV. The dark background outside the FOV in the retinal image is easy to segment. It is obvious an advantage in measuring the true negatives pixels when the whole image is considered. We have calculated the percentage of pixels outside the FOV in the images for the two datasets, which represents approximately the 25% of the pixels in the whole image. However, it does not affect all the measurement metrics, only where the true negative value is involved (e.g. Accuracy rate). On the other hand, most of the methods utilize the whole image for the performance measures, making the comparion fair. Considering the accuracy rate our method has the best performance on the DRIVE dataset. On STARE the TPR shows that the graph cut outperformance over other approaches, including some of the supervised methods.

Any pathology presence in an image may obscure and confuse the blood vessel appearance, making it difficult to segment. Table 4.3 presents the results of normal cases (10 images) and abnormal cases (10 images) separately. Our graph cut method presents the best TPR values for normal and abnormal images.

Method	TPR	FPR	Accuracy
Human observer B[Martinez-Perez et al., 2007]	0.7760	0.0275	0.9473
Staal[Staal et al., 2004]	0.6780	0.0170	0.9441
Mendonca[Mendonca and Campilho, 2006]	0.7344	0.0236	0.9452
Martinez[Martinez-Perez et al., 2007]	0.7246	0.0345	0.9344
Usman[Usman Akram et al., 2009]	-	-	0.9469
Graph Cut	0.6782	0.0271	0.9478

Table 4.2: Performance comparison of the blood vessel segmentation on the DRIVE dataset.

Normal cases			
Method	**TPR**	**FPR**	**Accuracy**
Mendonca[Mendonca and Campilho, 2006]	0.7258	0.0209	0.9492
Hoover[Mendonca and Campilho, 2006]	0.6766	0.0338	0.9324
Graph Cut	0.7417	0.0359	0.9471
Abnormal cases			
Method	**TPR**	**FPR**	**Accuracy**
Mendonca[Mendonca and Campilho, 2006]	0.6733	0.0331	0.9388
Hoover[Mendonca and Campilho, 2006]	0.6736	0.0528	0.9211
Graph Cut	0.6978	0.0311	0.9487

Table 4.3: Performance comparison of the blood vessel segmentation on the STARE dataset, normal versus abnormal cases

Unsupervised methods have also been reported in previous studies such as [Cai and Chung, 2006]. An experimental comparison between supervised and unsupervised methods is presented in [Cai and Chung, 2006]. These results, combined with ours, are shown in Figure 4.13 in the form of receiver operating characteristic (ROC) curves. ROC curve is a graphical plot of the TPR versus FPR for a binary classifier, where its discrimination threshold is varied producing different TPR for different FPR. We compute different TPRs by changing the initialization of the weight edges for the pixels with the terminals S (foreground) and T (background). The performance of the second observer B has been marked into the graphic as a reference as well.

These results show that our algorithm outperforms the unsupervised method presented in [Cai and Chung, 2006]. The supervised methods perform slightly better but at cost of an extra, and potentially intensive, training process.

Blood vessel segmentation is an important process in the analysis of reti-

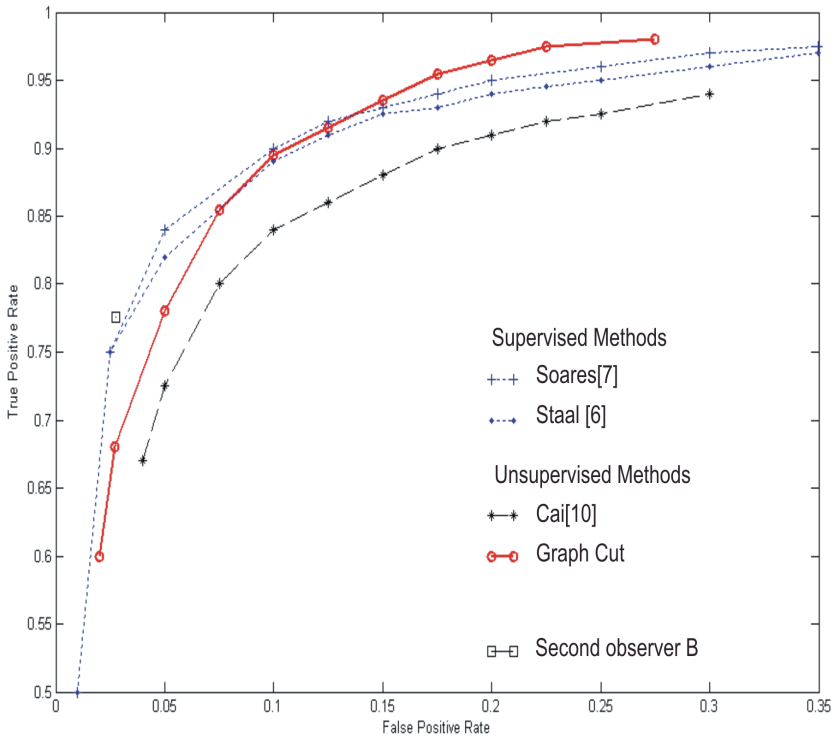

Figure 4.13: ROC curve for the blood vessel segmentation performance for supervised and unsupervised methods in DRIVE dataset

nal images. Integrating the mechanism of flux into the graph cut method provides a good balance between flux stretching and length shrinking along the boundary. Our method does not require ad hoc tuning of parameters on different datasets. Experimental results on the DRIVE and STARE datasets show that out method outperforms other unsupervised methods and is comparable to the supervised methods in the previous studies.

4.5 Summary

In this chapter our method for the segmentation of retinal blood vessels has been presented. The method takes as a first step the creation of a rough segmentation of vessels by applying AHE and pruning the resultant image. Next a distance map is created and the gradient from the centre pixels is taken as flux. This and the spatial pixel connections are used to construct the graph. Finally the graph is cut by minimizing the energy function and the optimal segmentation is found.

Our method has been tested on three different datasets (STARE, DRIVE and DIARETDB1). Quantitative evaluation of results has been presented for STARE and DRIVE datasets. The comparison with other methods results has demonstrated the outperformance of our method.

Chapter five is dedicated to the segmentation of the optic disc. The segmentation of overlapping tissues (optic disc and blood vessels) in the medical imaging field is explored. Two complementary methods have been designed and implemented.

Finally Chapter six presents the consolidation of our research by utilizing the segmented retinal structures to create a background template. This template is the used to detect any suspicious area within the retinal image.

Chapter 5

Optic Disc Segmentation

5.1 Introduction

The optic disc appears as the brightest round object in the fundus retinal images, see Figure 5.1. The structure of the optic disc is an important part of the eye screening test. Eye screening is based on a group of tests which include evaluation of the intraocular pressure, optic disc morphology and visual field. The tests should be safe for the patients. The analysis of fundus images represents a non invasive method to determine the optic disc condition.

The segmentation of the optic disc can be used to determine its morphologic. In addition, it will make possible to discriminate the optic disc from the searching area for retinal lesion.

In this chapter we present two methods for the automatic segmentation of the optic disc. Firstly the process to localize the optic disc is explained. Next we discuss the segmentation of overlapping tissues (blood vessels and

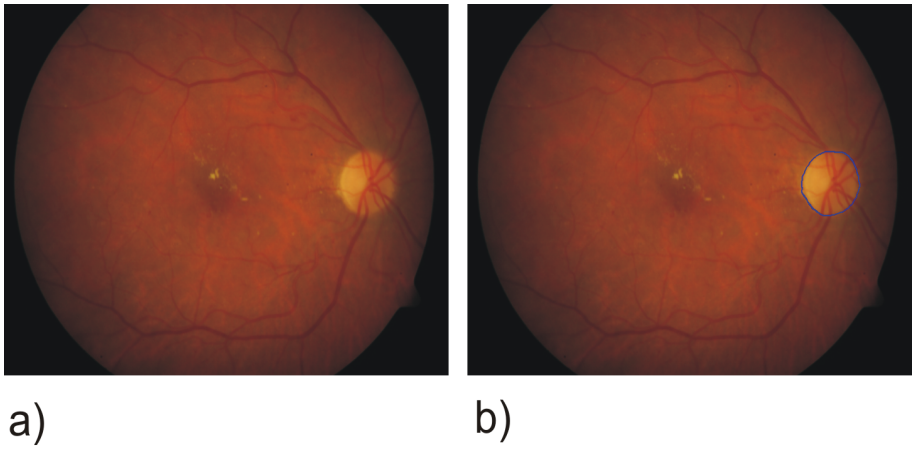

Figure 5.1: Retinal optic disc. a) retinal image, b) retinal optic disc hand labeled segmented.

optic disc) by reviewing the blood vessels role in the segmentation of the optic disc. In this section we explain the need of explore two different methods. Next, the methods are explained with detail. Finally we present the evaluation of results when the methods are tested on two public datasets.

5.2 Optic Disc Localization

Inspired by the work presented in [Welfer et al., 2010a] we use the segmented vessel network to localize the optic disc. The binary image is pruned by using a morphologic open process in order to keep the main arcade. Afterwards the centroid of the arcade is located using the following formulation:

$$C_x = \sum_{i=1}^{K} \frac{x_i}{K} \qquad C_y = \sum_{i=1}^{K} \frac{y_i}{K} \tag{5.1}$$

where x_i and y_i are the coordinates of the pixel in the binary image and K is the number of pixels set to "1", which is the pixels marked as blood vessels in the binary image.

Using the gray intensity of the retinal image, 1% of the brigthest pixels are selected. The algorithm detects the brightest area with the most number of elements in the image to determine the position of the optic disc with respect to the centroid (left, right, up, down, etcetera). Considering that the main arcade is narrowing until the vessels converge, the algorithm adjusts the centroid point iteratively until it reaches the center of the arcade.

The centroid point is then adjusted by reducing the distance with the optic disc, and correcting its central position inside the arcade. The center of the arcade is presumed to be the vessels convergence point and the center of the optic disc. Figure 5.2 shows an example of the localization process of the optic disc center. It is important to detect with accuracy a point inside of the optic disc, since this point will be used to automatically mark foreground seeds. A point just inside the border of the optic disc may result in some false foreground seeds.

We constrain the image to a small area in order to minimize the processing time. The region of interest (ROI) is constrained to a square of 200 by 200 pixels concentric with the detected optic disc center. We have selected an automatic initialization of seeds (foreground and background) for the graph. A neighborhood of 20 pixels of radius around the centre of the optic disc is marked as foreground pixels, while a band of pixels around the

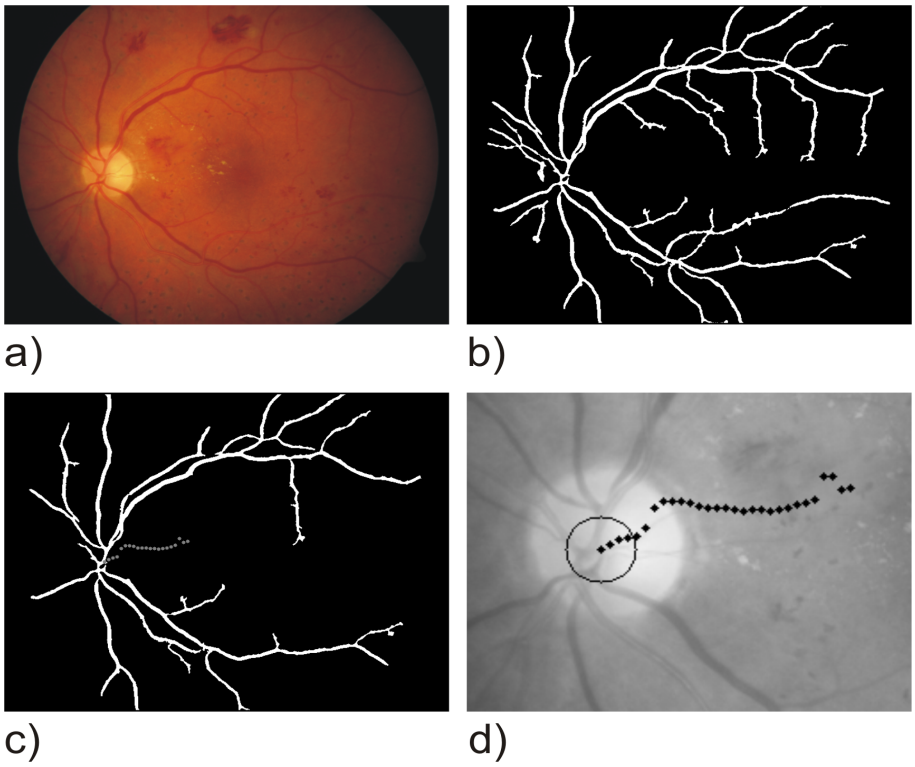

Figure 5.2: Optic disc localization. a) retinal image, b) blood vessel segmentation, c) blood vessel segmentation after pruning and d) sequence of points from the centroid to the vessels convergence.

perimeter of the image are considered as background seeds(see Figure 5.3).

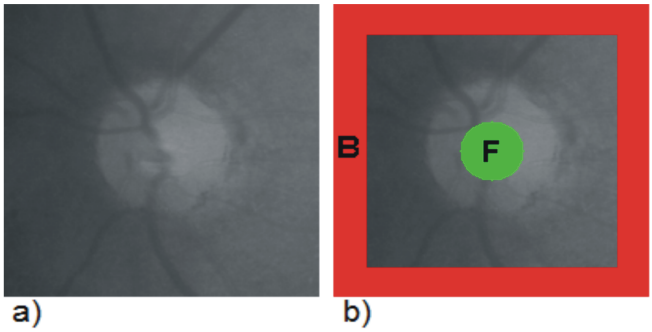

Figure 5.3: a) constrained image, b) foreground **F** and background **B** seeds initialization in the constrained image.

5.3 Segmentation of overlapping tissues

The retinal blood vessels have a double role in the optic disc segmentation. On the one hand, blood vessels break the continuity of the optic disc creating an obstruction for its segmentation; and on the other hand blood vessels inside the optic disc are part of the object to be segmented. The overlapping of tissues is a common issue to address in the analysis of medical images.

Figure 5.4 shows some retinal images where the optic disc was segmented using the traditional formulation of the graph cut technique. Note that blood vessels interrupt the continuity in the segmentation of the optic disc. The high contrast of vessels inside of the optic disc misguides the

segmentation trough the shortest path.

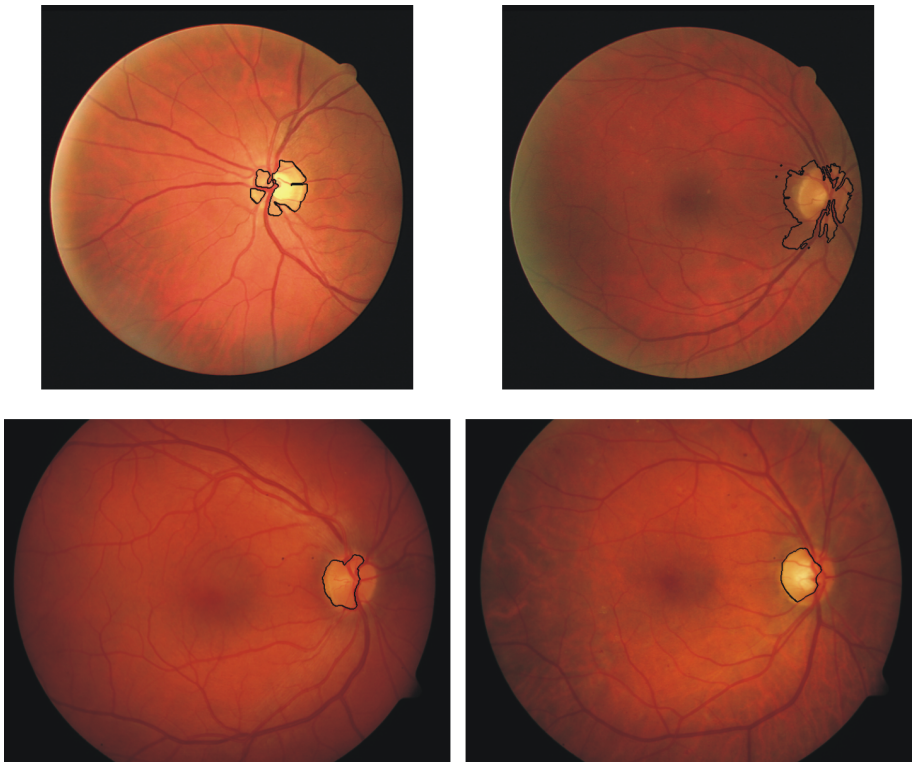

Figure 5.4: Retinal optic disc segmented using traditional formulation of graph cut technique. Top: DRIVE dataset samples; bottom: DIARETDB1 dataset samples.

For the reason exposed above the segmentation of the optic disc process requires of special attention for the blood vessels. There are two main premises by using prior blood vessel segmentation, eliminate them prior to the segmentation process and incorporate them into the formulation technique. By exploring this opposing research lines the study is extended to cover both premises and the results could be used as guideline for other overlapping structures cases. Our proposed methods are based on these two premises and they are summarized next.

- **Discrimination of vessels (MRF reconstruction).** Prior blood vessels segmentation is used to perform a MRF reconstruction. Vessels pixels are considered as unknown, and the rest of the image is used to find the statistical best matching to substitute the missing pixels. As a result the optic disc appears as a well defined round bright object and is ready to segment. Traditional Graph formulation is then used to segment the optic disc in the reconstructed image.

- **Incorporation of vessesl (Graph Cut with compensation factor Vad).** While most of the methods for the optic disc segmentation have addressed this problem by trying to eliminate the vessels, we have incorporated them into the formulation. We introduced a compensation factor in the graph cut technique. The compensation factor is calculated by using prior vessel segmentation.

In both methods the convergence of the blood vessels is localized and assumed as the centre of the optic disc. Seeds are initialized automatically and used to create a general pixel intensity template for foreground and background. Foreground seeds are taken from the centre of the optic disc and Background seeds from a perimeter band.

5.4 Discrimination of vessels

In our first method the segmented vessels are discriminated from the retinal image. Figure 5.5 shows the methodology of our method. First vessels are segmented and used to localize the optic disc. Then the blood vessels are reconstructed by using MRF formulation. Vessel pixels are considered as unknown and the statistical best matching pixel is found to substitute the

missing pixel. Later traditional graph cut formulation is used to segmented the resultant well defined optic disc in the reconstructed image.

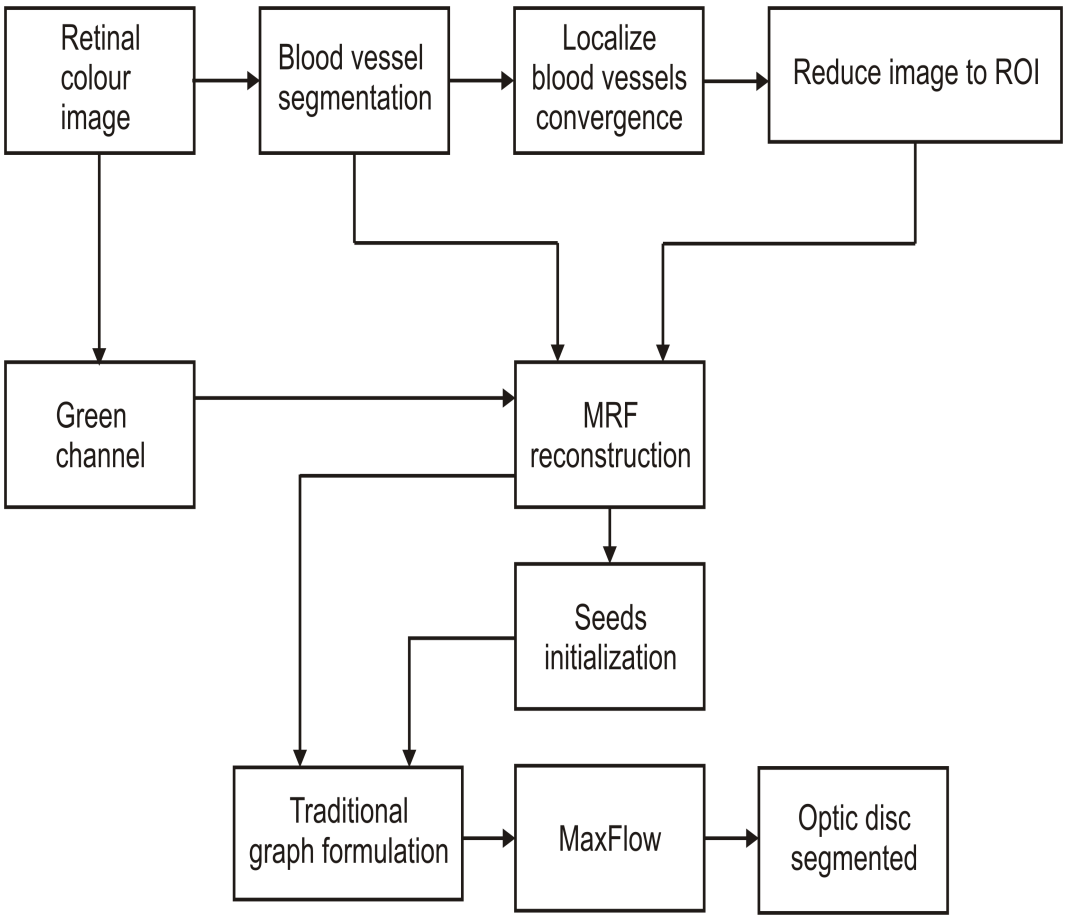

Figure 5.5: Graph cut optic disc segmentation methodology using prior MRF reconstruction.

The MRF reconstruction is performed using previous blood vessel segmentation. Blood vessel pixels are considered as unknown and the surrounded pixels are used to fill these vacancies. We have selected Markov Random Field based reconstruction technique because of its robustness. The general idea is to find the best matching for the missing pixels. One of

the disadvantages of this approach is the intensive computation required. We address this problem by limiting the reconstruction to the region of interest. The method is summarized in Table 5.1.

Input: Colour retinal image I_{in}
1. Segment the blood vessels from I_{in} [Salazar-Gonzalez et al., 2010];
2. I_c = Localize the optic disc and constrain the image;
3. I_r = Perform the MRF reconstruction of I_c;
4. Initialize Fg_s and Bg_s in I_r;
5. I_{out} = Construct graph for I_r and resolve;
Output: Optic disc segmented I_{out}

Table 5.1: Optic disc segmentation process using prior MRF reconstruction.

5.4.1 MRF Reconstruction

In order to minimize the obstruction of blood vessels trought the optic disc segmentation process we performed a reconstruction using prior vessels segmentation. As a results the reconstructed image provided a well defined optic disc. Later a traditional formulation of the graph cut technique is used to segment the optic disc.

Using prior blood vessel segmentation we perform the reconstruction in the ROI. We have selected a Markov Random Field based method to perform the reconstruction [Efros and Leung, 1999] for its robustness. In the beginning blood vessel pixels are considered as unknown. The general idea is to find a collection of patches statistically similar to the patch where a pixel p ($p = 0$) is missed. Then we create a histogram of the pixels that are in the same position as p in the collection of patches and obtain the best approximate value to substitute the missing pixel.

A pixel neighborhood $w(p)$ is defined as a square window of size W, with center on pixel p. The image that is going to be reconstructed is I. Some of the pixels in I are missing and the objective is to find the best approximate value for them. Let $d(w1, w2)$ indicate a perceptual distance between two patches that indicate how likely they are. The exact matching patch would be the one that $d(w', w(p)) = 0$. If we define a set of these patches as $\Omega(p) = \{\omega' \subset I : d(\omega', \omega(p)) = 0\}$ the probability density function of p can be estimated with a histogram of all center pixel values in $\Omega(p)$.

But owing to the fact that we are considering a finite neighborhood for p and the searching is limited to the image area, there might not be any exact matches for the patch. For this reason in our implementation we find a collection of patches whose match falls between the best match and a threshold. The closest match is calculated as $\omega_{best} = argmin_{\omega} d(\omega(p), \omega) \subset I$. And all the patches ω with $d(\omega(p), \omega) < (1 + \epsilon) d(\omega(p), \omega_{best})$ are included in the collection ω'. In our implementation $d(w', w(p))$ is defined as the sum of the absolute differences of the intensities between patches, so identical patches will result in $d(w', w(p)) = 0$. We have set $\epsilon = 0.1$ and $W = 5$. Using the collection of patches we create a histogram and select the one with highest mode.

The reconstruction starts with the unknown pixels with most number to know pixels. In this way the patch represents with more accuracy the neighborhood intensity distribution and the image is actualized after each unknown pixel is filled.Table 5.2 shows the pseudo function for the MRF image reconstruction.

The success of the reconstruction process depends in part of the segmentation of the blood vessels. Simply vessel sections than are not detected cannot be reconstructed. Figure 5.6 shows some examples of reconstructed images. It is possible appreciate the segmented vessels and their reconstruction on the retinal images. The optic disc appears as a well defined object in the reconstructed images and it ready to segment.

Inputs: Retinal gray scale image I_g and binary blood vessel image I_{bv}.
1. If $I_{bv}(p) = vessel$ then $I_g(p) = 0$; 2. Create a list of unknown pixels p in I_g, $I_g(p) = 0$ and their neighborhood $w(p)$; 3. Sort out the list according with the number of unknown pixels included as part of the neighborhood $w(p)$; 4. for $i = 0$ to $i = W - 1$; for each element in the list; $patch$ = w(p) if unknown neighbors number is equal to i; find $\omega_{best} = argmin_{\omega} d(\omega(p), \omega) \subset I$; collection of patches $d(\omega(p), \omega) < (1 + \epsilon) d(\omega(p), \omega_{best})$; create a histogram of collection of patches; Substitute p in I_g by the intensity with highest mode; $i++$ end for end for

Table 5.2: Pseudo function for the MRF image reconstruction in the constrained retinal image.

5.5 Incorporation of vessels

The second method proposes the incorporation of vessels into the graph formulation by using a compensation factor Vad. Figure 5.7 shows the algorithm for the method. Retinal green channel, blood vessels and the ROI are needed for the graph construction. The graph formulation is limited to the ROI.

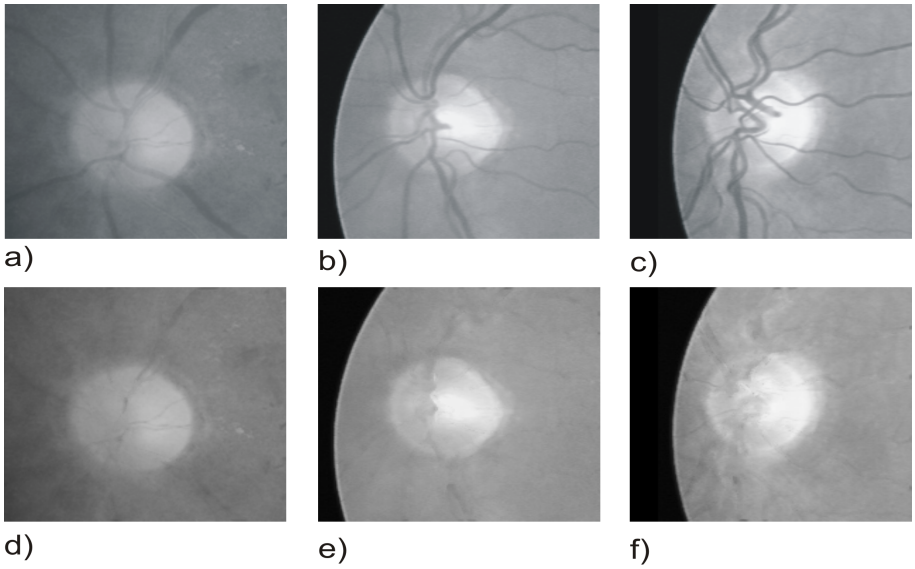

Figure 5.6: MRF reconstruction applied to retinal images. First row: original gray scale images, second row: reconstructed images using the MRF based method

We have selected the traditional edge weight assignment method as base for our formulation [Salazar-Gonzalez et al., 2011]. Prior blood vessel information is incorporated to the graph formulation using a compensation factor Vad.

The energy function consists of regional and boundary terms. Regional term is calculated from the likelihood of a pixel p belonging to the foreground and background generating the t-link weights. The boundary term is based on the own pixel properties (i.e. intensity), which is used to assign weights to the n-links. For our particular purpose we have designed a compensation factor for the foreground t-link. The original image is constrained to a ROI concentrating the analysis in a smaller area and minimizing the processing time. The ROI is centered on the optic disc. The constrained

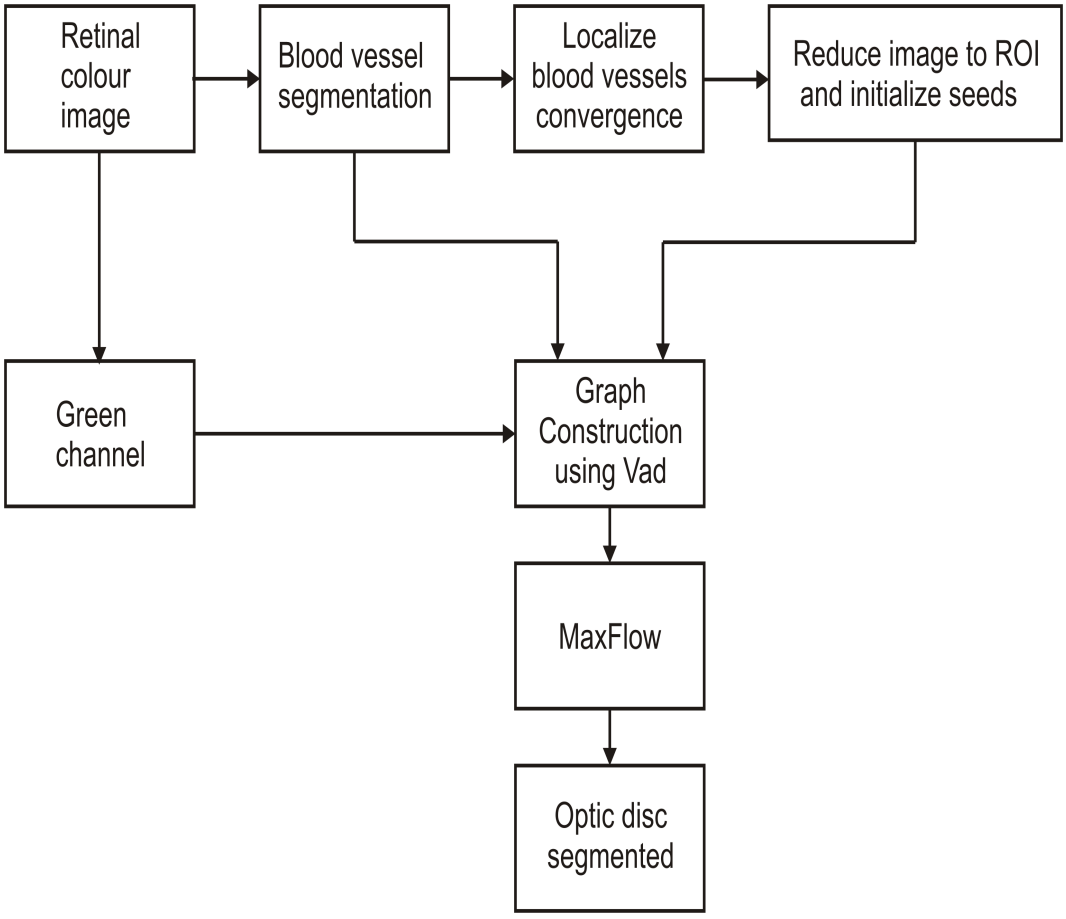

Figure 5.7: Optic disc segmentation methodology using Graph cut technique with compensation factor Vad.

image is preprocessed by applying a histogram equalization in order to enhance its contrast.

5.5.1 Graph Cut with compensation factor Vad

A grid of 16 neighbors N has been selected to create links between pixels in the image Im. The n-link weights are defined by:

$$B_{p,q} = exp\left(-\frac{(I_p - Iq)^2}{2\sigma^2}\right) \cdot \frac{1}{dist(p,q)} \tag{5.2}$$

where I_p and I_q are the pixel intensities between the pixel p and its neighbor q. The distance between p and q is represented by $dist(p,q)$. Using the definition of equation (2), it is obvious that pixels with similar intensities have strong connections. If pixels are very different, the connection between them will be very weak. The pixel links with the terminals S (foreground) and T (background) are defined by the likelihood of the pixel with the seeds. Fg_{seeds} and Bg_{seeds} are represented by the intensity distribution of the foreground and background seeds respectively. This link is calculated according to:

if $(p \neq Vessel)$

$$S_{link} = -lnPr\left(I_p|Fg_{seeds}\right)$$

$$T_{link} = -lnPr\left(I_p|Bg_{seeds}\right)$$

else

$$S_{link} = -lnPr(I_p|Fg_{seeds}) + Vad$$

$$T_{link} = -lnPr(I_p|Bg_{seeds})$$

where

$$Vad = max_{p \in Vessel}(-lnPr\,(I_p|Fg_{seeds})$$

$p \neq Vessel$ implies that the pixel is not part of the vessel network. For the pixels that belong to the blood vessel network a compensation factor Vad is added for the foreground link. The dark intensity characteristic of the blood vessel pixels makes them more likely to belong to the background than the foreground (optic disc). Even when vessels inside of the optic disc are less dark, the weak connection with their neighbors makes them more likely to be segmented as background.

By adding a compensation factor Vad to the foreground t-link we equilibrate this behavior. Vessels are classified using their neighborhood and not the likelihood with the terminals. Vessels inside of the optic disc will be classified according with their neighbors connections (Foreground). Vessel pixels outside of the optic disc will have the same compensation for the foreground t-link, but because of their strong n-links to their neighbors, and those with strong t-links to the background, they will be classified as background.

In summary, the blood vessel classification (foreground or background) is made primarily by their neighborhood characteristics instead of their own characteristics. Fg_{seeds} and Bg_{seeds} are linked to the terminals S(Source) and T(Sink) by using the traditional formulation presented in [Boykov and Jolly, 2001]. Finally the maxflow technique is used to compute the optimal

segmentation.

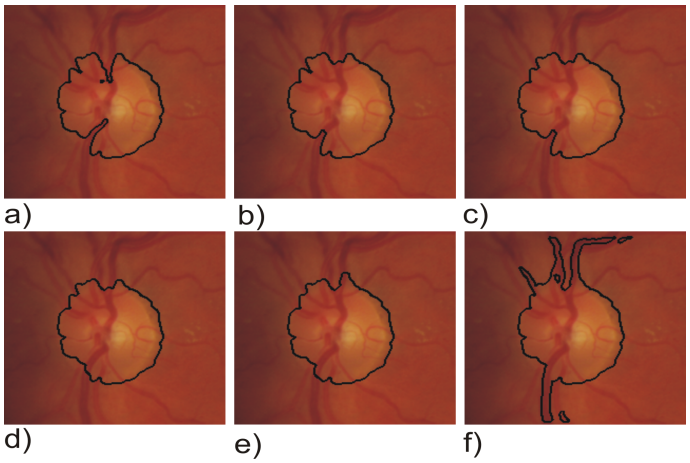

Figure 5.8: Optic disc segmentation via graph cut with different foreground t-link compensation factor Vad for blood vessels: a) $Vad = 20$, b) $Vad = 50$, c) $Vad = 100$, d) $Vad = 150$, e) $Vad = 200$ and f) $Vad = 250$

Figure 5.8 shows an example of our method applied to a retinal image. The image is segmented using different values of Vad adjusted manually. For a low value of Vad, the segmentation is affected by the presence of the blood vessels inside or near by the optic nerve. When Vad is increased, the segmentation performance improves until it starts to segment the blood vessels as part of the foreground as well.

5.6 Experiments and Results

Our proposed method was tested on two public datasets, DIARETDB1 [Kauppi et al., 2007] and DRIVE[Staal et al., 2004]. Our algorithm detected the optic disc centre successful in 96.7% on the DIARETDB1 dataset and in 97.5% of the images on DRIVE. The localization of the optic disc is used

to initialize foreground and background seeds.

We created hand labeled sets for DIARETDB1 and DRIVE in order to have a ground truth to compare our results. The performance of the methods was evaluated by the overlapping ratio ($Oratio$) and the mean absolute distance(MAD). The overlapping ratio is defined as:

$$Oratio = \frac{G \bigcap S}{G \bigcup S}$$

where G represents the manually segmented area and S is the area as result of the algorithm segmentation. MAD is defined as:

$$[\ \mathrm{MAD}(\mathrm{G}_c, S_c) = \tfrac{1}{2}\big\{\tfrac{1}{n}\sum_{i=1}^{n} d(g_{ci}, S) + \tfrac{1}{m}\sum_{i=1}^{m} d(s_{ci}, G)\big\}]$$

where G_c and S_c are the contour of the segmented area in the ground truth and the resulting images, and $d(a_i, B)$ is the minimum distance from the position of the pixel a_i on the contour A to the contour B. A good segmentation implies a high overlapping ratio and a low MAD value.

We calculated the sensitivity of the methods when they are applied to DIARETDB1 and DRIVE, which is defined as:

$$Sensitivity = \frac{Tp}{Tp\ +\ Fn}$$

where Tp and Fn are the number of true positives and the number of false negatives respectively. Sensitivity is an indicator of the foreground pixels detected by the segmentation method.

Our results are compared to those provided in [Welfer et al., 2010a]. This method was tested on the same datasets (DIARETDB1 and DRIVE) and results were measured under the same parameters. Also we have included the results of our experiments using the traditional graph cut technique without compensation and the ones using the topology cut technique [Zeng et al., 2008].

Unfortunately most of the methods do not use a unique ground truth to measure the results of the optic disc segmentation, so this makes the comparison of the results difficult.

Figures 5.9 and 5.10 present the segmentation results using different methods on DIARETDB1 and DRIVE datasets. The manually labeled images have been included to have a visual reference. It can be seen that our method performs better over the blood vessel interference. Particularly the traditional graph cut technique tends to segment the optic disc along the blood vessels edges. The topology cut technique succeeds in the brightest area of the optic disc where the blood vessels are more likely to look like part of the foreground. The topology cut technique was applied to the color image directly without any preprocessing. The topology cut is not an automatic technique, and it requires a manual marking of foreground seeds.

Figure 5.11 shows the segmentation results by our method on four representative images. The images represent different challenges due to their illumination, contrast, and focal characteristics. We have included the overlapping ratio ($Oratio$) and MAD values of the segmentation re-

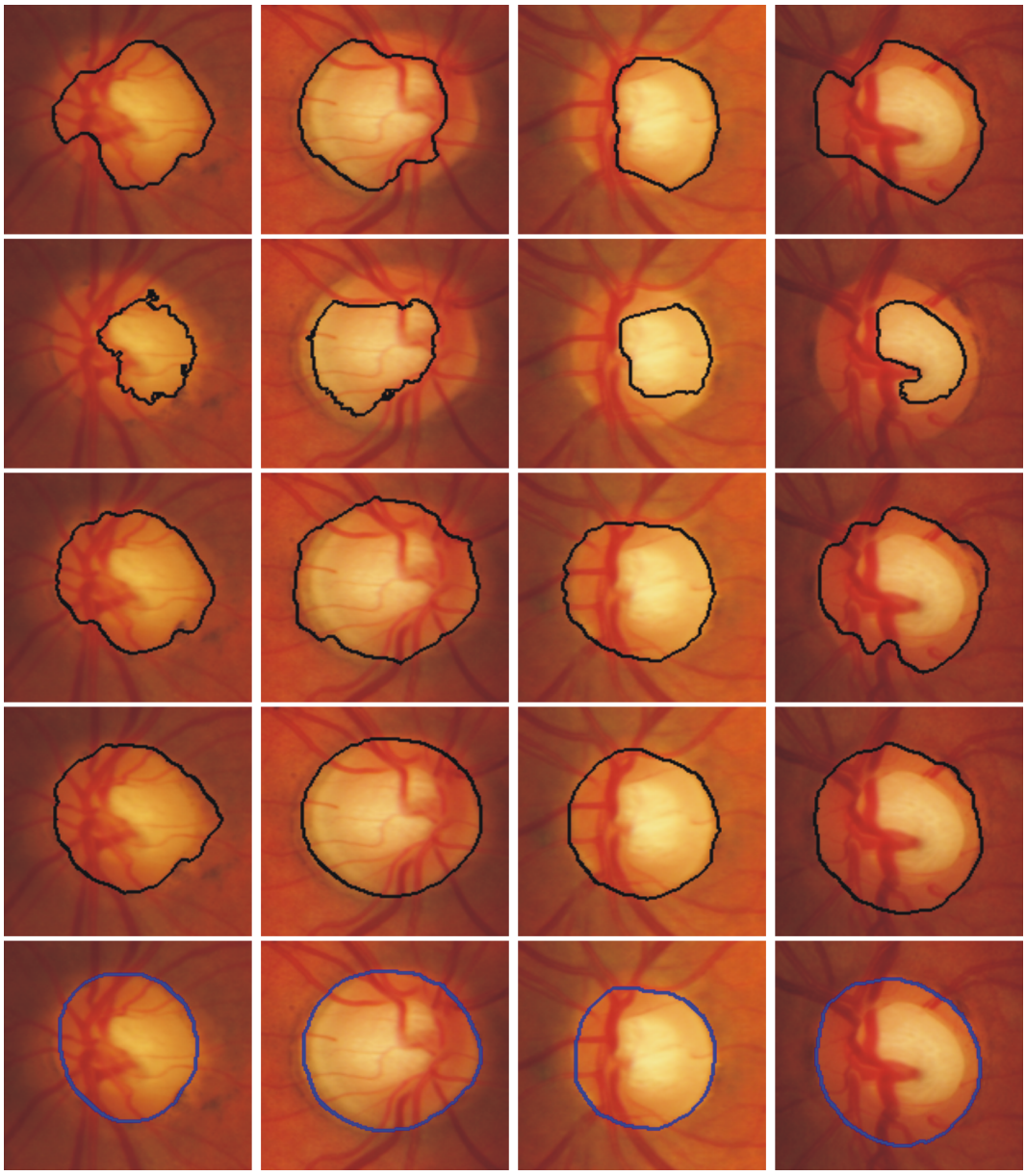

Figure 5.9: Optic disc segmentation using different methods for DIARETDB1 dataset. First row: Topology cuts, second row: Graph cut, third row: Graph cut with compensation factor Vad for blood vessels, fourth row: MRF + graph cut and fifth row: hand labeled

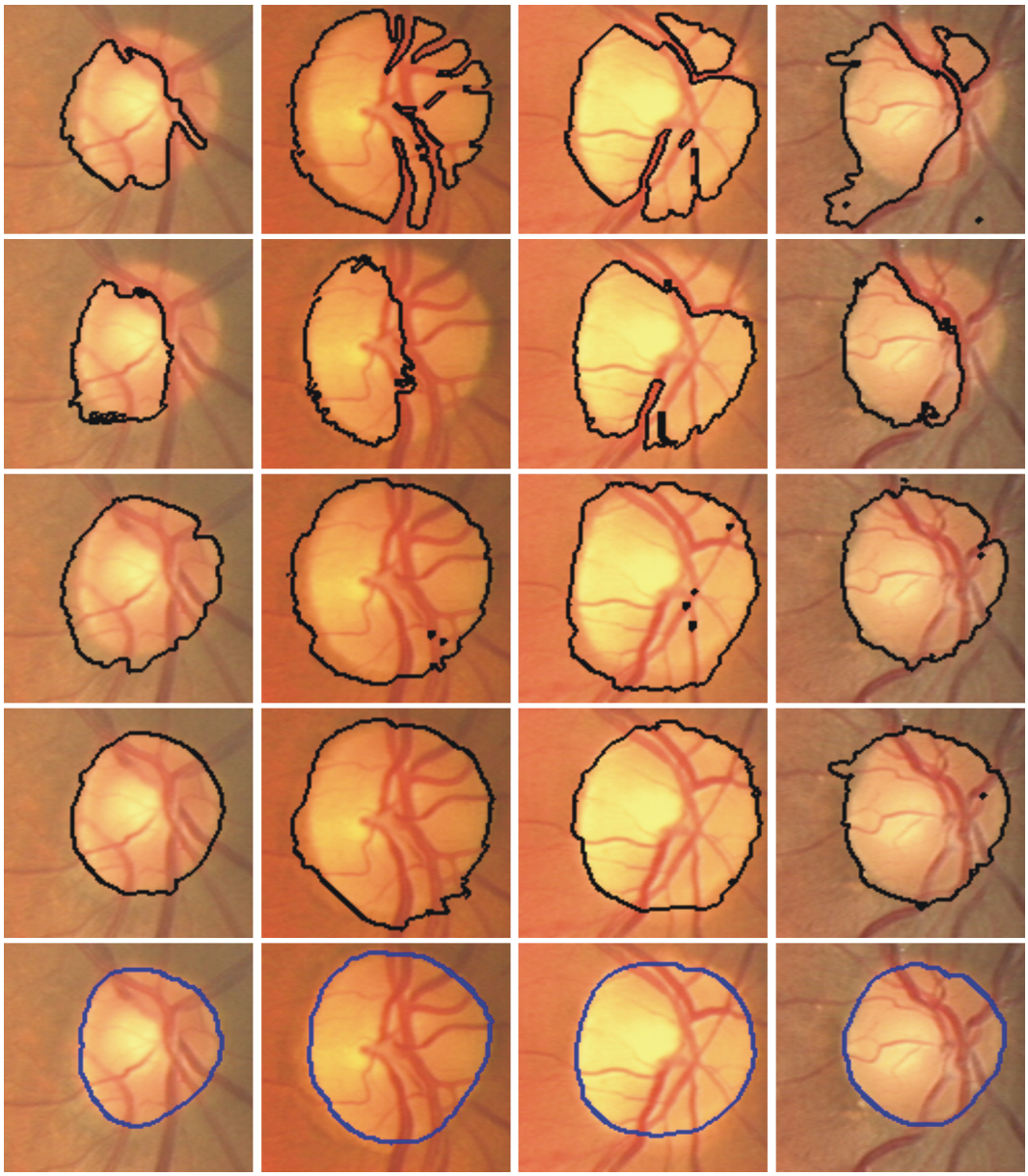

Figure 5.10: Optic disc segmentation using different methods for DRIVE dataset. First row: Topology cuts, second row: Graph cut, third row: Graph cut with compensation factor Vad for blood vessels, fourth row: MRF + graph cut and fifth row: hand labeled

sult. Some authors [Niemeijer et al., 2007a] consider a minimum Oratio of 0.50 as a successful segmentation. In this direction the 100% of the images in the Figure 5.11 have been segmented correctly.

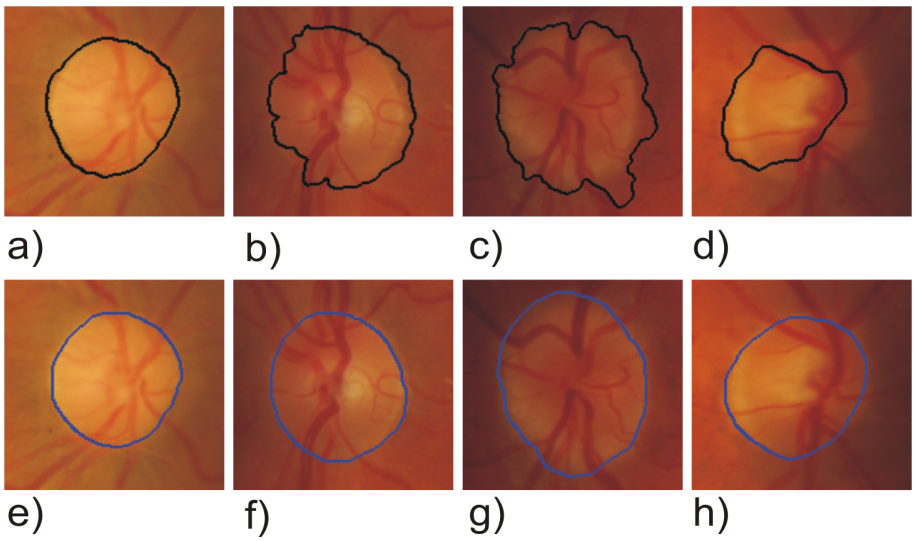

Figure 5.11: Top Row: optic disc segmentation using graph cut with compensation factor Vad for blood vessels: a) Oratio = 0.9003 MAD = 2.26, b) Oratio = 0.8320 MAD = 3.94, c) Oratio = 0.7857 MAD = 5.58 and d) Oratio = 0.6393 MAD = 9.80. Bottom row: hand labeled images

Table 5.3 and Table 5.4 show the comparison with different methods in terms of *Oratio*, MAD and *Sensitivity*. Our method achieved the highest overlapping ratio with the minimum MAD value. It can be seen that an increase in the overlapping ratio does not mean a decrease on MAD value necessarily. MAD value does not represent the best way to measure the segmentation results, but it provides a good reference of the contour matching with the ground truth contour reference.

Figures 5.12, 5.13, 5.14 and 5.15 show the distribution of the overlap-

Table 5.3: Performance comparison on the DIARETDB1 dataset.

Method	Average ORatio	Average MAD	Average Sensitivity
Topoly Cut	38.43%	17.49	55.30%
Adaptive morphologic [Welfer et al., 2010a]	43.65%	8.31	—
Graph Cut	54.03%	10.74	76.35%
Graph Cut with Vad	75.74%	6.38	86.55%
MRF + Graph Cut	78.3%	6.75	87.3%

Table 5.4: Performance comparison on the DRIVE dataset.

Method	Average ORatio	Average MAD	Average Sensitivity
Topoly Cut	55.91%	10.24	65.12%
Adaptive morphologic [Welfer et al., 2010a]	41.47%	5.74	—
Graph Cut	55.32%	9.97	73.98%
Graph Cut with Vad	70.70%	6.68	84.44%
MRF + Graph Cut	82.2%	3.59	97.99%

ping ratio on DIARETDB1 and DRIVE using the four different segmentation methods. We have included lines as a reference at $Oratio = 50\%$ and $Oratio = 70\%$. By using this reference lines it is possible appreciate the amount of image segmented over an $Oratio = 50\%$ and $Oratio = 70\%$

There are few specific cases where the segmentation of the optic disc resulted in null by using our methods. This cases are shared by the other methods as well. The characteristic of these images is the poor contrast, as a consequence all the pixels are linked with strong weight and is not possible to find a cut to segment it. This is an indication of the challenge of analyzing those specific images.

In these specific cases it is possible to address the problem by adjusting the parameters in the energy function and the edge weight assignment to attend the specific needs of these images. This change will move our methods from automatic to interactive mode, where the user can adjust

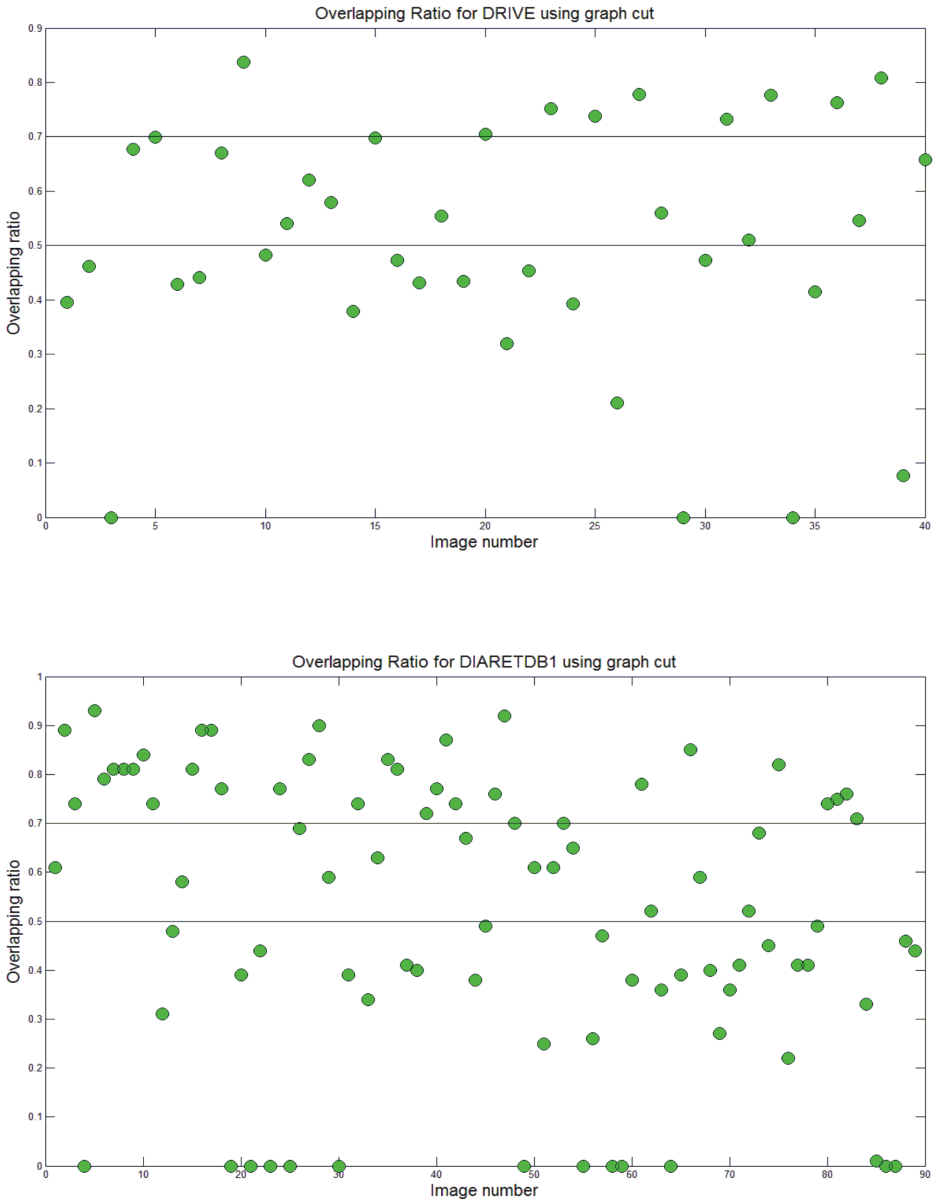

Figure 5.12: Overlapping ratio distribution for the optic disc segmentation using traditional graph cut formulation.

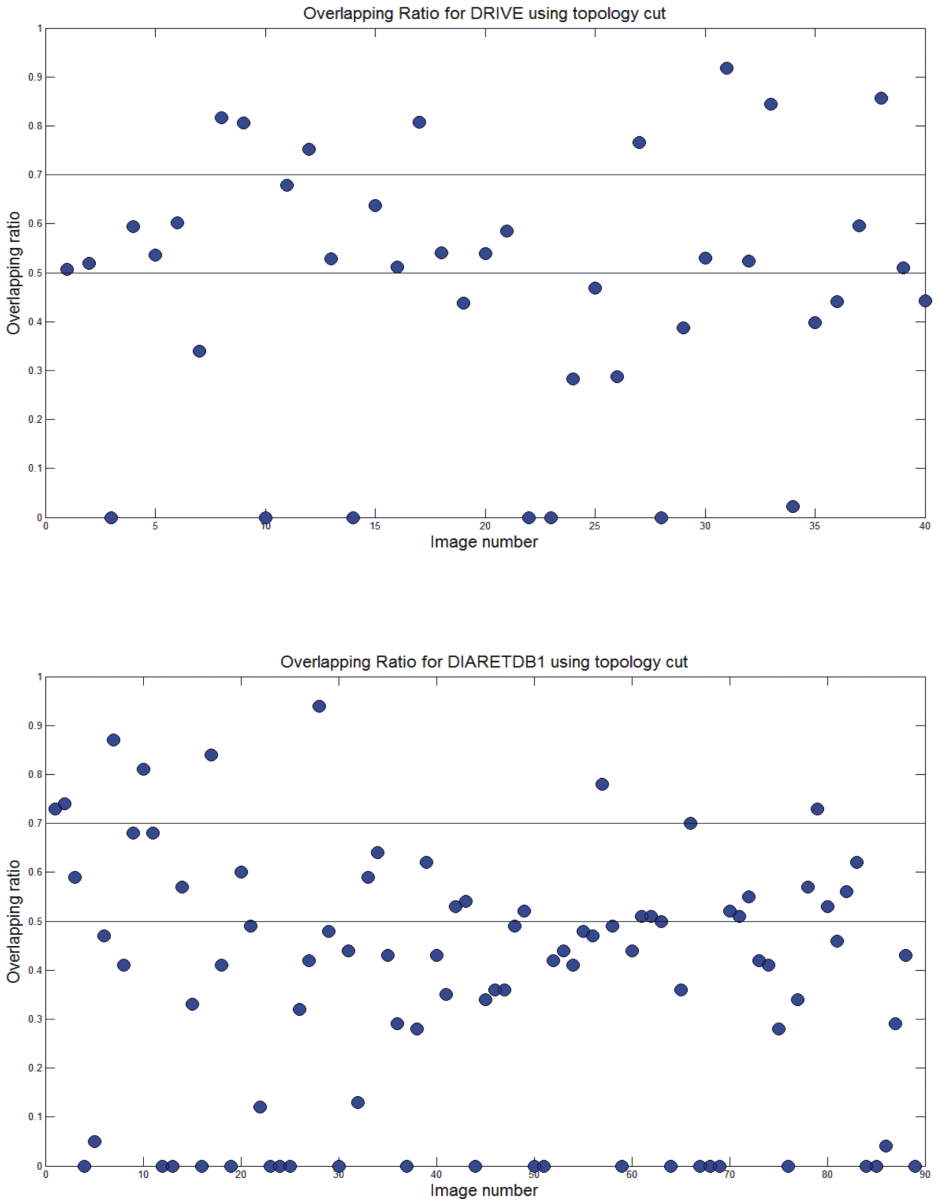

Figure 5.13: Overlapping ratio distribution for the optic disc segmentation using topology cut technique.

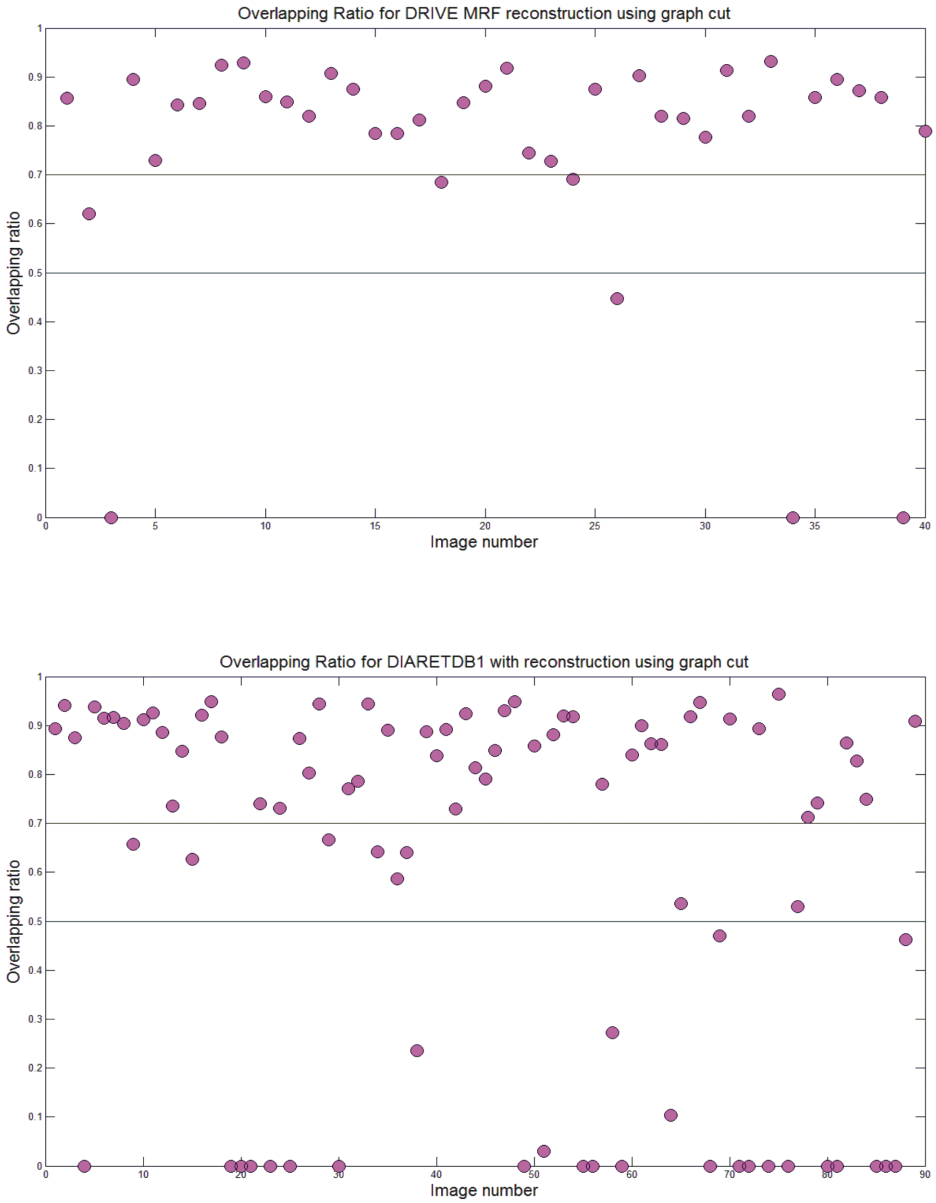

Figure 5.14: Overlapping ratio distribution for the optic disc segmentation using traditional graph cut formulation on MRF reconstructed images.

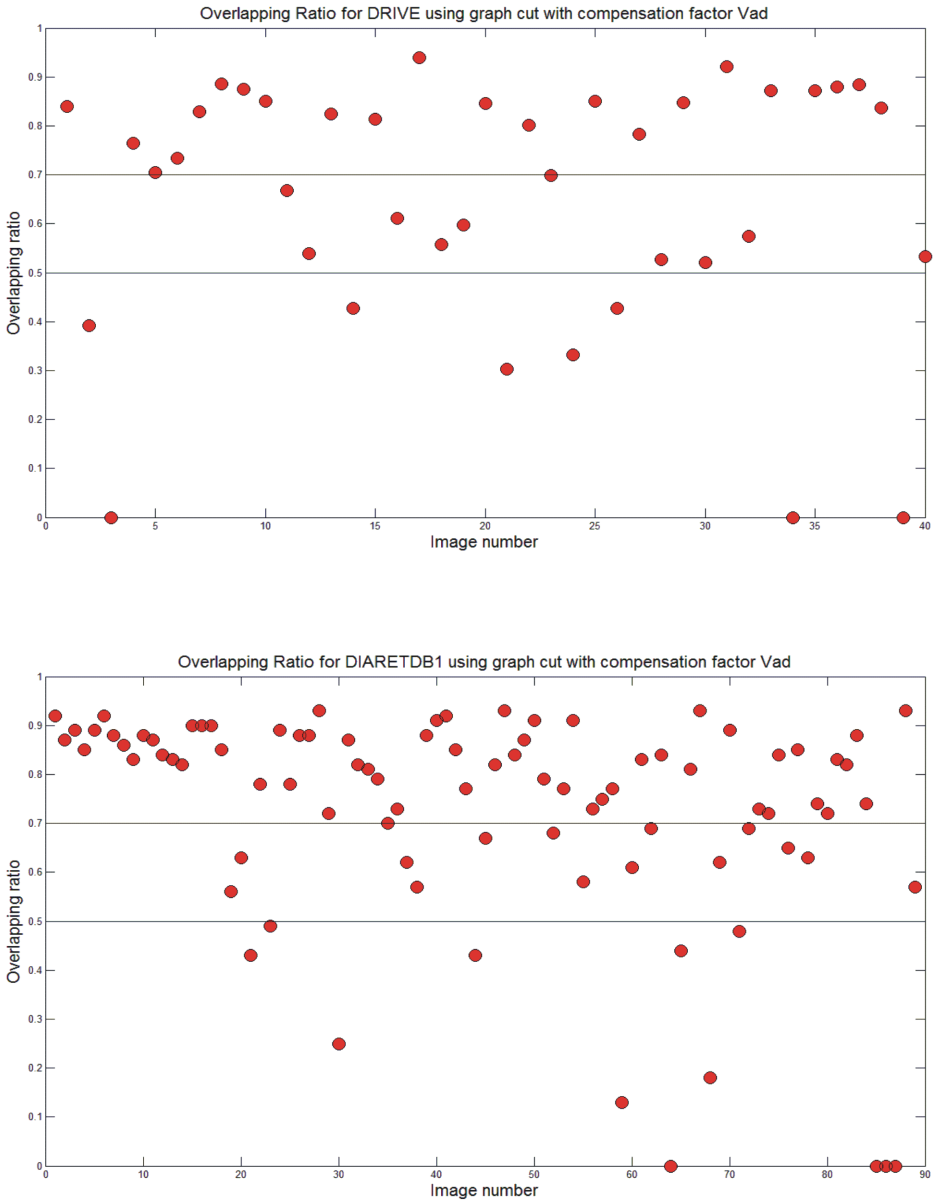

Figure 5.15: Overlapping ratio distribution for the optic disc segmentation using graph cut technique with compensation factor Vad.

parameters for each image analysis.

In order to make possible a comparison with the method presented in [Niemeijer et al., 2007a], we have addopted their assuption, which takes a minimum overlapping ratio of 50% as a successful segmentation. Table 5.5 presents the success of the methods based on this assumption ($Oratio > 50\%$).

Table 5.5: successful optic disc segmentation ($Oratio > 50\%$) on DRIVE and DIARETDB1 using different methods.

Method	DRIVE	DIARETDB1	No public dataset
Graph cut	21/40 = 52.5%	47/89 = 52.8%	
Topoly Cut	24/40 = 60.0%	30/89 = 33.7%	
MRF + Graph Cut	36/40 = 90.0%	62/89 = 69.6%	
Graph Cut with Vad	32/40 = 80.5%	77/89 = 86.5%	
[Niemeijer et al., 2007a]			94%

Figures 5.16 and 5.17 show the cumulative histograms comparison, for normalized overlapping ratio on DIARETDB1 and DRIVE datasets using different methods. The cumulative histogram shows the frequency of the $Oratio$ value when the segmentation is compared with the hand labelled image. In the case of a perfect matching, $Oratio = 1$, for all the images in the dataset the area under the curve would be zero. Since our method shows the minimum area under the curve, it is clear that graph cut technique using the compensation factor Vad outperforms other techniques. The cumulative histograms provide a summary of the success of our method.

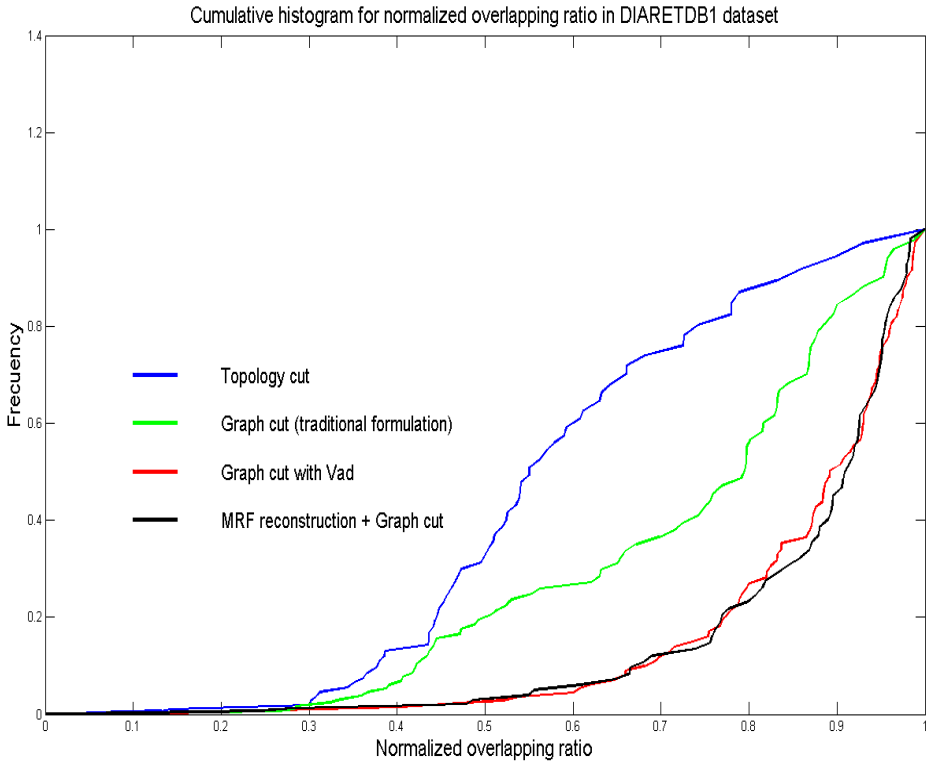

Figure 5.16: Cumulative histogram for normalized overlapping ratio on DIARETDB1 dataset using different methods.

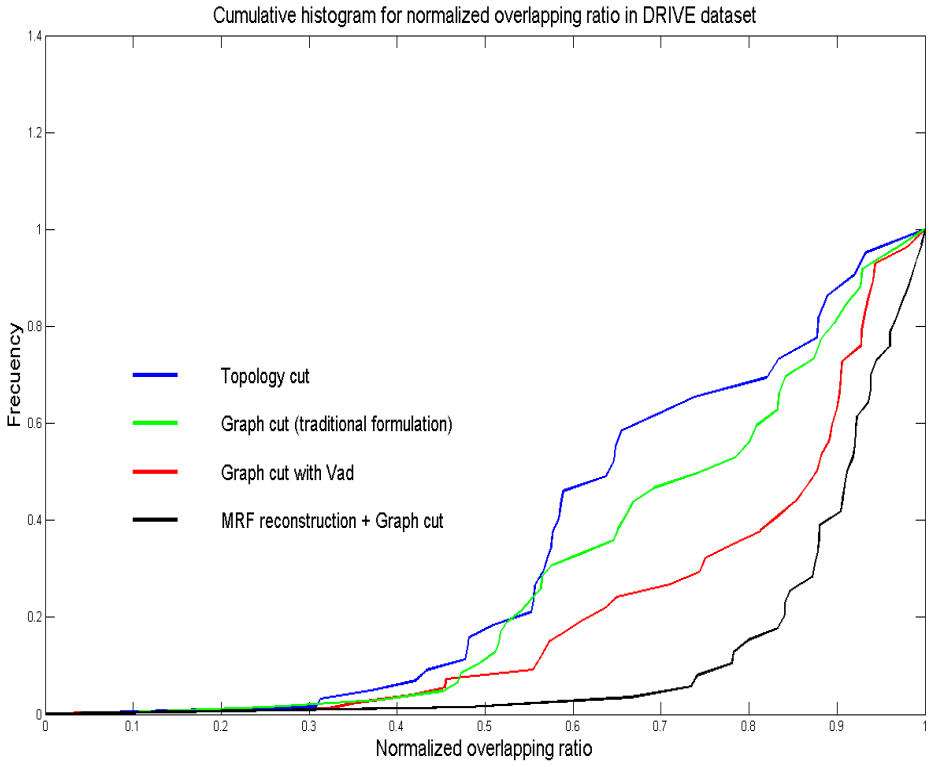

Figure 5.17: Cumulative histogram for normalized overlapping ratio on DRIVE dataset using different methods.

5.6.1 Discussion

Results are very clear, both methods have outperformed other methods in the literature. From tables 5.3 and 5.4 it is possible to observe the performance of both methods on DIARETDB1 and DRIVE datasets.

In the case of DIARETDB1, "MRF + graph cut" method performs slightly better than "Graph Cut with Vad" method by 2.56%. The outperformance is more visible in the case of DRIVE dataset, where the "MRF + graph cut" method reached an average ovelapping ratio of 11.5% more than "Graph Cut with Vad" method.

Nevertheless "MRF + graph cut" method produced a considerable amount of null segmentation when performing on DIARETDB1. While "Graph Cut with Vad" method produced only four cases of null segmentation.

The ideal conditions for the performance of "MRF + graph cut" method are that blood vessels have been detected with high confidence, then the reconstruction will produce a well defined optic disc and as a consequence a good segmentation will be achieved. On the other hand if the retinal image do not have the best conditions to perform the segmentation of vessels (e.g. severe damaged retina) the reconstruction will not offer a well defined object to segment and consequently the segmentation will not succeed.

In general the DIARETDB1 images are characterized by contain at least one sign of retinal lesion. This complicates the analysis of the images (blood vessels and optic disc segmentation), but precisely these type of im-

ages are the main concern in a retinal test.

The "Graph Cut with Vad" method performs the segmentation using the original data in the image. This method permits that misclassified vessel pixels (false positives and false negatives) are part of the graph as well, and with the declaration of seeds the optimal segmentation is found.

In general the optic disc on DRIVE dataset is segmented better by "MRF + graph cut" method; while "Graph Cut with Vad" method produced better segmentation of the optic disc on DIARETDB1 dataset.

5.7 Summary

Optic disc segmentation is an important process in the analysis of retinal images. The analysis of optic disc morphology is part of the retinal screen process. Retinal Blood vessel network requires special attention due to its overlapping with the optic disc.

In this chapter we have presented two methods for the segmentation of the optic disc based in the graph cut technique. We followed the two major premises: incorporating vessels into the graph formulation and masking them out prior to its segmentation by applying a MRF reconstruction.

The methods were tested in two public data sets: DIARETDB1 and DRIVE. The results were compared with the results of the traditional formulation of the graph cut and the topology cut techniques. The results

comparison shows the superior performance of our methods.

The next chapter presents the consolidation of our research. Segmented retinal structures are used to created a background template. This template is then used to perform the detection of suspicious areas in the retinal images.

Chapter 6

Retinal lesion detection

6.1 Introduction

Retinal lesions are the main indicator of the presence of a disease. Different types of lesions appear progressively during the development of a retinopathy.

Microaneurysm is usually the first lesion to be detected. It appears as a red spot and sometimes is seen next to small blood vessels. In general microaneuryms does not appear in patients that have had diabetes for less than three years. Around 70% of the people that have had diabetes type 1 (insulin dependent diabetes) for 10 years present this type of lesion. But in the case of people with diabetes type 2 (non-insulin dependent diabetes) only 55% of them present microaneuryms lesion.

In the second stage exudates begin to appears as yellow deposits. Exudates are originated as a consequence of capillary blood vessels and microaneuryms leaking, and they are composed in part by lipid materials.

The subsequent type of lesions to appear are the ones associated with ischemia. These stage is characterized by the dilatation of retinal capillars or small blood vessels. It may be possible to observe abnormalities in the large blood vessels. The next lesions to appear are those that belong to the proliferative retinopathy stage. The growth of new blood vessels is a typical indication of this stage.

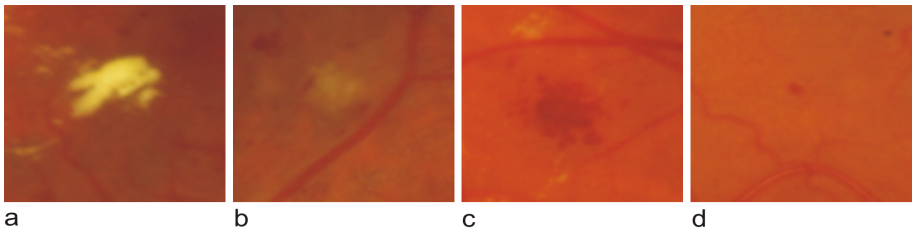

Figure 6.1: Examples of different type of lesions: hard exudate, soft exudate, hemorrhages and red spots.

In general we can classify typical retinal lesions as bright and dark according to their colour. Bright lesions include hard and soft exudates. Exudates are lipid formations from weak vessels precipitations. They appear as bright yellow areas in eye fundus images. Hard exudates show sharp edges, while soft exudates present fuzzy borders. Dark lesions are formed by hemorrhages and red spots and they appear as dark red areas in the retina. Bright lesions present a better contrast with their background than dark lesions. Figure 6.1 shows some examples of the different types of lesions.

An early and adequate treatment has demonstrated to be effective to avoid the loss of the vision as a consequence of any type of retinopathy. The

analysis of fundus images is a non-intrusive option for the periodic retinal screening. In order to provide a system to assist the retinal screening we have developed an automatic system capable to detect suspicious lesions areas inside the retina.

In this chapter we present the consolidation of our research by making use of the segmented retinal structures to perform the detection of lesions. Frequently false lesion pixels are detected inside the retinal structure areas due to their similar characteristics of colour and texture; bright lesions with optic disc and dark lesions with blood vessels.

Our proposal is to located the eye structures (e.g. optic disc and blood vessels) as first step and then by masking them out we create a clear field to perform the analysis of lesions. Using the masked image a background template is created. The template is used then to detect the objects that do not match with the general background template. The masked image is subtracted from the template to detect any discrepancy between them and suspicious areas are detected.

The aim of our work is to create a method able to detect any kind of suspicious lesion and assist the retinal test procedure. Since our method is completely automatic and unsupervised, it does not require ad hoc tuning of parameters on different datasets. Our method has been designed to detect any object that does not match with the general background. It does not perform a classification of the lesions. The results are evaluated using the DIARETDB1 ground truths for different type of lesions.

6.2 Lesions detection

The current methods for the detection of retinal lesions have been concentrated in bright lesions. In general bright lesions are easier to detect due to the high contrast with their background, so it is not surprising that the efforts have been concentrated on this type of lesions.

Chapter 2 presented a review of the current methods designed for the detection and segmentation of retinal lesions. Table 2.3 shows the compilation on the main interests of these methods. It is possible appreciate that all of them are dedicated to detect some type of retinal bright lesion.

For first time a system for the detection of retinal lesions, including dark lesions, is presented. The aim of our system is to detect any suspicious area within the retinal image. These suspicious areas attempt to correspond to bright or dark retinal lesions.

The methodoly of segment retinal structures prior to the analysis of lesions is a procedure explored before. It has been demonstrated that this methodology minimizes the false positive rate of lesion detection due to the similar colour characteristics between lesions and retinal structures [Sopharak et al., 2008, Fang et al., 2010, Walter et al., 2002, Sanchez et al., 2004].

In our research the blood vessels are segmented by using the method proposed in [Salazar-Gonzalez et al., 2010]. The method utilizes a prior rough segmentation of vessels to create a graph. The formulation of the graph includes the flux term that represents the flow of the gradient from

the centre of the vessels. Finally the graph is cut by minimizing the energy function and the optimal segmentation is found. The method has been detailed previously in Chapter 4.

The segmented blood vessels are used to detect the optic disc. By detecting the convergence of vessels the center of the optic disc is localized. The optic disc is then segmented by following the procedure described in [Salazar-Gonzalez et al., 2011]. The method incorporates prior blood vessel segmentation into the formulation of a graph. The graph represents the energy function that describe the relationship of pixels with their neighborhood and with prior foreground and background knowledge. Chapter 5 contains details about this method for the segmentation of the optic disc.

The next step is to mask out the optic disc and blood vessels from the retinal images. Table 6.1 outlines the keysteps of the method. The discrimination of retinal structures will reduce the field for the lesions searching. Also, by using the remained pixels it will be possible to create a background template. This template will be then used to detect any suspicious area.

Input: Colour retinal image I_{in}
1. Segment the blood vessels using graph cut technique; 2. Segment the optic disc using MRF reconstruction and graph cut technique; 3. Mask out the eye structures in the retinal colour image; 4. Apply median filtering to the masked image creating a background template; 5. Subtract the masked image from the background template; 6. Apply thresholding;
Output: Retinal lesions detected I_{out}

Table 6.1: Method for the detection of retinal lesions.

The background template is created by using the masked image. A median filtering is applied just to the areas that have not been masked. The

median filtering is a nonlinear technique, and is often used to remove noise. As with all smoothing techniques median filtering has an adverse affect on edges. Precisely with this effect we can create a background template using the masked image.

The aim of the filtering process is to create a smooth region free of any relevant object. After the masking the retinal image is divided in two sets $I = R \bigcup M$, where R represents the retinal area without eye structures and M is the masking. The filtering process considers only the pixels that are not part of the masking. Table 6.2 shows the pseudo function to create the background template.

Input: Retinal masked image I_{mask}

for each $p \in I_{mask}$
if $p \notin M$
p = median$_{(s,t)\in W \bigcap (s,t)\notin M}$ $\{W(s,t)\}$
else
p = 0;

Output: Background template I_{Bg}

Table 6.2: Pseudo function for the background template.

For each pixel in the image that is not part of the masking a neighborhood window W is defined. The original pixel is substituted by the median of the pixel intensity distribution in the window.

The objective of filter process is to create a background template, where retinal structures (blood vessel and optic disc) and possible retinal lesions are not included. By using prior segmented retinal structures the image is masked out. Then a median filter is used to smooth the rest of enhanced regions.

Experimental trial was performed in order to localize the largest blob of pixels that did not correspond to any of the retinal structures (blood vessel or optic disc).

In order to ensure that any blob of pixels will be cover by the filter, the result of the experiment was used to select the size of the filter window W as 81x81 pixels including a safety margin.

Figure 6.2 shows some examples of retinal images masked and their background templates generated after filtering. The background template is compared and subtracted from the masked image. Later an adaptive thresholding is used to extract the regions that less agree with the background template.

6.3 Experimental work

In order to evaluate our method we have used the DIARETDB1 dataset. DIARETDB1 [Kauppi et al., 2007] is a particular dataset of retinal images. The dataset is compoused of 89 images of which 84 contain at least one indication of diabetic retinopathy. Images were captured to 50 degree field of view using a digital fundus camera. But the uniqueness of this dataset is the ground truth marking. The images were marked independently by 4 medical experts considering the type of lesions separately. The experts were instructed to report their marking confidence using three levels: Confidence $< 50\%$, Confidence $> 50\%$ and Confidence 100%. These levels

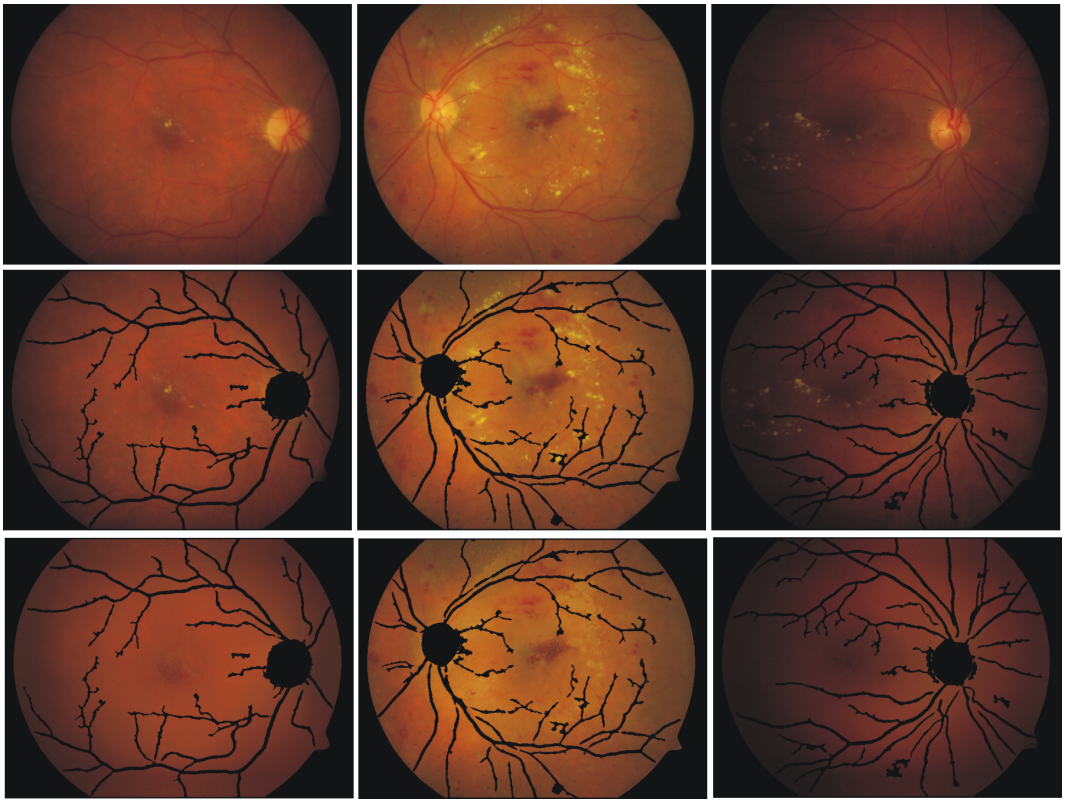

Figure 6.2: First row: Retinal images, second row: masked retinal images, third row: background template.

represent the certainty of the decision that the mark is correct. The fact that the ground truth was generated independently by each expert avoid the mutual influence on their decisions.

The confidence of the markings in the DIARETDB1 ground truth is represented by different levels of gray in the image. The brigthest areas are those that were marked with highest confidence by most of the experts. Some markings are hard to notice because of their low gray intensity. This areas were marked with low confidence and probably not all the experts agreed in the presence of a lesion in this region. Figure 6.3 shows some examples of the retina image and its ground truth for each type of lesion.

We present the results of our method using the confidence level reported by the experts. In this way our experiments results are evaluated considering the opinion of the four experts. For example we can consider a case where an image is declare as healthy by 3 of the 4 experts, and the only expert that marked a small suspicsious area has declared a very low confidence level on it (e.g. Confidence $< 50\%$). If a particular method declare this image as healthy, the decision will agree with the diagnosis of 3 of the 4 experts, instead of disagree with one general ground truth opinion.

6.3.1 DIARETDB1: Ground Truth confidence level quantification

The markings confidence made by the experts are represented by the gray level intensity in the ground truth images but unfortunatelly they are not quantified. Using the gray level intensity of the ground truth in the DI-

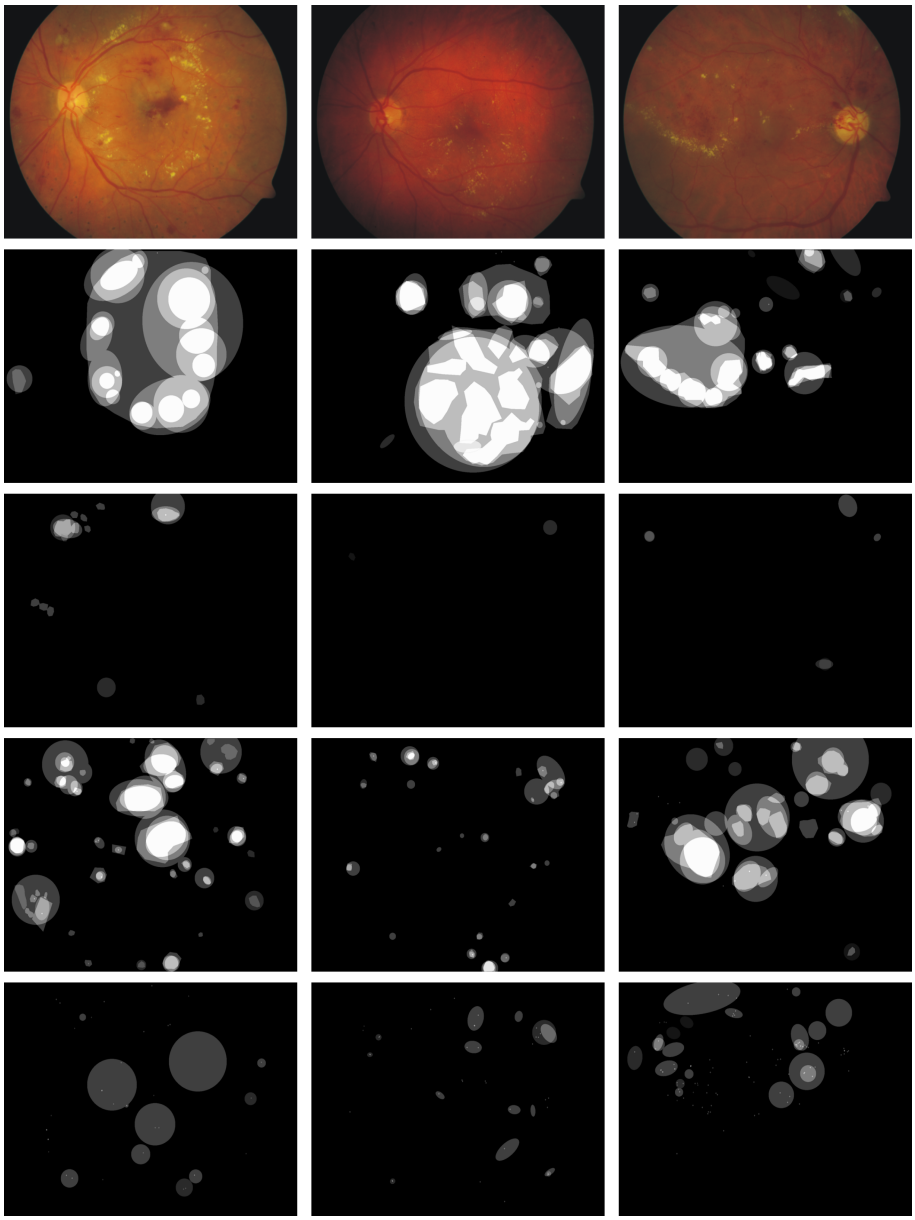

Figure 6.3: DIARETDB1, first row: retinal images, second row: hard exudates ground truth, third row: soft exudates ground truth, fourth row: hemorrhages ground truth, fifth row: red spots ground truth.

ARETDB1 dataset the confidence level of the marks is quantified.

The maximum and minimum gray level intensity in the ground truth are found for each type of lesion. These are assumed as the maximum and minimum level of confidence level. Later the confidence is normalized to [0, 1]. This confidence will be referred in the future as general ground truth confidence level $conf_{GT}$. So we have four $conf_{GT}$ one for each type of lesion.

Similary we also calculate the local confidence level, using the maximum and minimum gray level intensity within each ground truth image. This confidence will be referred in the future as local ground truth confidence level $conf_{local}$.

6.3.2 Evaluation

Sensitivity and Specificity terms are very common in the evaluation of retinal analysis methods. They correspond to typical medical practices evaluation, they are defined as follows.

$$Sensitivity = \frac{Tp}{Tp + Fn} \qquad Specificity = \frac{Tn}{Tn + Fp} \tag{6.1}$$

where Tp and Tn are the number of true positives and true negatives; and Fp and Fn are the number of false positives and false negatives. The evaluation of our method is done separately for the different retinal lesions. In our experiment we have selected two different evaluation basis:

1. Evaluation image based. A true positive image is considered when the detected lesion match total or partially with the ground truth for

an specific lesion. If the algorithm does not detect any lesion that match with the ground truth for an specific lesions it is count as false negative image. This measures are used to calculate the sensitivity and is reported along with the ground truth confidence level. In our evaluation specificity does not provide a meaningful information. Due to the fact that our method does not classify the lesions, a detected lesions that does not match with the ground truth of an specific lesion, it does not mean that does not match with any other. Therefore false positives are difficult to be considerated.

2. Evaluation lesion based. To evaluate the performance of our method to detect lesions within the image we use the local ground truth confidence level. We calculate the average of the $conf_{local}$ for the areas detected by the algorithm. For a good detection the average of the $conf_{local}$ will be near to 1. In the case to evaluate the detection of lesions we are interested to know if the lesions were found inside of a high local confidence region.

We cannot use the general confidence $conf_{GT}$ to evaluate the performance of our method on the basis of detected lesions. The general confidence $conf_{GT}$ has been calculated using the total of ground truth images for an specific lesion. Therefore a ground truth image with low $conf_{GT}$ indicates that the image does not show a dramatic presence of lesions and the markings were label with low confidence. To evaluate the detection of lesions in a image we are interested to know if the detected lesions were found inside of the markings made by the specialist, even if the markings general confidence is low. Then we evaluate the detected areas using the local confidence $conf_{local}$.

6.3.3 Results

Figure 6.4 shows some examples of lesions detected. We have included the overlapping of the lesions on the ground truth. The brightest areas represent our method results matching with the the highest confidence marks made by the experts. The black marks are false positives detections. The dark gray area represents the general ground truth marked by the experts.

As expected most of the detected areas correspond to a type of bright lesion, hard or soft exudates. Some dark lesions were detected as well. Figure 6.5 shows the detected lesions on the ground truth for haemorrhages. It is possible appreciate that the most relevant dark lesions are detected, nevertheless the smooth dark lesions were not detect.

Table 6.3 shows the number of images reported with lesions by our method for each type of lesion. They are compared with the number of images reported by experts. We have considerated any ground truth marking with the minimum confidence $conf_{GT} > 0$ as the true presence of the lesion.

Method	Mark	hard exudates	soft exudates	hemorrhages	red spots
DIARETDB1 experts	positive	48	36	54	80
	negative	41	53	35	9
Our method	positive	43	24	40	45
	negative	41	53	35	9

Table 6.3: Number of images reported with lesions by our method respect to the experts report.

Table 6.4 shows the number of true positives and false negatives report image based. The image based evaluation reports a sensitivity of 89.58% (43/48) in the case of hard exudates. This report has considered a mini-

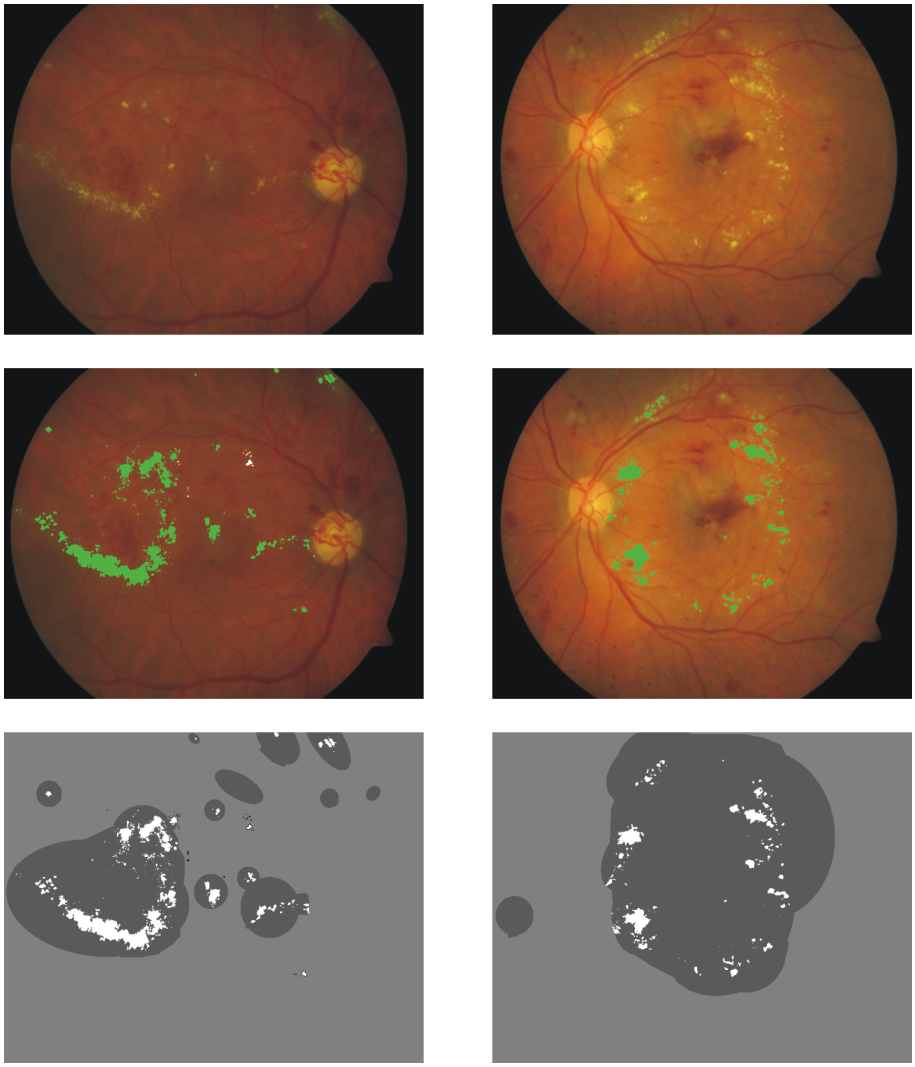

Figure 6.4: Example of lesions detection. First row: retinal colour images, second row: detected lesions($conf_{local} = 0.7908$ and 0.9146), third row: detection matching with exudates ground truth.

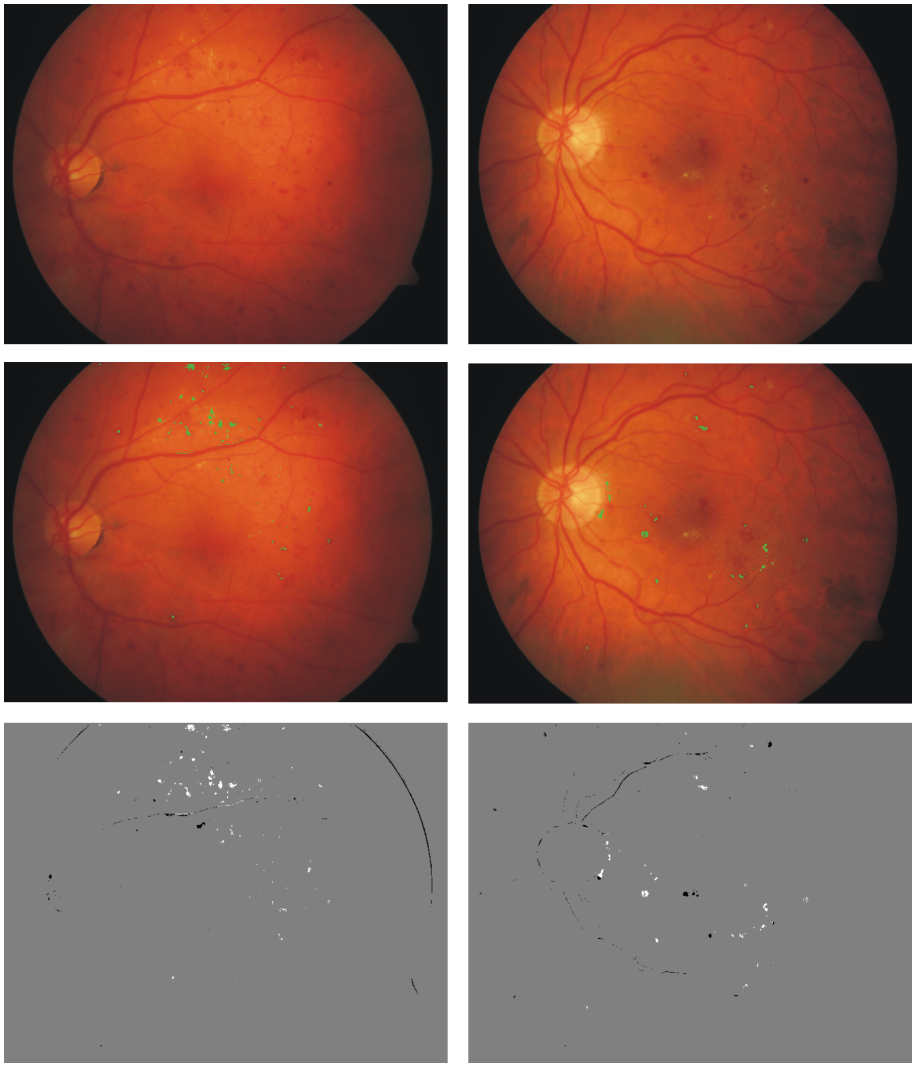

Figure 6.5: Example of lesions detection. First row: retinal colour images, second row: detected lesions($conf_{local} = 0.7702$ and 0.7459), third row: detection matching with haemorrhages ground truth.

	hard exudates	soft exudates	hemorrhages	red spots
true positive	43	24	40	45
false negative	5	12	14	35

Table 6.4: Number of true positives and false negatives images considering the truth presence of lesion when ($conf_{GT} > 0$).

mum confidence level mark ($conf_{GT} > 0$) as the truth presence of the lesion.

Let us now present an example to ilustrate the following evaluation of results. We consider the case of the retinal image 32 in DIARETDB1 and its ground truth (see Figure 6.6). In this case the retinal image does not show a visible sign of lesions. The ground truth for hard and soft exudates do not indicate the precence of lesions. Nevertheless the ground truth for hemorrhages and red spots indicate some lesion markings. The $conf_{GT}$ for hemorrhage and red spots are $conf_{GT} = 0.0846$ and $conf_{GT} = 0.2304$ respectively. This rate indicates a very low confidence level marked by the experts. Perhaps just one of the four experts marked this area as suspicious and gave it a very low confidence (e.g. $< 50\%$). Any method that classify this image as healthy will disagree with a low level confidence ground truth. It is posible that the algorithm result matchs with more than one expert opinion.

If we limit the confidence to different margins, we can present more meaningful results. In this case we have considered different confidence level marks as the truth presence of the lesion. Table 6.5 presents the sensitivity for different margins of ground truth confidence levels.

Fixing $conf_{GT} > 0.2$ the performance of our method is compared with other methods. Most of the methods in the literature are focused in the detection of hard exudates, so our comparative study is limited to this type

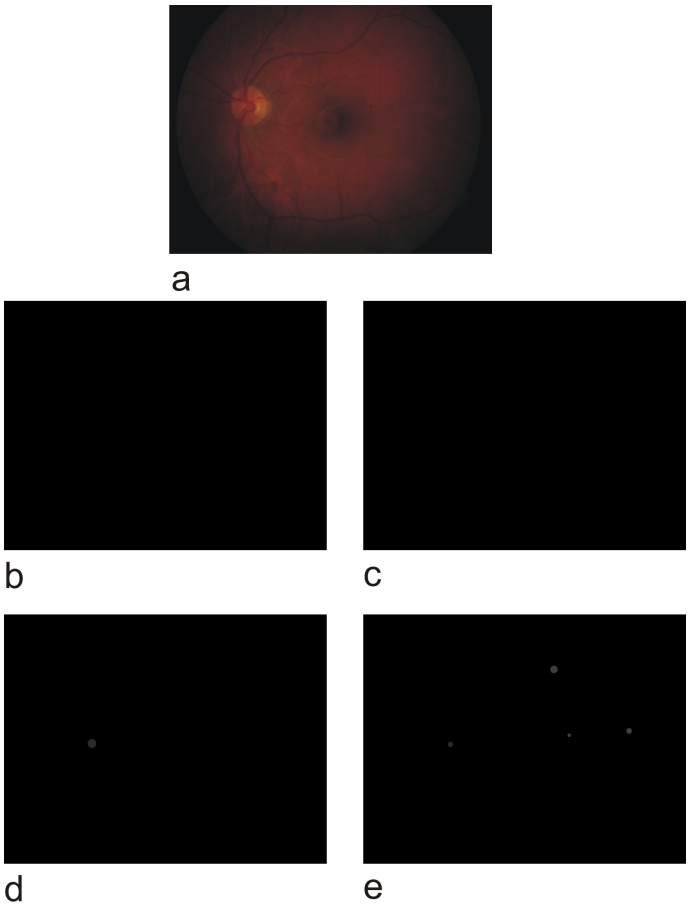

Figure 6.6: DIARETDB1 dataset: a) retinal image #32, b) hard exudate ground truth, c) soft exudate ground truth, d) hemorrhages ground truth $conf_{GT} = 0.0846$ and e) red spot ground truth $conf_{GT} = 0.2305$.

	$conf_{GT} > 0$	$conf_{GT} > 0.1$	$conf_{GT} > 0.2$
Hard exudates	89.58%	97.73%	97.73%
Soft exudates	66.67%	82.76%	88.89%
Hemorrhages	74.07%	86.96%	93.02%
Red spots	56.25%	62.5%	71.43%

Table 6.5: Average sensitivity for different margins of ground truth confidence levels.

of lesion. Table 6.6 shows the comparative analysis. Due to the lack of a common database the comparison is complex.

Method	Dataset	Average sensitivity
Morphologic reconstruction [Walter et al., 2002]	30 images	100%
Boosted soft segmentation [Fang et al., 2010]	DIARETDB1 83 images	100%
Statistical classification [Sanchez et al., 2009]	80 images	100%
Machine learning [Niemeijer et al., 2007b]	1789 images	87%
Computational intelligence [Osareh et al., 2009]	150 images	96%
Our method	DIARETDB1 89 images	97.73%

Table 6.6: Comparative study for hard exudate detection using different method considering image based criterion.

Table 6.7 presents the average local confidence of the detected areas marked by out method. Since hard exudates present the highest contrast, are the type of lesions detected with the highest $conf_{local}$ by our method.

Due to the low false positive rate, and considering that most of the regions is cover by non lesions the value for specificity is very close to 100%. Consequently the specificity value is not a good indicator of the performance of the algorithm. Table 6.7 presents the average local confidence of the detected areas marked by out method. As we can see our method detects lesions inside the ground truth with high $conf_{local}$.

	hard exudates	soft exudates	hemorrhages	red spots
Average $conf_{local}$	0.9123	0.7730	0.6416	0.4195

Table 6.7: Average local confidence $conf_{local}$ of the detected lesions.

We have presented the consolidation of our research by the detection of retinal lesions. Our method keeps the advantages of an automatic and unsupervised technique. The masking of eye structures prior to the detection

of lesions generates a clear area to perform the analysis. In general bright lesions are detected with higher confidence than dark lesions.

It is important to mention that we have quantified the ground truth confidence level using the gray level intensity of the ground truth images. The rates we have presented do not match necessarily with the original confidence levels reported by the experts.

6.4 Summary

In this chapter we have explained the process to detect retinal lesions. By using prior segmented retinal structures (blood vessels and optic disc) a background template is created and then used to detect any suspicious area.

The detected suspicious areas correspond to some type of retinal lesions. As expected, bright lesions are detected easier than dark lesions.

In the previous chapters we have presented the details about the design and implementation of our methods for the segmentation of structures and lesion detection from retinal images. The next chapter is dedicated to summary the research project, the contributions and the future work.

Chapter 7

Conclusions

7.1 Introduction

The aim of this chapter is to review the research presented in this thesis. Periodical eye screening is a highly recommended procedure for the early detection of signs of retinopathy. The main motivation of this research project was to provide a system to assist the retinal test.

Current methods for the analysis of retinal images have been designed for specific datasets characteristics, reducing modularity. Recognising the importance of an analysing method that can perform on retinal images with different characteristics (resolution, field of view, illumination, contrast), the research has been concentrated in the creation of this system.

For the reasons explained above we have concentrated our research in the development of an automatic system to assist the control and diagnosis of retinal diseases. A system with not need of user interaction or tunning of parameters. At the same time our selection of use the graph cut technique

provides to our model the flexibility to move from automatic to semiautomatic system if is required. During the development of our research we have test our methods on three different public datasets. This has demonstrated the versatility of our method.

This chapter has been divided in three sections. The first one is dedicate to make a summary of the research project. Then in Section 7.3 the contributions of our research are presented. Finally Section 7.4 makes a reflections about the possible limitations of the research and visualize the future work in this area.

7.2 Summary of research

The analysis of medical images is a specialized area of research. In general medical images contain a good amount of noise due to the capture process, and the control over this issue is limited. As a consequence poor contrast and illumination are characteristics of medical image.

Another issue to attend is the overlapping of tissues, this situation is common in medical images. In the case of retinal images optic disc and blood vessels are overlapped. This condition makes difficult the segmentation of retinal structures. In our research we explored two opposed research lines, the discrimination and the incorporation of vessels. This was an opportunity to study the blood vessels role into the segmentation of the optic disc.

Our research project can be divided in three major stages: segmentation of blood vessels, segmentation of optic disc and retinal lesions detection.

7.2.1 Retinal blood vessels segmentation

The morphology of blood vessels can provide valuable information about the health condition of the eye. Also vessels can be used to detect other retinal structures, such as optic disc.

For the segmentation of the retinal vessel using the graph cut technique we were limited by the "shrinking" problem. Basically, the issue appears when the energy function is minimized and the segmentation follows the shortest path. The segmentation boundary "shrinks" around the object to segment. But in the case of vessels, they are thin elongated structures "spreading" into the retinal image and the "shrinking" becomes a problem.

We confronted the problem by incorporating the flux term into the graph formulation. This innovative method has the modularity to segment vessels in different retinal datasets. Our method was tested in three different public datasets. Results have shown the outperformance of our method when is compare with other methods in the literature.

The processing time to perform the segmentation of vessels depends in part of the resolution of the image. An image with high resolution requires of more nodes and as a consequence more edges must be declared. To find the optimal segmentation on a big graph requires of more processing time than in a small graph. This is a disadvantage of our method. But considering that the medical image analysis area do not require strictly of real

time processing this is not a major drawback.

7.2.2 Retinal optic disc segmentation

The second stage is concentrated in the segmentation of the retinal optic disc. The morphology of the optic disc is considered by the experts as part of the procedure to provide a diagnosis. Also if the location of vessels and optic disc is known, these regions can be discriminated for the detection of retinal lesions in order to reduce the searching field.

Our method for the optic disc detection relies on prior blood vessel segmentation. The convergence of blood vessels is locate and assumed as the centre of the optic disc. From this location seed are initialized to construct the graph. In general images with a clear contrast between vessels and their background have an excellent prognostic to succeed in the detection of the optic disc centre, and then the initialization of seed will be precise.

Blood vessel network has a double roll in the segmentation of the optic disc. In one side blood vessels inside of the optic disc are part of the object to segment. On the other side they are part of the background. We designed two different methods for the segmentation of the optic disc. The methods attend both premises mask out the vessels prior to the optic disc segmentation and made then part of the segmentation formulation.

To attend the first premise we performed a MRF reconstruction on the retinal images. Assuming blood vessel pixels as unknown the method find the statistical best match in the rest of the image to substitute the missing

pixel. The back draw of this method is the high computational processing that MRF reconstruction requires. We limited the MRF reconstruction and the graph formulation to the ROI in order to minimize the processing time.

For our second method we incorporated prior blood vessel segmentation into the graph construction. The vessel pixels were linked to the foreground terminal using a compensation factor. In general all the pixels in the image were segmented using the traditional formulation of graph cut technique. It means using the neighbour links and the likelihood of them to belong to the foreground and background (boundary and regional terms). But in particularly vessel pixels were segmented using their neighbourhood links. Thus vessel pixels inside the optic disc, surrounded by foreground pixels, were segmented as foreground. And vessel pixels outside of the optic disc, surrounded by background pixels, were segmented as background.

Both of our methods were implemented and tested in two public datasets. Results have demonstrated the outperformance of our methods. Optic disc was segmented with high accuracy. The exceptional cases where the segmentation by using our methods resulted in null were shared cases by other segmentation methods. This due to the poor contrast between optic disc and background that difficult the achievement of an acceptable segmentation.

To evaluate the segmentation results we needed a ground truth of the optic disc. As exposed in Chapter three, none of the three public datasets used in our research provide hand label of the optic disc. We labelled by hand the optic disc in two datasets, DRIVE and DIARETDB1, in order to

create a ground truth where the results could be evaluated. These ground truth is now available for research purposes and can be used as ground truth or as a second observer for experimental work.

The seeds have been initialized automatically by using the optic disc centre location. There are two special cases in the initialization of seeds. If the method fails to locate the centre of the optic disc and instead locate an area in the background the initialization of seeds will be erroneous. If the method locates the area half inside the boundary of the optic disc the initialization will be spurious. These special cases are reduced to only one case for the DRIVE dataset (40 images) and three for DIARETDB1 dataset (89 images).

7.2.3 Retinal lesions detection

Retinal lesions are the main indicator of the presence of a disease in the retina. By considering the colour retinal lesions can be classified in two: bright retinal lesions (hard and soft exudates) and dark retinal lesions (red spots and haemorrhages). In general bright retinal lesions are easier to detect and segment due to the high contrast with their background.

Current methods in the literature are focused on the detection of bright lesions. Table 2.3 shows a compilation of methods designed for the detection of retinal lesions, it is possible appreciate they are dedicated to detect and segment bright lesions.

For first time a method to detect any type of suspicious lesion, including

dark lesions, has been presented. Our method made use of prior segmented retinal structures (optic disc and blood vessels) to create a background template. The template is then used to localize any suspicious area that do not match with the background.

The detected areas are then evaluated on DIARETDB1 by using the provided ground truth. As expected before most of the suspicious areas correspond to bright lesions (hard and soft exudates). Dark lesions were detected with acceptable level.

To evaluate the detected areas the confidence of the markings made by experts was quantified, this permitted to have more meaningful results evaluation. Unlike to other methods our evaluation was not based on only one expert opinion. Instead the opinions of four experts were condensate on the ground truth confidence and under this basis our method was evaluated.

7.3 Contributions

Besides the innovative and authentic characteristics of our research, the development of this project has permitted make significant contributions. Valuable commentaries and critics from the research community have worked for the enrichment of our project. We summarize the contribution of our research project next.

- An auntomatic and unsupervised model. Traditional methods for the analysis of retinal images are based on supervised systems. These systems have been trained by using a collection of hand labelled retinal

images. The training process demands of time processing and hand labelled images. Often the systems designed for the analysis of retinal images are based on specific characteristics of the retinal structures such as, size, shape, and colour. Unfortunately is difficult to keep control on these parameters in order to provide the optimal conditions for the best performance of the models, specially for retinal with lesions. For the reasons exposed above we have concentrated our research in the development of an automatic and unsupervised system for the analysis of retinal images. Our methods can perform on retinal images with different characteristics without adjustment of parameters.

- Incorporation of prior knowledge. For the segmentation of retinal structures (blood vessels and optic disc) we based our design on the graph cut technique. The use of this technique permitted to incorporate prior information to guide the model in order to find the optimal segmentation. Prior segmented vessels are used to localize the optic disc. Then by using the location of the optic disc foreground and background seeds are initialized and used to construct the graph. Finally the segmented structures are used to create a background template to detect retinal lesions.

- Segmentation of other blood vessel structures. Due to our method for the segmentation of blood vessels does not rely on the characteritics (size, resolution) of the images, it can be applied to other medical images like angiograms.

- Segmentation of overlapping tissues. The main issue to attend for the segmentation of the optic disc is the overlapping of vessels. This is a common situation on the analysis of medical images. By using prior vessel segmentation we have explored to complementary research lines, discrimination and incorporation of vessels. As results new knowledge is available to attend this problem, and results of our experimental work can be used to take a decision in the case of overlapping tissues segmentation.

- Dark and bright retinal lesions detection. In general bright lesions are easier to detect than dark lesions. This due to the high level contrast with their background. Current methods designed for the detection of retinal lesions are concentrated in the detection of brigth lesions, leaving to a side dark lesions. Our method detects any suspicious area that do not match with the general background template, this includes dark and bright lesions.

- Confidence based evaluation for the retinal lesion detection. Until now the evaluation of the methods for the detection of lesions has been performed based on a unique ground truth. By means of the DIARETDB1 dataset use we perform the evaluation of detected lesions based on the confidence marks made by more than one expert.

- Creation of ground truth for the optic disc in public datasets. A common interest within the research comunnity in retinal imaging is the availability of ground truth images to perform experimental work. Different public retinal datasets are available, but unfortunately they

do not included a ground truth of the optic disc. We have created hand labelling of the optic disc on two public dataset, DRIVE and DIARETDB1. These ground truth sets are available and have been shared within the research comunity.

7.4 Future work

The detection of retinal lesions is a controversial area to address. Is in fact very useful to achieve a detailed segmentation of the lesions? or is the truly important to recognize the suspicious areas in the image?

Our method does not classify the detected lesion areas. Until now it is not clear how much this classification can help to the experts with the screen test procedure. We consider that detect the suspicious lesions areas is the main process to assist the retinal scanner. The exact condition, diagnosis and decision respect to a patient should be left to the medical professionals.

Still the question is open, which one is a good method to detect retinal lesions, the one that is able to detect most of them or the one that detect the lesions in crucial areas or the one that is able to segment lesions with high detailed boundary? The answer perhaps is coming in the next years when the retinal analysis systems will be put in practice by the hands of the experts. And then new adaptation and information can be incorporated into the systems in order to compensate the limitations.

It is possible that for some new applications the automatic initialization

of seed limited the performance of the method, in this case the initialization can be done manually. And is precise this one of the best characteristics of our method, the flexibility to move from automatic to interactive method easily. The overall results of the research have demonstrated the outperformance of our methods for the segmentation of retinal structures. Even though there are opportunities to improve.

The creation of a graph and the consequent energy function optimization demand of high processing time. In general the analysis or medical image does not require of real time performance, but there will be situations where a faster solution is demanded. It is possible to reduce the time processing by limiting the graph construction to only the region of interest. This can be achieve by the manual initialization of seeds. In this way the user can select the region of interest and the analysis will be limited to this.

The formulation of the graph link weights has been based on the pixel intensity distribution and the euclidian distant with the pixels in the neighborhood. There are other medical images applications where this formulation is not enough and new formulation is needed. It is possible to extent the assignment of link weights by including other features such as texture. In the one hand the graph will be more complex and to find the optimal cut will require of more intensive processing, but on the other hand the image information will be represented better by the graph.

The research work presented in this thesis has been concentrated to the analysis of fundus retinal images in 2D. In order to create a the formulation can be extend to perform on retinal images in 3D. This extension should

be a straight forward process. If a grid of 26 neighbors is used for the 3D representation each pixel will be linked with eight neighbors in the same plane and with two in the adjacent planes, one pixel in each plane. In order to capture the retinal image it would be necessary to refer to a Heidelberg Retina Tomography.

Perhaps the most important feedback and the one that will establish the agenda for the immediate future of our system will be the report of the opticians after the systems is put in use. The system will need be modified to attend the specific request of the opticians.

Bibliography

S.Y Ababneh and M.N Gurcan. An efficient graph cut segmentation for knee bone osteoarthritis medical images. *IEEE International Conference on Electro/Information Technology (EIT)*, pages 1–4, 2010.

A. Aquino, M.E. Gegundez-Arias, and D. Marin. Detecting the optic disc boundary in digital fundus images using morphological, edge detection and feature extraction techniques. *IEEE transactions on medical imaging*, 29(10):1860–1869, 2010.

Y. Boykov and G. Funka-Lea. Graph cuts and efficient n-d image segmentation. *International Journal of Computer Vision*, 70(2):109–131, 2006.

Y. Boykov and M-P. Jolly. Interactive organ segmentation using graph cuts. *In Proceedings of International Conference on Medical Image Computing and Computer-Assisted Intervention*, pages 276–286, 2000.

Y. Boykov and M-P. Jolly. Interactive graph cuts for optimal boundary and region segmentation of objects in n-d images. *In Proceedings of Eighth IEEE International Conference on Computer Vision, ICCV.*, 1:105–112, 2001.

Y. Boykov and V. Kolmogorov. An experimental comparison of min-

cut/max- flow algorithms for energy minimization in vision. *IEEE Transactions on Pattern Analysis and Machine Intelligence*, 26(9):1124–1137, 2004.

W. Cai and A. Chung. Multi-resolution vessel segmentation using normalized cuts in retinal images. *In Proceedings of International Conference on Medical Image Computing and Computer-Assisted Intervention*, 1: 928–936, 2006.

J.H Chen and L.G Shapiro. Medical image segmentation via min s-t cuts with sides constraints. *19th International Conference on Pattern Recognition ICPR*, pages 1–4, 2008.

V Chen and S Ruan. Graph cut segmentation technique for mri brain tumor extraction. *2nd International Conference on Image Processing Theory Tools and Applications, IPTA*, pages 284–287, 2010.

D.R. Chittajallu, G. Brunner, U. Kurkure, R.P. Yalamanchili, and I.A. Kakadiaris. Fuzzy-cuts: A knowledge-driven graph-based method for medical image segmentation. *Proceedings of the twenty third IEEE coference on computer, vision and Pattern recognition.*, pages 715–722, 2009.

A.S Chowdhury, A.K Rudra, M Sen, A Elnakib, and A El-Baz. Cerebral white matter segmentation from mri using probabilistic graph cuts and geometric shape priors. *Proceedings of the IEEE 17th international conference on image processing.*

R. Chrastek, M. Wolf, K. Donath, H. Niemann, D. Paulus, T. Hothorn, B. Lausen, R. Lammer, C. Y. Mardin, and G. Michelson. Automated segmentation of the optic nerve head for diagnosis of glaucoma. *Medical Image Analysis*, 9(1):297–314, 2005.

A. A. Efros and T. K. Leung. Texture synthesis by non-parametric sampling. *In Proceedings of the ICCV 1999.*, pages 1033–1038, 1999.

S Esneault, N Hraiech, E Delabrousse, and J.L Dillenseger. Graph cut liver segmentation for interstitial ultrasound therapy. *Proceedings of the 20th annual international conference of the IEEE EMBS.*

G. Fang, N. Yang, H. Lu, and K. Li. Automatic segmentation of hard exudates in fundus images based on boosted soft segmentation. *Proceedings of the International Conference on Intelligence Control and Information Processing*, pages 633–638, 2010.

A.D Fleming, S Philip, K.A Goatman, G.J Williams, J.A Olson, and P.F Sharp. Automated detection of exudates for diabetic retinopathy screening. *Physics in medicine and biology*, 52:7385–7396, 2007.

D Fong, L Aiello, F Ferris, and R. Klein. Diabetic retinopathy. *Diabetes Care*, 27(10):2540–2553, 2004.

D Freedman and T Zhang. Interactive graph cut based segmentation with shape priors. *Proceedings of the IEEE computer society conference on computer vision and pattern recognition.*

P Furnstahl, T Fuchs, A Schweizer, L Nagy, G Szekely, and M Harders. Automatic and robust forearm segmentation using graph cuts. *5th IEEE International Symposium on Biomedical Imaging: From Nano to Macro.*

M Garcia, C.I Sanchez, M.I Lopez, D Abasolo, and R Hornero. Neural network based detection of hard exudates in retinal images. *Computer methods and programs in biomedicine*, 93:9–19, 2009.

A. Hoover and M. Goldbaum. Locating the optic nerve in retinal image using the fuzzy convergence of the blood vessels. *IEEE Transactions on Medical Imaging*, 22(8):951–958, 2003.

A Hoover, V Kouznetsova, and M Goldbaum. Locating blood vessels in retinal images by piecewise threshold probing of a matched filter response. *IEEE Transactions on Medical Imaging*, 19(3):203–210, 2000.

X Jiang and D Mojon. Adaptive local thresholding by verification-based multithreshold probing with application to vessel detection in retinal images. *IEEE Transactions on Pattern Analysis and Machine Intelligence*, 25(1):131–137, 2003.

Gordon J. Johnson, Darwin C. Minassian, Robert A. Weale, and 2nd Edition Sheila K. West. *The Epidemiology Of Eye Disease*. Arnold, 2003.

T. Kauppi and H. Kalviainen. Simple and robust optic disc localisation using colour decorrelated templates. *Proceedings of advanced concepts for intelligence vision systems*, pages 719–729, 2008.

T Kauppi, V Kalesnykiene, J Kamarainen, L Lensu, I Sorri, A Raninen, R Voitilainen, H Uusitalo, H Kalviainen, and J Pietila. Diaretdb1 diabetic retinopathy database and evaluation protocol. *In Proceedings of British Machine Vision Conference.*, 2007.

V. Kolmogorov and Y. Boykov. What metrics can be approximated by geo-cuts, or global optimization of length/area and flux. *In Proceedings of Tenth IEEE International Conference on Computer Vision, ICCV.*, 1:564–571, 2005.

B.S.Y. Lam and H. Yan. A novel vessel segmentation algorithm for the

pathological retinal images based on the divergence of vector fields. *IEEE transactions on medical imaging*, 27(2):237–246, 2008.

H. Li and O. Chutatape. Automated feature extraction in color retinal images by a model based approach. *IEEE Transactions on biomedical engineering*, 51(2):246–254, 2004.

W Li Yun, U Rajendra-Acharya, Y.V Venkatesh, C Chee, L Choo-Min, and E.Y.K Ng. Identification of different stages of diabetic retinopathy using retinal optical images. *Information Sciences*, 178:106–121, 2008.

L Liang, K Rehm, R.P Woods, and D.A Rottenberg. Automatic segmentation of left and right cerebral hemispheres from mri brain volumes using the graph cuts algorithm. *NeuroImage*, 34:1160–1170, 2007.

X Lin, B Cowan, and A Young. Model based graph cut method for segmentation of the left ventricle. *Proceedings of the IEEE engineering in medicine and biology 27th annual conference*, pages 3059–3062, 2005.

J. Lowell, A. Hunter, D. Steel, A. Basu, R. Ryder, E. Fletcher, and L. Kennedy. Optic nerve head segmentation. *IEEE Transactions on Medical Imaging*, 23(2):256–264, 2004.

M. E. Martinez-Perez, A. D. Hughes, S. A. Thom, A. A. Bharath, and K. H. Parker. Segmentation of blood vessels from red-free and fluorescein retinal images. *Medical image analysis*, 11(1):47–61, 2007.

F. Mendels, C. Heneghan, P.D. Harper, R.B. Reilly, and J. Ph. Thiran. Extraction of the optic disc boundary in digital fundus images. *In Proceedings of the 1st Joint BMES/EMBS Conf*, page 1139, 1999.

A. M. Mendonca and A. Campilho. Segmentation of retinal blood vessels by combining the detection of centerlines and morphological reconstruction. *IEEE Transactions on Medical Imaging*, 25(9):1200–1213, 2006.

M. Niemeijer, M. D. Abramoff, and B. van Ginneken. Segmentation of the optic disc, macula and vascular arch in fundus photographs. *IEEE Transactions on Medical Imaging*, 26(1):116–127, 2007a.

M. Niemeijer, M. D. Abramoff, and B. van Ginneken. Automated localization of the optic disc and the fovea. *Proceedings of the 30th Annual International IEEE EMBS conference*, pages 3538–3541, 2008.

Meindert Niemeijer, Bram van Ginneken, Stephen R. Russell, Maria S. A. Suttorp-Schulten, and Michael D. Abrmoff. Automated detection and differentiation of drusen, exudates, and cotton-wool spots in digital color fundus photographs for diabetic retinopathy diagnosis. *IOVS*, 48:2260–2267, 2007b.

T Nuzhnaya, E Cheng, H Ling, D Kontos, P.R Bakic, and V Megalooikonomou. Segmentation of anatomical branching structures based on texture feature and graph cut. *IEEE International Symposium on Biomedical Imaging: From Nano to Macro*.

A. Osareh, B. Shadgar, and R. Markham. A computational-intelligence-based approach for detection of exudates in diabetic retinopathy images. *IEEE TRANSACTIONS ON INFORMATION TECHNOLOGY IN BIOMEDICINE*, 13:535–545, 2009.

N. Patton, T.M. Aslam, T. MacGillivray, I.J. Deary, B. Dhillon, R.H. Eikelboom, K. Yogesan, and I.J. Constable. Retinal image analysis: Concepts,

applications and potential. *Progress in Retinal and eye research*, 25:99–127, 2006.

Patrick J. Saine and Marshall E. Tyler. *Ophthalmic Photography: Retinal Photography, Angiography, and Electronic Imaging, 2nd Edition*. 2002.

A. Salazar-Gonzalez, Y. Li, and X. Liu. Retinal blood vessel segmentation via graph cut. *In Proceedings of the 11th International Conference on Control, Automation, Robotics and Vision, ICARCV*, 1:225–230, 2010.

A. Salazar-Gonzalez, Y. Li, and X. Liu. Optic disc segmentation by incorporating blood vessel compensation. *In Proceedings of IEEE SSCI, International Workshop on Computational Intelligence In Medical Imaging*, pages 1–8, 2011.

C.I Sanchez, R Hornero, M.I Lopez, and J Poza. Retinal image analysis to detect and quantify lesions associated with diabetic retinopathy. *Proceedings of the 26th annual international conference of the IEEE EMBS*, pages 1–5, 2004.

Clara I. Sanchez, Maria Garcia, Agustin Mayo, Maria I. Lopez, and Roberto Hornero. Retinal image analysis based on mixture models to detect hard exudates. *Medical Image Analysis*, 13:650–658, 2009.

G Slabaugh and G Unal. Graph cuts segmentation using an elliptical shape prior. *IEEE International Conference on Image Processing, ICIP*.

J. Soares, J. Leandro, R. Cesar, H. Jelinek, and M. Cree. Retinal vessel segmentation using the 2-d gabor wavelet and supervised classification. *IEEE Transactions on Medical Imaging*, 25(9):1214–1222, 2006.

Z Song, N Tustison, B Avants, and J Gee. Adaptive graph cuts with tissue priors for brain mri segmentation. *3rd IEEE International Symposium on Biomedical Imaging: Nano to Macro.*

A Sopharak, B Uyyanonvara, S Barman, and T.H Williamson. Automatic detection of diabetic retinopathy exudates from non-dilated retinal images using mathematical morphology methods. *Computerized medical imaging and graphics*, 32:720–727, 2008.

J. Staal, M. D. Abramoff, M. Niemeijer, M. A. Viergever, and B. van Ginneken. Ridge-based vessel segmentation in color images of the retina. *IEEE Transactions on Medical Imaging*, 23(4):501–509, 2004.

K. W. Tobin, E. Chaum, V. P. Govindasamy, and T. Karnowski. Detection of anatomic structures in human retinal imagery. *IEEE Transactions on Medical Imaging*, 26(12):1729–1739, 2007.

M. Usman Akram, A. Tariq, and S. Khan. Retinal image blood vessel segmentation. *Proceedings of the international conference on information and communication technology*, 978(1), 2009.

A. Vasilevskiy and K. Siddiqi. Flux maximizing geometric flows. *IEEE transactions on pattern analysis and machine intelligence.*, 24(12):1565–1578, 2002.

S. Vicente, V. Kolmogorov, and C. Rother. Graph cut based image segmentation with connectivity priors. *In Proceedings of IEEE Conference on Computer Vision and Pattern Recognition, CVPR*, 1:1–8, 2008.

T. Walter, J-C Klein, P. Massin, and A. Erginay. A contribution of image processing to the diagnosis of diabetic retinopathy: Detection of exu-

dates in color fundus images of the human retina. *IEEE Transactions on Medical Imaging*, 21(10):1236–1243, 2002.

D. Welfer, J. Scharcanski, C. Kitamura, M. Dal Pizzol, L. Ludwig, and D. Marinho. Segmentation of the optic disc in color eye fundus images using an adaptive morphological approach. *Computers in Biology and Medicine*, 40(1):124–137, 2010a.

D. Welfer, J. Scharcanski, and D. Ruschel Marinho. A coarse to fine strategy for automatically detecting exudates in color eye fundus images. *Computerized Medical Imaging and Graphics*, 34:228–235, 2010b.

S Wild, G Roglic, A Green, R Sicree, and H King. Global prevalence of diabetes. *Diabetes Care*, 27(5):1047–1053, 2004.

D. Wu, M. Zhang, and J. Liu. On the adaptive detection of blood vessels in retinal images. *IEEE Transactions on Biomedical Engineering*, 53(2): 341–343, 2006.

X. Yang, P. Morrow, and B. Scotney. Optic nerve head segmentation in hrt images. *Proceedings of the international conference on image processing*, pages 65–68, 2006.

A. Youssif, A. Ghalwash, and A. Ghoneim. Optic disc detection from normalized digital fundus images by means of a vessels's directed matched filter. *IEEE Transactions on Medical Imaging*, 27(1):11–18, 2008.

Y. Zeng, D. Samaras, W. Chen, and Q. Peng. Topology cuts: a novel min-cut/max-flow algorithm for topology preserving segmentation in n-d images. *Journal of computer vision and image understanding.*, 112(1): 81–90, 2008.

J Zhang, Y Wang, and X Shi. An improved graph cut segmentation method for cervical lymph nodes on sonograms and its relationship with node's shape assessment. *Computerized medical imaging and graphics*, 33:602–607, 2009.

J. Zhu-Jacquot and R. Zabih. Graph cuts segmentation with statistical shape prior for medical image. *Proceedings of the third international IEEE conference on signal-image technologies and internet-based system.*, pages 631–635, 2008.

Appendix A

MinCut/MaxFlow Algorithm

The min-cut/max-flow algorithm used in our research implementation belongs to the group of augmenting paths based algorithms. It builds two search trees for detecting augmenting paths, one from the source and one from the sink. The algorithm does not start the trees from scratch, instead it reuses the previous trees.

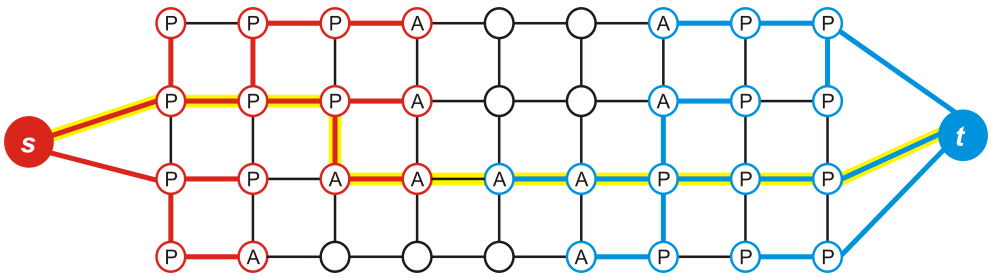

Figure 7.1: Example of search tree S (red) and T (blue) at the end of the growth stage when a path (yellow line) from the source s to the sink t is found.

Figure 7.1 illustrates the max flow algorithm. The algorithm keeps two non-overlappiong search trees S(source root) and T(sink root). For the tree S all edges from each parent node to its children are non-saturated, and for the tree T edges from children to their parents are non-saturated. The nodes that are not part of S ar T are called "free". Then we have

$$S \subset \nu, \quad s \in\subset S, \quad T \subset \nu, t \in\subset T, S = \oslash$$

The nodes in the search trees can be "active" or "passive". The active nodes are the ones that are in outer border in each tree, while the passive nodes are the internal ones. The active nodes allow the trees to grow by acquiring new children. The passive nodes are blocked by other nodes from the same tree and they cannot grow. It is important that the active nodes are in contact with the nodes from the other tree. As soon as an active node detects a neighboring node that belong to the other tree an augmenting path is found. The algorithm iterates repeating the following three stages:

- "growth" stage: search trees S and T grow until they touch givint an $s \rightarrow t$ path
- "augmentation" stage: the found path is augmented, search tree(s) break into forest(s)
- "adoption" stage: trees S and T are restored

In the "growth" stage the search tree expands. The active nodes explore non satuated adjacent nodes ans acquire new children from the set of free nodes. These new nodes become active members of the corresponding search tree. When all the neighboors of an active node haven explored the active node become passive. This stage finishes if an active node finds a neighboor that belongs to the oposite tree.

In the augmentation stage the path found in the growth stage is augmented. Because the largest possible flow is pushed some edges in the path

become saturated. As a consecuence, some of the edges linking the nodes to their parents are not loger valid and the nodes in the trees S and T become "orphans". The augmentation phase may split the search trees S and T into a "forest". Terminals s and t are still roots of two of the search trees, and the orphans form roots of all other trees.

Finally the "adoption" stage restores the single tree structure S and T with roots in the source s and in the sink t. A new valid parent for each "orphan" is found. The new parent and the "orphan" should belong to the set S ot T. The parent also should be connected through a non saturated edge. If a no qualified parent is found the "orphan" is removed from S or T and is declared as free node altogether with its children. The "adoption" stages terminates when no "orphans" are lef and the search trees structures S and T are restored.

After the "adoption" stage the algorthm returns to the "growth" phase. The algorithm finishes when the search trees cannot grow (no active nodes) and the trees are separated by saturated edges. In this point the maximum flux has been reached, and the minimum cut is determinated by $S = S$ and $T = T$.

Implementation

Assuming a direct graph $G =< V, E >$, for each augmenting path the flow f and the residual graph Gf are maintained. We also keep the list of active nodes, A and all the "orphan" nodes, O. The general structure of the lagorithm is:

initialize: S=s, T=t, A=s,t, O=⊘

while true

grow S or T to find an augmenting path P from s to t

if P=⊘ terminate

augment on P

adopt orphans

end while

The content of the search trees S and T are stored by indicating the affiliation of each node p

$$TREE(p) = \begin{cases} S\ if\ p\ \in\ S \\ T\ if\ p\ \in\ T \\ \oslash\ if\ p\ is\ free \end{cases}$$

If node p belongs to one of the search trees then the information about its parent will be stored as $PARENT$(p). The roots of the search trees, orphans, and free nodes are declared as $PARENT$(p)= ⊘. The notation $tree_cap(p\ \rightarrow\ q)$ is used to describe the residual capacity of the edges (p, q) in the search tree S and the edges (q, p) in the search tree T. p should be a valid parent for its child q,in the case of tree S, so the nodes are not saturated.

Growth stage

The active nodes require of new children from the set of free nodes

while $A \neq \oslash$

pick an active node $p \in A$

for every neighbor q such that $tree_c app \rightarrow q) > 0$

if $TREE(q) = \oslash$ then add q to search tree as an active node:

$TREE(q) := TREE(p),\ PARENT(q) := p,\ A := A \cup q$

if $TREE(q) \neq= \oslash$ and $TREE(q) \neq= TREE(p)$ return $P = PATH_{s \rightarrow t}$

end for

remove p from A

end while

return $P = \oslash$

Augmentation stage

In the begining of this stage the orphan set is empty, but at the end there may be some orphans in the set since at least one edge in P becomes saturated.

find the bottleneck capacity Δ on P

update the residual graph by pushing flow Δ through P

for each edge (p, q) in P that becomes saturated

if TREE(p) = TREE(q) = S then set PARENT(q):= $\oslash$ and $O := O \cup q$

if TREE(p) = TREE(q) = T then set PARENT(p):= $\oslash$ and $O := O \cup p$

end for

Adoption stage

All orphan nodes in O are processed until O becomes empty. Each node p will try to find a new valid parent within the same search tree. If p finds a new valid parent will remain in the tree, otherwise it will become a free node and all its children are added to O.

while $O = \oslash$

pick an orphan node $p \in O$ and remove it form O

If the orphan node p finds a new valid parent q then, PARENT(p)=q

else

p becomes free node

scan all the neighbors q of p such that TREE(q)=TREE(p)

if $tree_cap(q \rightarrow p) > 0$ add q to the active set A

if PARENT(q)=p add q to the set of orphans O and set $PARENT(q) :=$

$TREE(p) := \oslash$, $A := A - p$

end while

During the "process p" the orphan node p is trying to find a new valid parent among its neighbors. A valid parent q should satisfy the following conditions:

- they should belong to the same tree, TREE(q)=TREE(p)
- the residual capacity should be bigger than zero, $tree_cap(q \rightarrow p) > 0$
- the origin of the new parent q should be one of the main roots, source or sink

If the orphan node p finds a new valid parent q then, PARENT(p)=q, p remains in its search tree and keeps its status (active or passive). If the

orphan node does not find a valid parent the algorithm scan all neighbors of p and sort them out. When the orphan node does not find a new valid parent and becomes free all its neighbors connected through non-saturated edges should became active. It is possible that some neighbor q did not qualify as a valid parent during the adoption stage because it did not originate from the main roots, but this node could be a valid parent after adoption stage is finished. For more details about the MinCut/MaxFlow algorithm, its background, formulation, implementation, please refer to the work of Boykov and Kolmogorov, [Boykov and Kolmogorov, 2004].